INVESTIGATIONS TOWARDS THE PREPARATION OF PHOTORESPONSIVE POLYMERS BASED ON PHOTOCLEAVABLE TELLURIUM-CONTAINING CROSS-LINKS

BY

CHRIS GENDY, B.Sc. (H.)

A THESIS

SUBMITTED TO THE SCHOOL OF GRADUATE STUDIES IN PARTIAL FULFILLMENT OF THE REQUIREMENTS FOR THE DEGREE

MASTER OF SCIENCE

MCMASTER UNIVERSITY

M.Sc. (2011) McMaster University

(Chemistry) Hamilton, ON

TITLE: Investigations towards the preparation of photoresponsive polymers based on photocleavable tellurium-containing cross-links.

AUTHOR: Chris Gendy

SUPERVISORS: Dr. Ignacio Vargas-Baca and Dr. Kalaichelvi Saravanamuttu

NUMBER OF PAGES: xxvii, 94

ABSTRACT

Refractive index changes within a material are most commonly induced by either physical or photochemical changes such as the electro-optic or Kerr effects. The former processes can elicit a range of nonlinear phenomena including optical self-trapping and modulation instability which have been studied extensively. However, the corresponding processes due to photochemical transformations in a material have been studied to a lesser extent. The potential for application in photonics and optoelectronics technologies has made this an exciting and growing field. One convenient platform for the study of *opto-chemical* nonlinear phenomena is a siloxane matrix that contains photo-polymerizable methacrylate substituents. These functional groups undergo polymerization upon irradiation, which results in densification and an overall increase in the refractive index of the material. Studies of such materials have revealed a range of nonlinear opto-chemical phenomena including self-trapping, modulation instability and self-phase modulation.

The goal of this research project is to synthesize, characterize, and examine the properties of a material that undergoes a decrease in refractive index upon exposure to light. It is anticipated that such photoresponses could elicit previously unknown nonlinear phenomena including self-trapped black beams. An appropriate material for these investigations would be a polymer cross-linked by groups that can undergo dissociation by exposure to light, causing relaxation and expansion of the polymer matrix, and consequently a $\Delta n < 0$. Given the detailed optical studies already carried out with a frequency doubled Nd-VO_4 laser (λ = 532 nm), the crosslinks should be sensitive to green

light. Organo-ditellurides, molecules that contain a Te-Te bond, would be appropriate for the crosslinks as their $\sigma^*_{Te-Te} \leftarrow n_{Te}$ transition usually absorbs light between 400 and 500 nm, and can lead to photodissociation of the chalcogen-chalcogen bond.

Initial attempts to directly functionalize a polymer (polystyrene) resulted in intractable solids. A more promising approach relies on the preparation of cross-linking agents followed by co-polymerization. Progress to date includes the preparation of a bis(p-vinylbenzyl) telluride. Despite literature claims, to date, there is no structurally authenticated photoresponsive molecule that simultaneously contains vinyl and telluride functional groups. The work in this thesis has yielded what would be the first example, in addition to a crystal structure obtained by X-ray diffraction, the compound has been characterized by multinuclear NMR (^{1}H, ^{13}C, ^{125}Te) and vibrational spectroscopy with the support of DFT calculations.

ACKNOWLEDGEMENTS

I would like to thank Dr. Ignacio Vagas-Baca and Dr. Kalaichelvi Saravanamuttu for not only their supervision and guidance, but for inspiring in me a passion for research in chemistry. I thank my committee member Dr. Alex Adronov for his guidance in my time as a student at McMaster University.

I thank all the group members for their assistance, support, and making the lab an enjoyable place to work. I would especially like to thank Philip J. W. Elder for his mentorship and for preliminary calculations towards the vibrational analysis of the Te-Cl bonds. I thank Andy Tran for his contribution to the literature research towards a method for the polymerization of the acrylate and styrene systems.

I thank Dr. Gary J. Schrobilgen for running samples of supermesityltellurenyl(II) chloride on his FT-Raman system, and for his guidance.

I would like to thank the NMR, and optical spectroscopy personnel for instrument training, and advice. In particular, I thank Dr. Steve Kornic for instrument training, switching over the optics in the Nicolet FT-IR spectrometer and ongoing technical advice. I thank Dr. Jim Britten and Hilary Jenkins for all X-Ray work covered in this thesis.

I thank the Natural Science and Engineering Research Council of Canada (NSERC) for funding, specifically, the NSERC CREATE program in photovoltaics, and SHARCNET for CPU time.

TABLE OF CONTENTS

ABSTRACT.....**iii**

ACKNOWLEDGEMENTS.....**v**

LIST OF FIGURES.....**x**

LIST OF SCHEMES.....**xiii**

LIST OF COMPOUNDS.....**xv**

LIST OF ABBREVIATIONS AND SYMBOLS.....**xxv**

1 Chapter 1: Introduction **1**

1.1 Photoresponsive polymers. 1

1.1.1 Photoresponsive organic materials.....2

1.1.2 Photoresponsive inorganic-based materials.....9

1.2 Chemical change and refractive index. 12

1.3 Objective of this project. 14

1.4 Proposed Material 17

2 Chapter 2: Experimental **20**

2.1 Materials. 20

2.2 Infrared Spectroscopy. 21

2.3 Raman Spectroscopy. 21

2.4 NMR Spectroscopy. 22

2.5 Ultraviolet-Visible Absorption Spectroscopy. 22

2.6 Electron Ionization Mass Spectrometry. 23

2.7 Single Crystal X-Ray Diffraction. 23

2.8 Functionalization of polystyrene with TMS-Cl. 24

2.9 Attempted synthesis of polystyrene functionalized with elemental tellurium. 25

2.10 Synthesis of [Te(bipy)Cl_2] 39. 25

2.11 Attempted synthesis of the tellurated polymer using [Te(bipy)Cl_2]. 25

2.12 Test reaction of the "one-pot ditelluride synthesis" from 2-iodotoluene. 26

Following a procedure by Singh 26

2.13 Attempted synthesis of [4-[[[4-(hydroxymethyl)phenyl] methylditellanyl]methyl]phenyl]methanol. 26

2.14 Synthesis of 4-iodostyrene. 27

2.15 Attempted synthesis of 1-vinyl-4-[[(4-vinylphenyl)methyl ditellanyl]methyl]benzene starting from 4-iodostyrene. 27

2.16 Attempted synthesis of Te-(2-methylprop-2-enoyltellanyl)2-methylprop-2-enetelluroate from in situ generated sodium ditelluride. 27

2.17 Synthesis of Na_2Te. 28

2.18 Attempted synthesis of sodium 2-methylprop-2-enetelluroate 52. 29

2.19 Attempted synthesis of sodium (4-vinylphenyl)methanetellurolate 54. 29

2.20 Preparation of (bis)vinylbenzyl telluride. 30

2.21 Attempted synthesis of sodium (4-vinylphenyl)methane tellurolate with a catalytic amount of 15-crown-5. 30

2.22 Attempted synthesis of sodium (4-vinylphenyl)methane tellurolate with a stoichiometric amount of 15-crown-5. 31

2.23 Bromination of 1,3,5-tri-tert-butylbenzene. 32

2.24 Synthesis of (bis)supermesitylditelluride. 32

2.25 Synthesis of phenyltellurium(IV) trichloride 47. 33

2.26 Synthesis of supermesityltellurenyl(II) chloride 45. 34

2.27 Synthesis of supermesityltellurium(IV) trichloride 46. 34

2.28 Computational Details. 35

3 Chapter 3: Direct Functionalization of Polystyrene with n-BuLi and TMEDA.....36

3.1 Introduction. 36

3.2 Functionalization of polystyrene with TMS. 37

3.3 Reaction of lithiated polymer with elemental sulfur. 45

3.4 Reaction of lithiated polymer with elemental tellurium. 45

3.5 Reaction of 2 with [Te(bipy)Cl_2].....46

4 Chapter 4: Vibrational Analysis of R-$TeCl_n$ Groups.....48

4.1 Synthesis and vibrational analysis of organo-tellurium chlorides.....48

5 Chapter 5: Polymerizable Cross-Linking Agents 60

5.1 Introduction. 60

5.2 bis(4-vinylphenyl)ditelluride. 61

5.3 Bis(methacryloyl)ditelluride. 64

5.4 4-vinylbenzylditelluride 55. 68

6 Chapter 6: Conclusions and Suggestions for Future Work 85

6.1 Conclusions. 85

6.2 Suggestions for future work. 86

6.2.1 Synthesis of a ditelluride cross-linking agent.....86

6.2.2 Tellurium cross-linking agents from acetylides and elemental tellurium. 88

REFERENCES.....89

LIST OF FIGURES

Figure 1.1: Example of an azobenzene cross-linked methacrylate.....6

Figure 1.2: Example of a spirobenzopyran based cross-linking agent.....7

Figure 1.3: Photo-reversible coumarin cross-linking system.....9

Figure 1.4: Photocleavable M-M dimers containing Mo and Fe.....11

Figure 1.5: Intensity profiles over an area of the development of a self trapped dark beam. As time progresses, a decrease in intensity is observed. A self-trapped black beam is observed at 270s. ..16

Figure 1.6: Candidates for a polymerizable cross-linking agent.....18

Figure 3.1: Structure of TMEDA - phenyllithium dimer as determined by X-Ray diffraction. 37

Figure 3.2: Triplicate thermograms of the decomposition of polystyrene. 38

Figure 3.3: Triplicate thermograms of the decomposition of polystyrene functionalized with TMS. 39

Figure 3.4: Infrared spectra of a) TMS functionalized polystyrene; b) Polystyrene lab reference. 41

Figure 3.5: ^{1}H-NMR spectrum of a TMS functionalized polystyrene (DCM, 500MHz). 42

Figure 3.6: ^{13}C-NMR spectrum of a TMS functionalized polystyrene. 43

Figure 3.7: ^{1}H-^{13}C HMBC of polystyrene functionalized with TMS by direct lithiation. 44

Figure 3.8: ^{1}H-^{29}Si HMBC of polystyrene functionalized with TMS by direct lithiation. 44

Figure 4.1: Far IR spectra of Ph-$TeCl_3$. a) calculated for a single molecule; b) calculated for an SBI dimer forming the $[Te-Cl]_2$ supramolecular synthon; c) experimental. 51

Figure 4.2: Schematic representation of the organization of $PhTeCl_3$ molecules in the crystal. 52

Figure 4.3: Far IR spectra of $MesTeCl_3$. a) Calculated for a single molecule; b) calculated for a dimer; c) experimental. 54

Figure 4.4: Bonding motif of the dimer observed in the crystal of $SMesTeCl_3$. 55

Figure 4.5: Far IR spectra of RTeCl. a) Calculated for PhTeCl; b) experimental determination for SMesTeCl. The bands marked with a "*" are attributed to the trichloride present as an impurity. 56

Figure 4.6: Far-IR spectra of a polyethylene standard (top) and polyethylene dispersed with 40 (bottom). 58

Figure 5.1: ^{1}H NMR spectrum of the crude reaction mixture from the reaction in Scheme 5.3. 65

Figure 5.2: Powder diffraction pattern of Na_2Te. 66

Figure 5.3: ^{1}H NMR spectrum of 4-vinylbenzyl telluride. 70

Figure 5.4: ^{125}Te NMR spectrum of 4-vinylbenzyl telluride.....71

Figure 5.5: Mass spectrometric data of (bis)vinylbenzyl telluride, 55.72

Figure 5.6: Perspective view of the two components of the crystal structure of (bis)vinylbenzyl telluride with populations 46.6%:53.4% A:B. 75

Figure 5.7: Packing view of the "A" component perpendicular to (010)..75

Figure 5.8: Normal coordinate analysis of a C_{2v} idealized (bis)vinylbenzyl telluride. 76

Figure 5.9: Comparison of the experimentally determined (A) and geometry optimized structure (B) of (bis)vinylbenzyl telluride. 76

Figure 5.10: Stokes Raman spectrum of (bis)vinylbenzyl telluride (785nm). 78

Figure 5.11: UV-Visible spectra of (bis)vinylbenzyl telluride in hexanes. 79

Figure 5.12: NMR spectrum of 55 following attempted photolysis with 532nm light. 80

Figure 5.13: ^{1}H NMR spectrum of the product from the reaction of sodium telluride with vinylbenzyl chloride using a stoichiometric amount of 15-crown-5. 83

Figure 5.14: ^{125}Te NMR spectrum of the product from the reaction of sodium telluride with vinylbenzyl chloride using a stoichiometric amount of 15-crown-5. 84

Figure 6.1: *trans*-2,4-dibenzylidine-1,3-ditelluretan.....88

LIST OF SCHEMES

Scheme 1.1: Photocleaveage and recombination of polystannanes.....10

Scheme 1.2: Photo-dissociation of polymer cross-links.....17

Scheme 3.1: Functionalization of polystyrene with TMS.....36

Scheme 4.1: Stretch vibrations of a trichlorotellurane and their symmetries under the C_s point group.....49

Scheme 4.2: Synthesis of supermesityl ditelluride.....50

Scheme 4.3: Synthesis of supermesityltellurenyl(II) chloride and supermesityltellurium(IV) trichloride. 50

Scheme 4.4: Synthesis of phenyltellurium(IV) trichloride.....51

Scheme 5.1: Proposed synthesis of the polymerizable cross-linking agent **28**. 62

Scheme 5.2: Decomposition pathway of diorganyl ditellurides in the presence of alcohols. 62

Scheme 5.3: Synthesis of bis(methacryloyl)ditelluride.....64

Scheme 5.4: Synthesis of sodium telluride.....66

Scheme 5.5: Proposed syntheses of (bis)methacryloyl ditelluride and (bis)vinylbenzyl ditelluride from Na_2Te.....68

Scheme 5.6: Synthesis of (bis)vinylbenzyl telluride.....81

Scheme 5.7: Synthesis of sodium vinylbenzyl tellurolate.....81

Scheme 6.1: Synthesis of a trialkylsilyl protected organotellurium species through a (bis)trialkylsilyl telluride intermediate. ..86

Scheme 6.2: Synthesis of a trialkylsilyl protected organotellurium species through a sterically hindered trialkylsilyl tellurolate. 87

Scheme 6.3: Preparation of a 1,3-ditellurole.....88

LIST OF TABLES

Table 1.1: Molar refractivities $R_m/(cm^3mol^{-1})$ of common bonds and ions at 589nm. Data taken from reference 14

Table 3.1: Summarized thermogravimetric data for polystyrene and polystyrene functionalized with TMS. 40

Table 4.1: Experimental and calculated far-IR vibrations for the dimeric structure of $PhTeCl_3$. 53

Table 4.2: Experimental and calculated far-IR vibrations of the dimeric structure of $SMesTeCl_3$. 55

Table 4.3: Experimental and calculated far-IR vibrations of SMesTeCl..57

Table 4.4: Factor group splitting analysis of SMesPhTeCl.....58

Table 5.1: Experimental and calculated reflections of Na_2Te. 67

Table 5.2: Crystallographic information for (bis)vinylbenzyl telluride. 74

Table 5.3: Bond length comparison of the experimentally determined and geometry optimized structures. 77

Table 5.4: Bond Angle and torsion angle comparison of the experimentally determined and geometry optimized structures. 77

Table 5.5: Raman assignments based on the calculated frequencies.....78

LIST OF COMPOUNDS

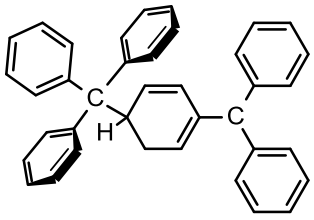

1

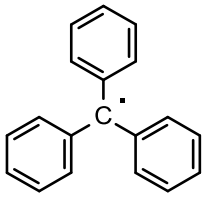

2

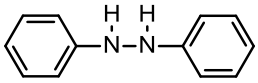

3

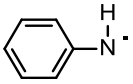

4

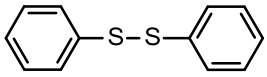

5

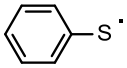

6

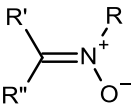

7

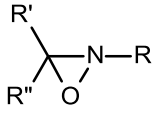

8

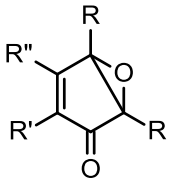

9

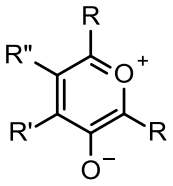

10

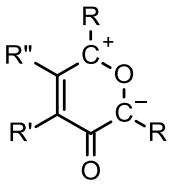

11

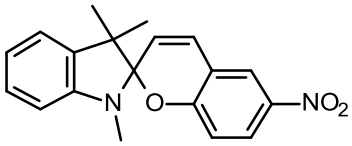

12

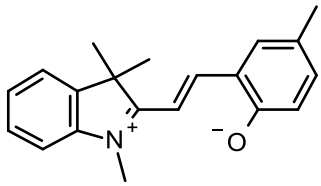

13

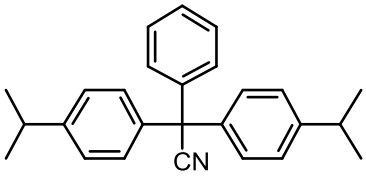

14

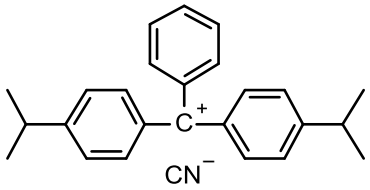

15

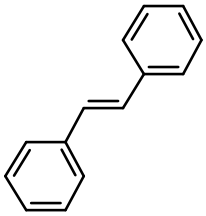

16

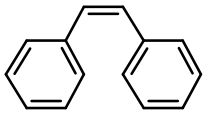

17

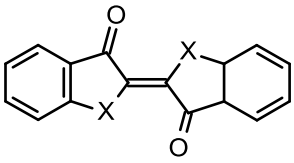

18

X = S, Se, O, N-R

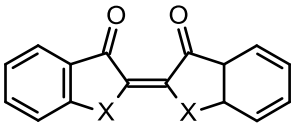

19

X = S, Se, O, N-R

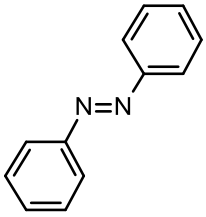

20

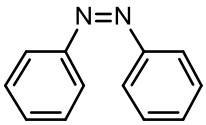

21

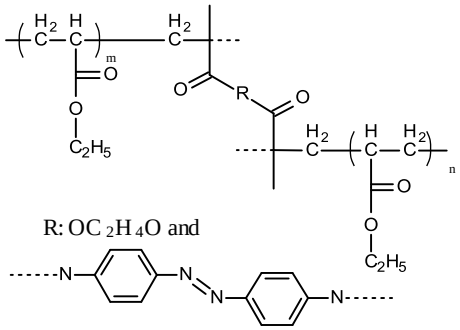

22

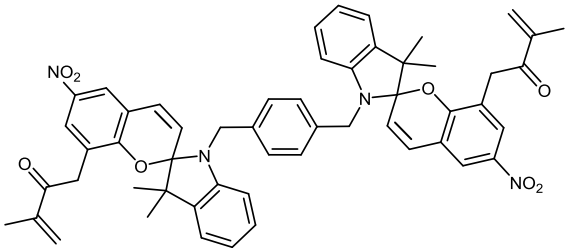

23

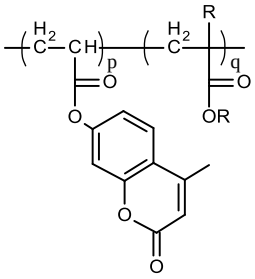

24

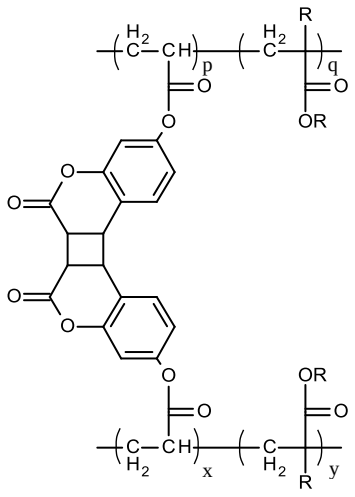

25

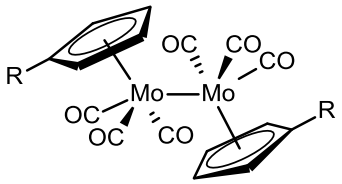

26

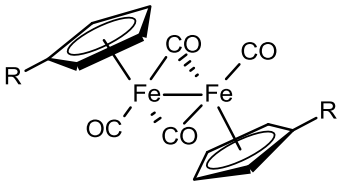

27

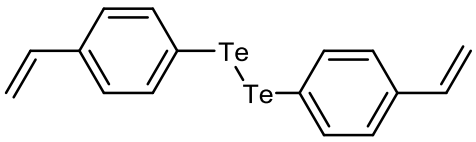

28

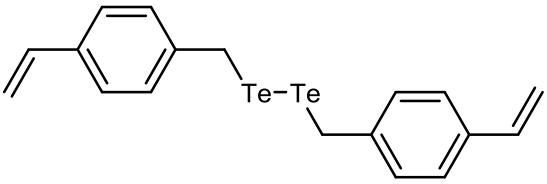

29

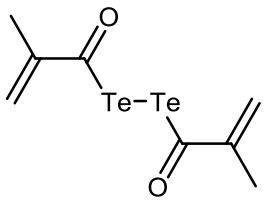

30

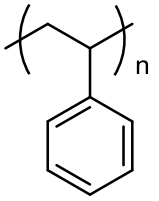

31

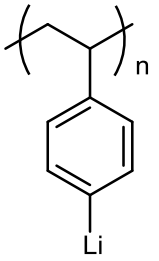

32

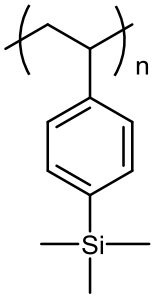

33

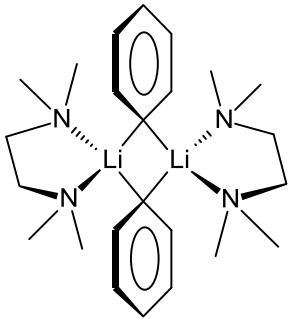

34

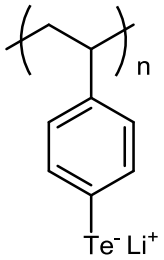

35

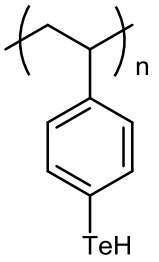

36

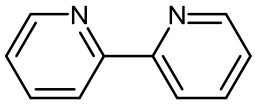

37

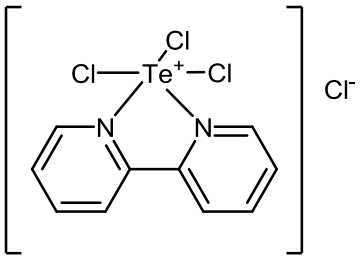

38

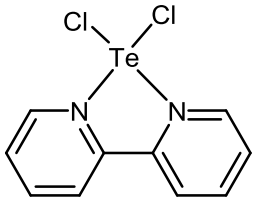

39

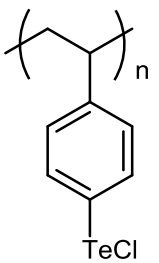

40

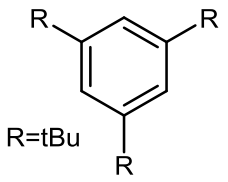

41

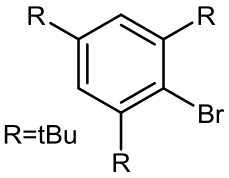

42

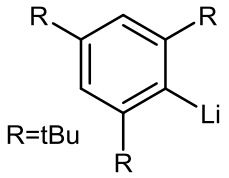

43

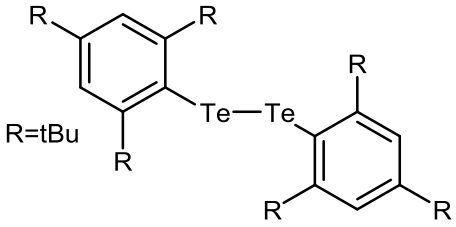

44

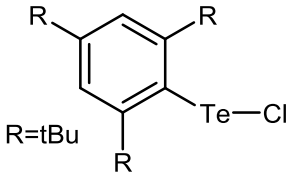

45

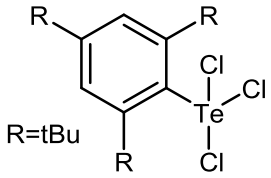

46

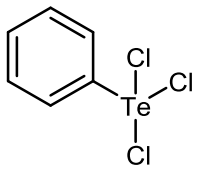

47

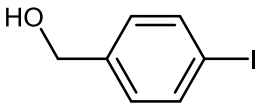

48

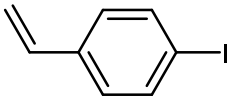

49

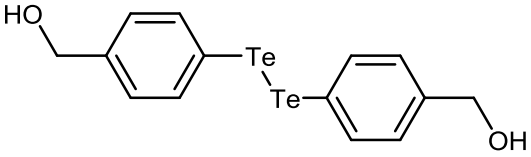

50

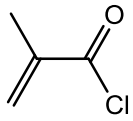

51

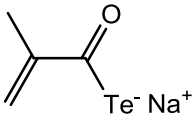

52

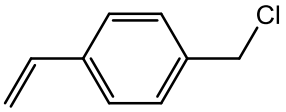

53

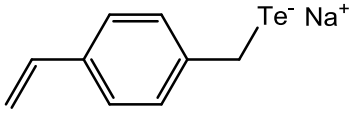

54

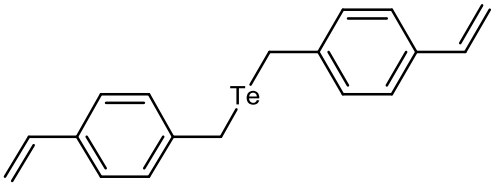

55

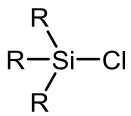

56

R = Me, tBu, Ph

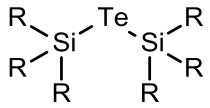

57

R = Me, tBu, Ph

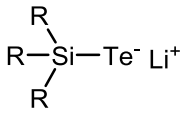

58

R = Me, tBu, Ph

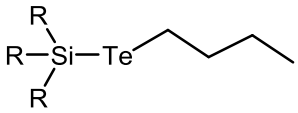

59

R = Me, tBu, Ph

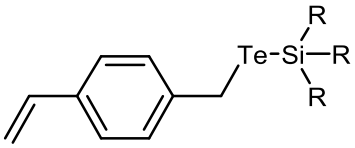

60

R = Me, tBu, Ph

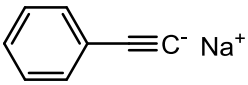

61

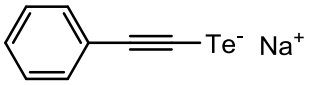

62

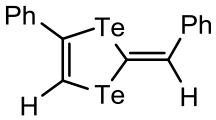

63

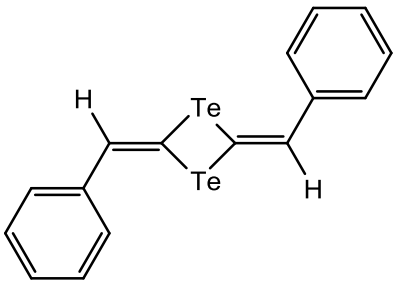

64

LIST OF ABBREVIATIONS AND SYMBOLS

α	Polarizability
Δ	Heat
δ	Chemical shift, ppm (parts per million)
ε	Dielectric permittivity in optics
ε	Extinction coefficient in UV-Visible spectroscopy
λ	Wavelength
μ	Magnetic permeability
ν	Frequency
ρ	Density
Å	Angstrom
a, b, c, α, β, γ	Unit cell parameters (in crystallography)
ACN	Acetonitrile
ADF	Amsterdam Density Functional software
c	Speed of light in vacuum
CCD	Charge-coupled device
cm^{-1}	Inverse centimetres (wavenumbers)
CSD	Cambridge structural database
DFT	Density functional theory
DMF	Dimethyl formamide
DMSO	Dimethyl sulphoxide
d	Doublet
d of d	Doublet of doublets
FT	Fourier transform
GUI	Graphical user interface

h	Planck's constant
HMBC	Heteronuclear multiple-bond coherence (pulse sequence)
IR	Infrared
m	Multiplet
M	Molar mass
Me	Methyl
n	Refractive index
N	Avogadro's number
n-Bu	Butyl
n-BuLi	n-butyllithium
nm	Nanometer
NMR	Nuclear magnetic resonance
P	Molar polarization
ppm	Parts per million
PW91	GGA exchange correlation functional, Perdew and Wang
R_1	Unweighted residual factor (in crystallography)
R_m	Molar refractivity
r_{vdW}	van der Waals radii
S	Singlet
SBI	Secondary bonding interaction
t	Triplet
T	Temperature
TGA	Thermogravimetric analysis
THF	Tetrahydrofuran

TMEDA	Tetramethylethylenediamine
TMS	Tetramethylsilane
TMS-Cl	Trimethylsilyl chloride
TOF	Time-of-flight (in mass spectrometry)
TZ2P	Triple-ζ with two polarization functions (basis set)
UV-Vis	Ultraviolet-visible (spectroscopy)
VT	Variable temperature (in NMR)
wR_2	Weighted residual factor (in crystallography)
Z	Molecules per unit cell (in crystallography)
ZORA	Zeroth-order regular approximation, in DFT calculations

1 Chapter 1: Introduction

1.1 Photoresponsive polymers.

Examples of the use of polymer photochemistry date back approximately 4000 years. Unknowingly, Ancient Egyptians made use of sunlight to photo-cross-link linens for mummification and the waterproofing of papyrus boats. Photoresponsive polymers describe a class of materials which undergo a change in their physical and/or chemical properties upon photo-irradiation. This includes changes in their conformation and shape, surface wettability, membrane potential, membrane permeability, pH, solubility, sol-gel transition temperature, and phase separation temperature of polymer blends.[1] These changes in refractive index can be induced by photo-isomerization and a change in bonding composition, and photo-cross-linking and photo-cleavage within polymer materials. In order to build photoresponsive polymers, we must consider molecules that can be incorporated into a polymer, and contain bonds that elicit a photochemical or conformational change. The following sections will outline the major classes of photoresponsive polymers; this field of chemistry is large, and the review is not intended to be comprehensive.

1.1.1 Photoresponsive organic materials.

1.1.1.1 Photo-isomerizable systems.

In the literature, there are several well-known examples of chromophores that undergo reversible isomerization upon photo-irradiation following the general process in Eq. 1.

$$A \underset{h\nu',\,\Delta}{\overset{h\nu}{\rightleftharpoons}} B \qquad (1)$$

This type of isomerization can change the physical or chemical properties of a material through a change in material composition, a geometric change, a change in dipole moment, and separation of charges. In many cases, the photo-isomerization is also photochromic.[2] This behaviour is known to arise in molecules that undergo homolytic cleavage, heterolytic cleavage, and *trans-cis* isomerization.

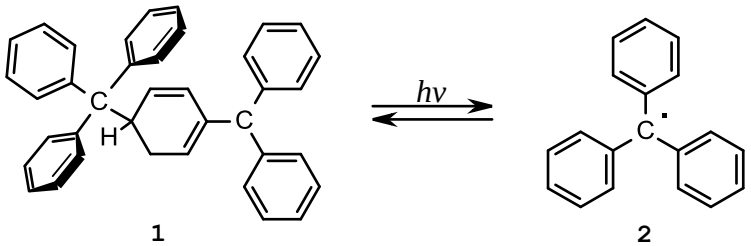

1 **2** (2)

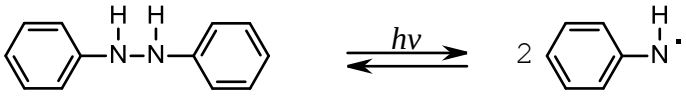

3 **4** (3)

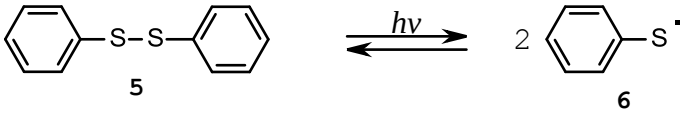

5 **6** (4)

Equations 2-4 illustrate photochromism by homolytic cleavage. The first example shows carbon-carbon bond cleavage in hexaarylethanes. Although little is known about the photochemical behaviour of this class of compounds, it has been shown that they undergo a photochemical transformation, resulting in a shift in the absorption spectrum, upon irradiation with a high-pressure mercury arc lamp.[3] 1,2-Diphenylhydrazine also undergoes homolytic cleavage upon irradiation with UV light. These experiments were conducted in alcoholic solution and no evidence of recombination of the radicals was reported.[4,5] The last example (Equation 4) shows the reversible photo-cleavage of diphenyl disulphide. This process is also known to be photochromic and typically occurs at wavelengths below 300nm.[6] 9.96 10.37

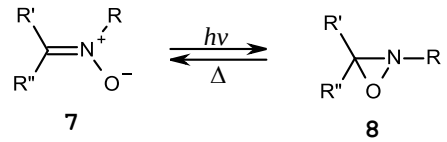

7 **8** (5)

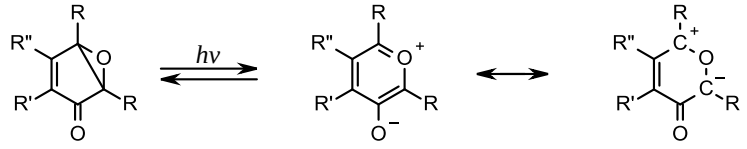

9 **10** **11** (6)

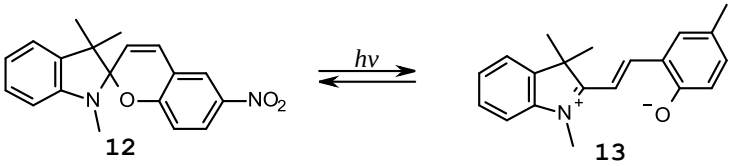

12 **13** (7)

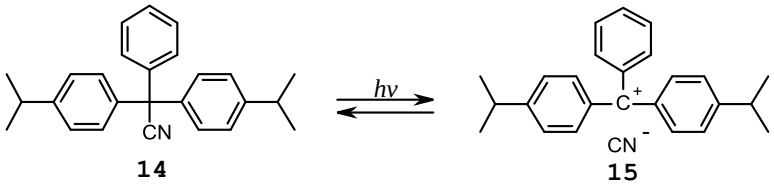

14 **15** (8)

Several examples exist of photoreversible heterolytic cleavage. A selection of these processes are presented in Equations 5-8 for nitrones, indenone oxides, spirobenzopyrans, and triarylmethanes. The photosensitivity of nitrones was first documented in 1910.[7] The oxazirane isomer **8**, however, was identified 55 years later in 1965. They are known to absorb strongly below 320 nm when they contain aryl functionals. The general isomerization of the nitrones is represented in the interconversion of **7** to **8**. Indenone oxides have been reported to isomerize with UV wavelengths to a red coloured species.[2] The process can be reversed with visible light. The zwitterionic pyrylium oxide **10** and **11** has been identified as the coloured isomer.[8,9] The spirobenzopyran and triarylmethane isomerizations will be discussed in detail in section 1.1.1.2 since their behaviour in polymer systems has been studied extensively.

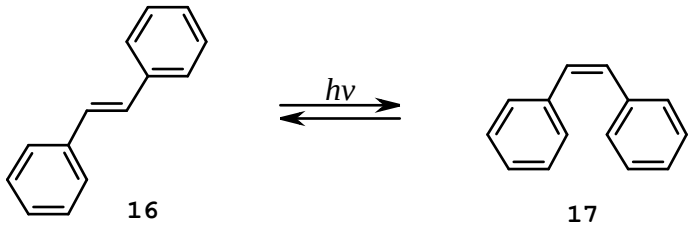

16 17 (9)

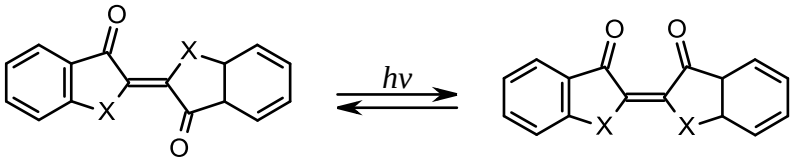

18 X = S, Se, O, N-R 19 (10)

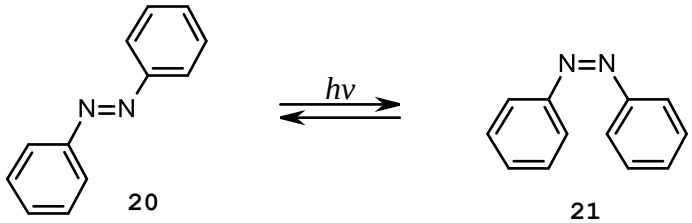

20 21 (11)

Trans-cis isomerization is known to involve photochromism. The examples shown in Equations 9-11 illustrate the general isomerization of stilbenes, indigoids, and azobenzenes. The *trans-cis* isomerization was discovered in 1946 upon exposure of *trans*-4,4'-diamidinostilbene to sunlight.[10] Based on the functionality, the conformational change caused by UV light can shift the absorption spectrum of stilbene into the visible region.[11] The indigoids are a set of versatile compounds which can be tuned to absorb in any region of the visible spectrum.[2] They are known to be photochromic in the cases outlined in Equation 10, however, indigo itself is not photo-isomerizable. It has been suggested that hydrogen bonding can prevent the *trans-cis* isomerization of the molecule.[12] Given the extensive research that has been done on

azobenzene functionalized polymers, the azobenze functional will be discussed in section 1.1.1.2.

1.1.1.2 Polymers containing photo-isomerizable substituents

Azobenzenes have been incorporated into polymer materials in the main chain, as components in copolymers, and as cross-linkers. Within the polymer matrix, the azobenzene functional groups can undergo a *trans-cis* isomerization upon irradiation with UV light ($410 > \lambda > 350$ nm).[13] This is shown schematically for the monomers in Equation 11 for the photo-isomerization of **20** to **21**. The resulting changes in the physical properties of a polymer functionalized with azobenzenes can include an increase in the maximum wavelength of absorption from 320nm ($\pi^* \leftarrow \pi$) to 440nm ($\pi^* \leftarrow n$), a change in polymer folding (due to a change in geometry), and a change in the dipole moment.[2,14]

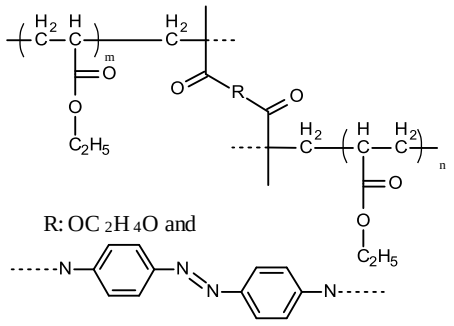

22

Figure 1.1: Example of an azobenzene cross-linked methacrylate.[15]

The photo-isomerization of **12** to **13** depicted in Equation 7 shows the photochemical change of spirobenzopyran upon irradiation with UV light. This chemical change results in the formation of highly coloured merocyanine species. Similar to the case of the azobenzenes, the

reverse process can be caused by irradiation with visible light.[16,17] The photochemical reaction in the spirobenzopyran drastically changes the physical properties of the molecule. This is manifested in a change in the absorption spectrum, dipole moment, and the refractive index.[18]

Spirobenzopyrans have been incorporated into polymer systems as cross-linkers through the addition of vinyl groups on the opposite ends of the molecule. Based on the expected change in refractive index between the chemical change in the spyrobenzopyran system, it should be possible to tune the refractive index of a polymeric material by irradiation with light of different wavelengths.

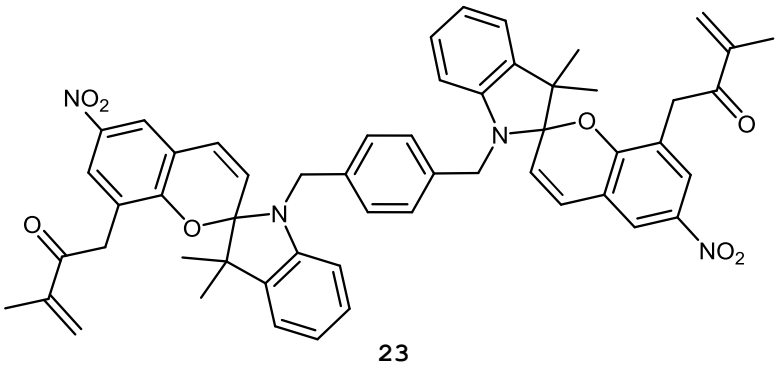

23

Figure 1.2: Example of a spirobenzopyran based cross-linking agent.

As with the monomeric spirobenzopyran species, a shift in the absorption spectrum to longer wavelengths (λ > 500m) has been observed in methacrylate polymer systems upon irradiation with UV light.[18]

Triarylmethane dyes are well-established photochromic molecules. As shown in Equation 8, irradiation of this type of molecule with UV light causes heterolytic dissociation from **14** to **15**. Unlike the above examples for the azobenzene and spirobenzopyran systems, which are incorporated into polymers by copolymerization, triarylmethanes are more commonly embedded into styrene based polymers through a method which is used to functionalize a preexisting polymer.[19]

Within the polymer matrix, the generation of positive charges following the photochemical transformation from **5** to **6** causes expansion of the polymer chains owing to electrostatic repulsion.[19] Much like the previous examples, the triarylmethane containing polymers are known to revert to their initial conformation when left in the dark.[20,21]

1.1.1.3 Photo-cross-linking and photo-cleavage.

Amongst the earliest synthetic investigations into photoresponsive polymers were material systems based on the [2+2] photo-cycloaddition of poly(vinyl cinnamate). The dimerization of the cinnamate functional groups resulted in the cross-linking of polymer chains. Similar examples of photo-induced cross-linking have been studied in anthracene, furan, and coumarin containing polymers. The coumarin functional group provides the unique advantage of a diverse range of derivatives, and is to date the only system of this type that undergoes photo-reversible cross-linking. These versatile chromophores have opened new avenues in the synthesis of electro-optical materials and photo-reversible polymer systems. Coumarin functionalized methacrylates have also shown varying degrees of substitution (between 1.2 and 30.4%).[1]

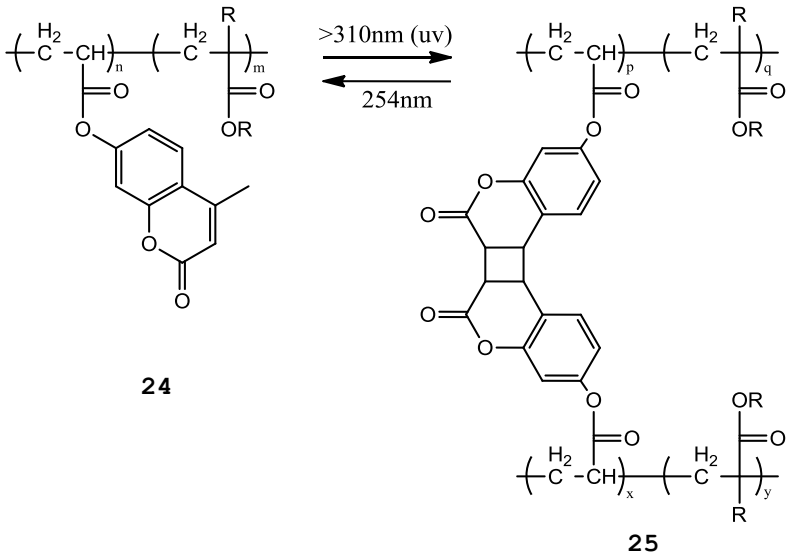

Figure 1.3: Photo-reversible coumarin cross-linking system.

1.1.2 Photoresponsive inorganic-based materials.

So far, this discussion has only considered organic-based photoresponsive systems. These systems have been observed to be both diverse and unique. Although some of the materials reviewed in the previous section are simple in terms of their synthesis, in many cases, their mechanism of photo-isomerization or photo-dissociation is complicated. This would make it difficult to predict the behaviour of these materials. The photo-dissociation pathways of the inorganic-based materials discussed in this section are much simpler.

1.1.2.1 Photocleavable heavy main-group polymers.

Some of the better studied systems of photoresposnive inorganic-based materials are those of the diorgano-polysilanes and diorgano-polystannanes. These materials consist of a repeating chain of Si-Si or Sn-Sn bonds as the backbone of a polymer. Interest in their development stems from the electronic properties of these polymers. Polysilanes

exhibit near-UV absorption due to σ-conjugation in the backbone of the polymers. These Si-Si bonds in the can be dissociated by photo-excitation. This property has made them useful for applications in lithography. They are also part of a new class of photo-conducting polymers. polysilanes absorb mostly in the UV. Their polystannane equivalents, however, absorb longer wavelengths of light.[22]

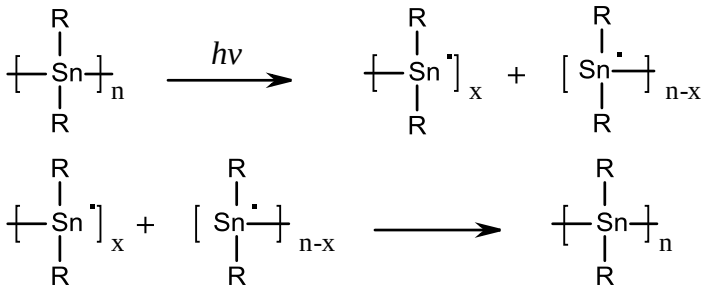

Scheme 1.1: Photocleaveage and recombination of polystannanes.[23]

One of the major drawbacks of working with these systems, however, is their instability. Polystannanes containing aromatic functional groups have shown photocleavage and recombination, and greater stability towards light than their analogous alkylated polymers.[23]

1.1.2.2 Photocleavable metal-metal bonds.

As with heavy main group elements, photosensitivity has been elicited in metal-metal bonds (λ≈500nm) of transition elements.[24] Dimers containing these metal-metal bonds are known to undergo homolytic cleavage upon irradiation with visible light. Examples of dimers which have shown this behaviour are presented in Figure 1.4.

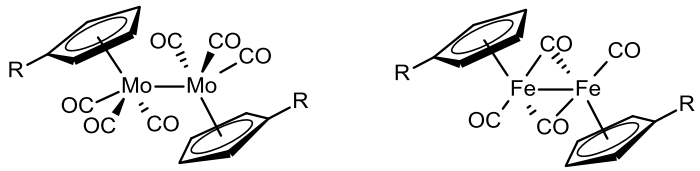

26 **27**

Figure 1.4: Photocleavable M-M dimers containing Mo and Fe.

These cyclopentadienyl (Cp) substituted dimers are particularly useful due to their ability to be functionalized with vinyl groups. However, it should be noted that synthesis of metal-metal dimers with substituted Cp rings is difficult due to the relatively weak metal-metal interaction ($BDE_{Mo-Mo} \approx 124 KJmol^{-1}$).[25,26,27] As a result, the Cp rings are substituted prior to coordinating the rings to the metals. This is done in order to circumvent exposure of the metal-metal bond to the conditions required to substitute the Cp rings.

Similarly to the cases of the spirobenzopyran, triarylmethane, and azobenzene systems, the photosensitivity of these metal-metal bonds is maintained when metal-metal dimers are incorporated into polymer systems. Typically, this is done through the radical polymerization of pendant vinyl functional groups attached to the Cp rings.[28] As with previous examples, these dimers can be incorporated into polymers in the backbone of a polymer chain, or as cross-linking agents. High molecular weight polymers can be difficult to synthesize, and are typically achieved by copolymerization.[29]

1.2 Chemical change and refractive index.

It has been shown that chemical changes in a photoresponsive material lead to changes in the microscopic refractive index. In order to understand these changes, fundamental background knowledge on the origins of refractive index is reviewed.

Refractive index, *n*, is the ratio of the speed of light in a material relative to its speed in vacuum[30] (Eq. 12).

$$n = c/v \tag{12}$$

Maxwell's equations lead to a relationship (Eq. 13) that describes refractive index in terms of the relative dielectric permittivity (ε) and magnetic permeability (μ) of a material. These parameters describe the response of a homogeneous medium to the application of an electric or magnetic field.

$$n^2 = \varepsilon \mu \tag{13}$$

Conventional optical materials have positive permittivity and permeability, resulting in a positive value for *n*.[30] Refractive index changes within a material are most commonly induced by either the electro-optic or Kerr effects or a physical or chemical change in the structure of the material. The change in the refractive index of a medium due to an applied electric field is called the electro-optic effect. This phenomenon can be observed in both liquids (e.g. CS_2) and noncentrosymmetric crystals (e.g. $SrBaNb_2O_6$).[31,32]

This process can be understood through the relationship between the refractive index and polarizability, α.[33] The net dipole moment per mole of a medium (molar polarization) is expressed in Eq. 14.

$$P = \frac{4\pi}{3} N\left(\alpha + \frac{\mu^2}{3kT}\right) \tag{14}$$

In this equation, $\mu^2/3kT$ represents the interaction of the permanent dipole moment of a medium with an external electric field. The polarizability, α, accounts for the induced dipole moment per molecule resulting from a temporary change in electron density in response to the external electric field. N represents Avogadro's number. The molar polarization is related to the dielectric constant (the electric permittivity at zero frequency) by the Clausius-Mosotti equation.[33]

$$\left(\frac{M}{\rho}\right)\left(\frac{\varepsilon - 1}{\varepsilon + 2}\right) = \frac{4\pi}{3} N\alpha \tag{15}$$

The permanent dipole term is neglected in Eq. 15 in order to better represent a medium unperturbed by an electric field. M represents molar mass and ρ represents density. Eq. 15 can then be related to the Maxwell equations in order to describe the relationship between the refractive index and α. This is known as the Lorenz-Lorentz equation (Eq. 16).

$$\left(\frac{M}{\rho}\right)\left(\frac{n^2 - 1}{n^2 + 2}\right) = \frac{4\pi}{3} N\alpha \tag{16}$$

The molar refractivity R_m, is then defined in Eq. 17.[34]

$$\left(\frac{M}{\rho}\right)\left(\frac{n^2-1}{n^2+2}\right)=R_m \qquad (17)$$

It is important to note that, to a first approximation, R_m is independent of temperature or physical state. More interestingly, for a large number of compounds, R_m is virtually additive for the atoms and bonds present on the molecular structure. With this information, it is possible to predict, with reasonable accuracy, the refractive index of a material based on its molecular structure. Consequently, a chemical change in a material would have a significant effect on the refractive index in polymer systems.

Table 1.1: Molar refractivities $R_m/(cm^3mol^{-1})$ of common bonds and ions at 589nm. Data taken from reference 35.

C-H	1.65	**Na^+**	0.46
C-C	1.20	**K^+**	2.12
C=C	2.79	**F^-**	2.65
C=O	3.34	**Cl^-**	9.30
S-S	16.05		

1.3 Objective of this project.

Refractive index changes within a material are most commonly induced by either the electro-optic or Kerr effects or a chemical change in the structure of the material. A convenient platform for the study of phenomena related to refractive index changes from a chemical change in a material is a siloxane matrix that contains photopolymerizable methacrylate substituents. These functional groups undergo

polymerization upon irradiation, which results in densification and an increase in the refractive index of the material.[36] In terms of the microscopic polarization, the polymerization would have created electronic interactions between local dipoles through the formation of bonds.

Studies of such materials have established that the initial polymerization rate is directly proportional to the intensity of light, and the positive refractive index changes are greatest in the most intense regions of irradiation. Since light propagates more efficiently in areas of higher refractive index, the light is trapped and the rate of refractive index change increases within these regions. There is competition between the confinement of light and its natural tendency to diverge. This gives rise to an effect known as self-trapping which results in highly localized regions in which light can propagate for long distances without diverging.[37] Related phenomena including moldulation instability and self-phase modulation have also been observed.[38,39,40] Since the photoinduced refractive index changes in the organosiloxane medium are permanent, microstructural changes induced by the self-trapped beam are discernible in optical and electronic micrographs.

The goal of this project is to synthesize, characterize, and examine the properties of a material, which undergoes a decrease in refractive index upon irradiation with visible light. We anticipate that this negative *change* in refractive index would lead to optical phenomena which would be different, yet related to the previously

mentioned self-trapping, and new microstructures. This could include the formation of self-trapped *dark beams*.

A prominent example of the self-trapping of *dark beams* was observed in strontium-barium niobate crystals by Chen and Segev in 1996. These are induced by the photorefractive effect when a laser beam containing a dark stripe, from a phase or amplitude discontinuity, is incident upon the crystal.[32] Self-trapped dark beams have also been observed in the photosiloxane medium through a positive change in refractive index by Kasala et al. in 2012.[41]

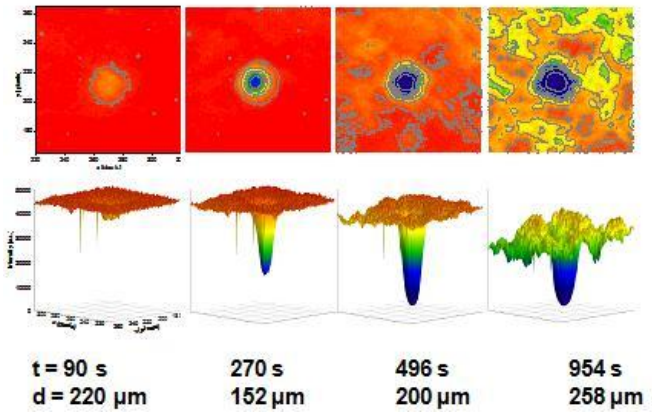

Figure 1.5: Intensity profiles over an area of the development of a self trapped dark beam. As time progresses, a decrease in intensity is observed. A self-trapped black beam is observed at 270s.[41]

While the self-trapped dark beam in the polysiloxane resulted from positive changes in refractive index, the objective of this project is to develop materials that undergo a negative change in refractive index upon exposure to light. An appropriate material for these investigations would be a polymer cross-linked by groups that can undergo dissociation by exposure to light. A negative change in refractive index would be

induced both by the dissociation of very polarizable bonds due to the relationship between polarizability and refractive index and expansion of the polymer matrix. Scheme 1.2 provides a graphical representation of the overall intended process. Given the detailed optical studies already carried out with a frequency doubled Nd-VO_4 laser (λ = 532 nm), ideally, the cross-links should be sensitive to green light.

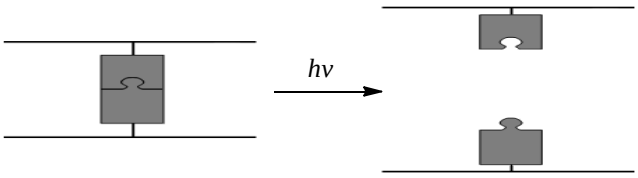

Scheme 1.2: Photo-dissociation of polymer cross-links.

1.4 Proposed Material

Of the materials outlined in the above sections, a good model for this project would be that of the metal-metal bond incorporated into a polymer. Based on the size of the atoms involved in the photo-dissociation, photo-cleavage of the Mo-Mo bond could potentially result in a large negative change in the refractive index of the material. However, the reactivity and relatively small bond dissociation energy ($BDE_{Mo-Mo} \approx 124 KJmol^{-1}$) of the molybdenum-molybdenum bond would make this chemistry challenging due to photosensitivity. Organo-ditellurides, molecules that contain a Te-Te bond, would be appropriate for the cross-link as their $\sigma^*_{Te-Te} \leftarrow n_{Te}$ transition usually absorbs between 400 and 500 nm and can lead to photo-dissociation of the chalcogen-chalcogen bond ($BDE_{Te-Te} \approx 227 KJmol^{-1}$).[42,43] The molar refractivity of the Te-Te bond is not reported, but the value for the S-S.[44] bond listed in Table 1.1, gives a good indication of the effect that the dissociation of ditelluride bonds

would have on the refractive index. The major advantage to studying ditellurides over the molybdenum-molybdenum bonds, is that their chemistry is well established, and many aryl ditellurides are air and moisture stable.

In order to incorporate such a cross-link during the synthesis of a polymer, the ditelluride should contain at each extreme a functional group capable of undergoing polymerization, such as pendant vinyl C=C bonds. Initial investigations would be based on styrenes and methacrylates, as their polymer chemistry is well understood. Figure 1.6 presents the cross-linking reagents discussed in this report.

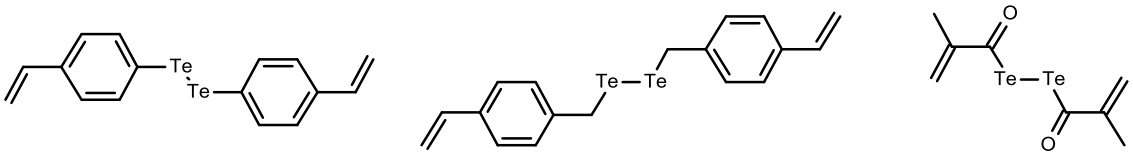

28 **29** **30**

Figure 1.6: Candidates for a polymerizable cross-linking agent.

An alternative approach would consist of the functionalization of an already-prepared polymer. Although such reactions are notoriously inefficient, a convenient method for the derivatization of polystyrene has been developed by Frechét.[45] The preparation of these ditelluride based materials would be strongly supported by spectroscopic characterization, including multinuclear NMR, vibrational spectroscopy (IR, Raman), and both single crystal and powder X-Ray diffraction in the case of the molecular cross-linking agents.

This thesis describes work done towards the direct functionalization of polystyrene with tellurium by various means and

outlines a method for the characterization of potential tellurium halide containing polymers by Far-IR spectroscopy. Attempted chemistry for the synthesis of a polymerizable cross-linking agent and future methods towards this goal are also explored. The chapter immediately following this introduction contains all experimental details. Chapter 3 presents studies of the direct functionalization of polystyrene. Chapter 4 covers work done towards the vibrational analysis of the Te-Cl functional group with the intention of characterizing materials synthesized in Chapter 3. Chapter 5 discusses work done towards the synthesis of polymerizable cross-linking agents. Finally, Chapter 6 presents conclusions and offers suggestions for future work.

2 Chapter 2: Experimental

2.1 Materials.

The manipulation of air sensitive materials was performed under an atmosphere of dry nitrogen using standard Schlenk and glove box techniques. All reagents were used as received unless otherwise specified: polystyrene (Aldrich) M_n = 170 KDa and M_w = 350 KDa (polydispersity 2.06), 2.5 M n-BuLi in hexanes (Acros Organics), ground elemental tellurium (Cerac), triphenyl antimony (III) (Aldrich), $TeCl_4$ (Alfa Aesar), and 2,2' bipyridine (Aldrich), phenylmercuric chloride (Aldrich), 1,3,5-tri-t-butylbenzene (Alfa Aesar), and SO_2Cl_2 (Aldrich), 4-iodobenzyl alcohol (Alfa Aesar), copper oxide nanopowder <50 nm (Aldrich), potassium hydroxide (Caledon), hydrazine monohydrate (Fisher Scientific), sodium hydroxide (Caledon), and 15-crown-5 (Alfa Aesar).

TMEDA (Aldrich) was distilled over CaH_2 (Aldrich), cyclohexane (Aldrich) was dried over potassium (BDH), and methylcyclohexane (Alfa Aesar) was dried over sodium. In the distillations of cyclohexane and methylcyclohexane, benzophenone (Lancaster) was used as an indicator for water and oxygen. Reagent grade diethyl ether (Caledon) was dried and deoxygenated through double distillation over sodium and benzophenone. Methacryloyl chloride (Aldrich), and vinylbenzyl chloride (Aldrich) were vacuum-distilled under an inert atmosphere of nitrogen prior to use.

Analytical grade solvents: THF (Caledon), acetonitrile (Caledon), methylene chloride (Caledon), and hexanes (Caledon) were purified with an Innovative Technology solvent purification system through columns of activated alumina to remove water and Cu_2O/alumina to remove oxygen.

2.2 Infrared Spectroscopy.

Samples were prepared in a glove box as compressed KBr or polyethylene pellets. Samples were transferred to the spectrometer under an atmosphere of nitrogen, and placed in a nitrogen purged sample casing. IR spectra were recorded at room temperature on a Nicolet 6700 spectrometer equipped with an Everglo or white light source. A solid-substrate beamsplitter and polyethylene windowed detector are used for far-IR at a resolution of 4 cm^{-1}. An extended range KBr window and doped triglycine sulfate (DTGS) detector are used for mid-IR. All spectra were obtained using 64 scans and processed with a multipoint baseline corrections using the GRAMS AI software package.

2.3 Raman Spectroscopy.

FT-Raman spectroscopy was done on air sensitive samples flame sealed in an NMR tube under an atmosphere of nitrogen. The samples were cooled to -160˚C with a stream of nitrogen to prevent thermal decomposition caused by the laser. Acquisition of these spectra was performed using a Bruker RFS 100 FT Raman spectrometer operating with a 1064nm Nd-YAG laser.

For acquisition using dispersive Raman spectroscopy, all samples were sealed in Pyrex melting point capillaries under an atmosphere of nitrogen. Dispersive spectra were acquired on a Renishaw inVia Raman microscope using the WiRE 3 software package at ambient temperature. The samples were irradiated with a 514.5nm argon-ion laser or a 785nm NIR diode laser, 30 mW, averaging 4 x 10 s scans. A multipoint baseline correction was applied to each spectrum.

2.4 NMR Spectroscopy.

A typical NMR sample was prepared by dissolving approximately 50 mg of material in 1 g of deuterated solvent. Measurements were done using a Bruker DRX (AVANCE) 500 (500.13 MHz), or AV 600 (600.13 MHz) spectrometer at ambient temperature or 298 K for high field acquisition. The DRX 500 is equipped with a 5 mm triple gradient broadband inverse probe used for ^{13}C, and ^{125}Te observation. An inverse triple resonance multinuclear (TBI-Z) probe was used for the acquisition of the ^{1}H spectra. The acquisition of all spectra was done by locking on the deuterium signal of the solvent on the AV 600. The ^{1}H and ^{13}C spectra were referenced to TMS (δ = 0, 298 K) using the deuterated solvent signals as secondary references. 128 scans were used for ^{1}H spectral acquisition, and 2048 scans for ^{13}C spectral acquisition and the data was processed with the Topspin software. ^{125}Te NMR experiments were performed on the 500 MHz instrument and referenced to an external standard of diphenyl ditelluride (δ = 423 ppm, 298 K based on the primary standard of dimethyl telluride).

2.5 Ultraviolet-Visible Absorption Spectroscopy.

Solutions of air sensitive compounds were prepared in volumetric glassware under an atmosphere of nitrogen in a glove box and transferred to air-free cuvettes for spectral acquisition. The absorption spectra were measured in quartz cuvettes on a Varian Cary 50 spectrometer. Samples were run in dual-beam mode by scanning from 200-800nm with a rate of 10 nm/s. The solvent background was subtracted automatically from external blank samples.

2.6 Electron Ionization Mass Spectrometry.

Pure crystals of a sample were flame sealed in melting point capillary tubes prior to introduction into the mass spectrometer via a probe inlet. The capillary tubes were opened immediately before acquisition. High-resolution electron-impact mass spectrometry experiments were obtained from a Waters/Micromass Q-TOF Ultima Global (ES TOF) Mass Spectrometer in probe mode. Samples were directly introduced into the ionization chamber on a melting point glass capillary tube mounted on a probe rod. The sample was heated to 200ºC for volatilization and fragmented by a 70eV electron stream. The resulting spectrum consisted of time averaged spectra corresponding to the maximized signal of the desired mass.

2.7 Single Crystal X-Ray Diffraction.

Samples were prepared under an atmosphere of nitrogen in a glove box where crystals were coated with Paratone-n oil and mounted onto borosilicate slides for selection. The crystals were mounted on nylon loops (Hampton, CA). Redundant data sets were collected on a P4 Bruker diffractometer with a Bruker SMART 1K CCD detector and a rotating anode using Mo-Kα radiation (λ=0.71073Å) from a sealed X-ray tube with a CCD area detector and an Oxford cryostream 700 low temperature accessory for acquisition at 173K. After data collection, the reciprocal lattice was visualized and integrated using the APEX2[46] software package. The final data set was obtained by refinement of the integrated reflections and absorption correction. The solution to the crystal structure was done by direct methods and refined by a full-matrix least squares on all F2 data with SHELX through a combination of the WinGX[47] and Olex2[48] software packages. All crystal structure refinement and modeling of disorder was

done using the WinGX software package. The atoms were refined anisotropically, and the H atoms were constrained to idealized positions. All images were produced using ORTEP-3[49] or POV-Ray[50].

2.8 Functionalization of polystyrene with TMS-Cl.

Following a literature procedure developed by Xue[51], A solution of polystyrene (1.0 g, 9.62 mmol) was dissolved in 25 mL of methylcyclohexane, mixed with TMEDA (1.5 mL, 9.62 mmol) was prepared in a side-arm round bottom flask fitted with a condenser. To this, n-BuLi (3.85 mL, 9.62 mmol) was added dropwise through a septum on the side arm of the flask. Following 2 hours of reflux, a black gel-like precipitate was observed. The solvent was decanted, and the polymer precipitate was redissolved in 20 mL of THF. TMS-Cl (1.2 mL, 9.62 mmol) was then added dropwise and left stirring overnight. A red mixture was observed in the flask the following morning. The product was obtained by precipitation into methanol followed by filtration. The compound was then purified by dissolution into THF and reprecipitation in methanol three times. 20.6% of the aromatic rings were functionalized based on the ^{1}H NMR spectrum. ^{1}H NMR (500.13 MHz, CD_2Cl_2, 5.32 ppm): δ = 0.20 ppm (s, 9H, CH_3), 1.48 (s, 2H, CH_2), 1.82 (s, 1H, CH), 6.60 (s, 2H, H_{aryl}), 7.08 (s, 3H, H_{aryl}). ^{13}C NMR (500.13 MHz, CD_2Cl_2, 54.00 ppm): δ = -0.71 ppm (s, 3C, CH_3), 41.16 (s, 1C, CH), 44.50 (m, 1C, CH_2), 126.21 (s, 1C, C_{aryl}), 128.50 (s, 4C, C_{aryl}), 131.27 (s, 2C, $C_{aryl,TMS}$), 133.66 (s, 2C, $C_{aryl,TMS}$), 137.60 (s, 1C, $C_{aryl,TMS}$), 139.72 (s, 1C, $C_{aryl,TMS}$), 145.89 (s, 1C, C_{aryl}).

2.9 Attempted synthesis of polystyrene functionalized with elemental tellurium.

A solution of polystyrene (1.00 g, 9.62 mmol) in 25 mL of methylcyclohexane, mixed with TMEDA (1.50 mL, 9.62 mmol) was prepared in a side-arm round bottom flask fitted with a condenser. To this, n-BuLi (3.85 mL, 9.62 mmol) was added dropwise through a septum on the side arm, and the reaction was left stirring from 4 to 6 hours. Elemental tellurium powder (1.23 g, 9.62 mmol) dispersed in THF was then added to the reaction mixture, and the reaction was left stirring for 16 hours. Unfortunately, the product of this synthesis was an intractable mixture.

2.10 Synthesis of [Te(bipy)Cl_2] 39.

$TeCl_4$ (1.00 g, 3.712 mmol) was reacted with 2,2' bipyridine (0.60 g, 3.8 mmol) in 5 mL of methylene chloride yielding [Te(bipy)Cl_3]Cl (1.40 g, 3.290 mmol). (1.00 g, 2.350 mmol) of this reagent was then reacted with a 10% excess of $SbPh_3$ (0.91 g, 2.585 mmol) in 5 mL of diethyl ether yielding the [Te(bipy)Cl_2] reagent (0.80 g, 2.255 mmol). The diethyl ether was removed by decanting, and the dark green product was washed three times with clean diethyl ether. ^{1}H and ^{13}C NMR spectra could not be acquired due to the rapid decomposition of the compound in solution.

2.11 Attempted synthesis of the tellurated polymer using [Te(bipy)Cl_2].

A solution of polystyrene (1.00 g, 9.62 mmol) in 25 mL of methylcyclohexane, mixed with TMEDA (1.50 mL, 9.62 mmol) was prepared in a side-arm round bottom flask fitted with a condenser. To this, n-BuLi (3.85 mL, 9.62 mmol) was added dropwise through a septum on the side arm, and the reaction was left stirring from 4 to 6 hours.

[Te(bipy)Cl_2] (3.5 g, 9.62 mmol) was dissolved in 5 mL of THF and the slurry was added to the reaction mixture at this point, and the reaction was left stirring for 16 hours. The reaction products were washed with DCM and hexanes for far-IR characterization.

2.12 Test reaction of the "one-pot ditelluride synthesis" from 2-iodotoluene.

Following a procedure published by Singh[52]; to a stirred solution of elemental tellurium powder (0.436 g, 2.0 mmol) and 2-iodotoluene (0.127 mL, 1.0 mmol) in 2 mL of dry DMSO, was added 50 nm CuO nanoparticles (0.00795 mg, 10 mol%) and KOH (0.112g, 2.0mmol). The reaction was set to 90˚C and left stirring overnight. The DMSO was removed by distillation under vacuum, and the orange-red product was characterized by GC-MS. LRMS (EI): *m/z* Found: 437.9, Calculated 437.9.

2.13 Attempted synthesis of [4-[[[4-(hydroxymethyl)phenyl] methylditellanyl]methyl]phenyl]methanol.

To a stirred solution of elemental tellurium powder (0.436 g, 2.0 mmol) and 10 (0.234 g, 1.0 mmol) in 2 mL of dry DMSO, was added CuO nanoparticles (0.00795 mg, 10 mol%) and KOH (0.112 g, 2.0 mmol). The reaction was set to 90˚C and left stirring overnight. This reaction was repeated several times due to difficulty encountered in the isolation and purification of the product. The DMSO was removed by distillation under vacuum, and purification of the orange-red product was attempted by sublimation or Soxhlet extraction with methylene chloride. ^{1}H NMR (500.13 MHz, Acetone-d6, 2.04 ppm): δ = 2.82 ppm (s), 4.22 (t, 2H, OH), 4.62 (d, 4H, CH_2), 7.25 (d, 4H, H_{aryl}), 7.66 (d, 4H, H_{aryl}). ^{125}Te NMR: δ = 667.05 ppm (s).

2.14 Synthesis of 4-iodostyrene.

Following a method developed by McNulty[53], 4-iodobenzyl alcohol (1.0 g, 4 mmol) was reacted with triethylphosphine hydrobromide (0.851 g, 4 mmol) for 24 hours at 110˚C under a continuous flow of nitrogen. The phosphonium salt was characterized by ^{31}P NMR and then reacted with aqueous formalin in basic medium in a microwave reactor at 100˚C for 30 minutes. The product of this reaction was isolated by liquid-liquid extraction into pentane, and passed through a plug of silica. The solvent was removed yielding pure 4-iodostyrene in 92% yield. ^{1}H NMR (200.13 MHz, CD_2Cl_2, 5.32 ppm): δ = 5.31 ppm (d of d, 1H, H_{vinyl}), 5.80 (d of d, 1H, H_{vinyl}), 6.68 (d of d, 1H, H_{vinyl}), 7.20 (d, 2H, H_{aryl}), 7.69 (d, 2H, H_{aryl}).

2.15 Attempted synthesis of 1-vinyl-4-[[(4-vinylphenyl)methyl ditellanyl]methyl]benzene starting from 4-iodostyrene.

To a stirred solution of elemental tellurium powder (0.436 g, 2.0 mmol) and 4-iodostyrene (0.227 g, 1.0 mmol) in 2 mL of dry DMSO, was added CuO nanoparticles (0.00795 mg, 10 mol%) and KOH (0.112 g, 2.0 mmol). The reaction was set to 90˚C and left stirring overnight. The following morning, the reaction mixture was centrifuged, and the supernatant was decanted and gravity filtered. The brown solution decomposed rapidly giving elemental tellurium and a pale yellow DMSO solution. The product could not be isolated for characterization.

2.16 Attempted synthesis of Te-(2-methylprop-2-enoyltellanyl)2-methylprop-2-enetelluroate from in situ generated sodium ditelluride.

Following a method developed by Klapoetke[54], to a mixture of powdered elemental tellurium (6.4 g, 50 mmol) and powdered NaOH (3.0 g,

75 mmol) in 30 mL of dry DMF, $N_2H_4 \bullet H_2O$ (0.625 g, 12.5 mmol) was added dropwise over the period of an hour through a dropping funnel. The reaction mixture was left stirring at room temperature for six hours. The reaction mixture gradually became viscous and purple. A 30% excess of methacryloyl chloride was then added slowly through the dropping funnel, and the reaction was left stirring overnight. During the addition of the acid chloride, HCl gas is generated due to the water generated as a byproduct in the synthesis of the sodium ditelluride in situ. The next morning, a black mixture was observed in the reaction vessel. This is due to the presence of elemental tellurium. The reaction mixture was gravity filtered into a round bottom flask immersed in a cooling bath at -78˚C to prevent decomposition. The yellow solution was characterized by ^{1}H-NMR revealing a mixture of products. This mixture could not be purified due to rapid decomposition and extrusion of elemental tellurium.

2.17 Synthesis of Na_2Te.

Using a procedure developed by Thiele[55], to a flask charged with rolled elemental sodium (0.60 g, 26.099 mmol) and powdered elemental tellurium (1.66 g, 13.055 mmol) was added a solution of 150 mg of sublimed naphthalene in 20 mL of dimethoxyethane. The reaction mixture turned blue within an hour, then green, and finally yellow over the course of 10 hours. The reaction was left stirring at room temperature overnight. The following day the reaction was filtered through a coarse frit. 2.25 g of a white solid was collected (99% yield). Powder diffraction (CoK_α = 1.7902): 24.62°, 28.54°, 40.70°, 48.04°, 50.74°, 58.30°, 64.82°, 66.70°, 74.16°, 78.94°, 87.86°, 92.64°, 95.14°, 101.48°, 105.94°, 108.78°.

2.18 Attempted synthesis of sodium 2-methylprop-2-enetelluroate 52.

Methacryloyl chloride (0.100 mL, 1.023 mmol) was reacted with Na_2Te (178 mg, 1.023 mmol) dispersed in 2 mL of dry and degassed acetonitrile. The reaction was allowed to proceed for four hours, at which point the mixture was centrifuged and decanted into a Schlenk tube. The product appeared to decompose, extruding elemental tellurium in the environment of the glovebox. The solvent was then removed at reduced pressure into a secondary trap through an external connection. After removal of the solvent, a yellow glass was left in the flask. ^1H NMR of the crude reaction mixture revealed a mixture of products. ^1H NMR (500.13 MHz, CD_3CN, 1.93 ppm): δ = 1.29 ppm (s), 1.46 (s), 1.65 (s), 1.87-2.06 (multiple resonances), 2.89 (s), 3.59 (s), 3.92 (s), 5.71-5.73 (multiple resonances), 5.88-5.98 (multiple resonances), 6.13-6.17 (multiple resonances).

2.19 Attempted synthesis of sodium (4-vinylphenyl)methanetellurolate 54.

4-vinylbenzyl chloride (0.100 mL, 0.709 mmol) was reacted with Na_2Te (210 mg, 1.209 mmol) dispersed in 2 mL of dry and degassed acetonitrile. The reaction was allowed to proceed for four hours in a dewar with cold copper sand at -10˚C. The mixture was then centrifuged and decanted into a Schlenk tube. The solvent was then removed at reduced pressure into a secondary trap through a connection to the glovebox. Following the removal of the solvent, brown crystals were observed in the flask. The ^1H NMR spectrum revealed (bis)vinylbenzyl telluride as the product. ^1H NMR (500.13 MHz, CD_3CN, 1.94 ppm): δ = 4.03 ppm (s, 4H, CH_2), 5.20 (d of d, 2H, H_{vinyl}), 5.75 (d of d, 2H, H_{vinyl}), 6.71

(d of d, 2H, H_{vinyl}), 7.18 (d, 4H, H_{aryl}), 7.32 (d, 4H, H_{aryl}). ^{125}Te NMR: δ = 640.85 ppm (s).

2.20 Preparation of (bis)vinylbenzyl telluride.

4-vinylbenzyl chloride (0.200 mL, 1.419 mmol) was reacted with Na_2Te (246 mg, 1.419 mmol) dispersed in 5 mL of dry and degassed acetonitrile. The reaction was allowed to proceed overnight under an inert atmosphere of either nitrogen or argon at room temperature. The mixture was then filtered through a glass frit separating NaCl and unreacted Na_2Te from the brown reaction solution. Dry and degassed hexanes (5x5 mL) was then used to extract the yellow product from the reaction mixture. The solvent was then removed at reduced pressure into a secondary trap. Following the removal of the solvent, a concentrated solution of the yellow product was prepared in hexanes. Yellow crystals were grown from this solution at -30ºC overnight and used for spectroscopic and X-ray characterization. M.P.: 44-48 ºC, decomposition noted between 70 and 110 ºC. ^{1}H NMR (500.13 MHz, CD_3CN, 1.94 ppm): δ = 4.03 ppm (s, 4H, CH_2), 5.20 (d of d, 2H, H_{vinyl}), 5.75 (d of d, 2H, H_{vinyl}), 6.71 (d of d, 2H, H_{vinyl}), 7.18 (d, 4H, H_{aryl}), 7.32 (d, 4H, H_{aryl}). ^{125}Te NMR: δ = 640.85 ppm (s). UV (hexanes): λ_{max} = 258 nm, ε = 3342 cm^2/mol. Raman (cm^{-1}): 1626(s) ($C{=}C_{vinyl}$), 556(s) (ν_s, C-Te-C), 531(w) (ν_{as}, C-Te-C), 213(w) (δ, C-Te-C). HRMS (EI): *m/z* Found: 364.0484, Calculated 364.0472.

2.21 Attempted synthesis of sodium (4-vinylphenyl)methane tellurolate with a catalytic amount of 15-crown-5.

4-vinylbenzyl chloride (0.200 mL, 1.419 mmol) was reacted with Na_2Te (246mg, 1.419mmol) and a catalytic amount of 15-crown-5 (0.0156

mg, 5 mol%) in 5 mL of dry and degassed acetonitrile. The reaction was allowed to proceed overnight under an inert atmosphere of argon at room temperature. The mixture was then filtered through a glass frit separating NaCl and unreacted Na_2Te from the red reaction solution. The solvent was then removed at reduced pressure into a secondary trap. Following the removal of the solvent, the crude product was analyzed by ^1H NMR spectroscopy. The major components of the ^1H NMR spectrum revealed a 3:1 mixture of (bis)vinylbenzyl telluride and a second tellurium containing product. ^1H NMR (500.13 MHz, CD_3CN, 1.94 ppm): δ = 3.58 ppm (s, $CH_{2\text{crownn ether}}$), 4.02 (s, 4H, CH_2), 4.11 (s, 2H, CH_2) 5.16 (d of d, 1H, H_{vinyl}), 5.20 (d of d, 2H, H_{vinyl}), 5.71 (d of d, 1H, H_{vinyl}), 5.74 (d of d, 2H, H_{vinyl}), 6.67 (d of d, 1H, H_{vinyl}), 6.70 (d of d, 2H, H_{vinyl}), 7.19 (d, 4H, H_{aryl}), 7.23 (d, 2H, H_{aryl}), 7.27 (d, 2H, H_{aryl}) 7.31 (d, 4H, H_{aryl}). ^{125}Te NMR: δ = 640.85 ppm (s).

2.22 Attempted synthesis of sodium (4-vinylphenyl)methane tellurolate with a stoichiometric amount of 15-crown-5.

4-vinylbenzyl chloride (0.100 mL, 0.710 mmol) was reacted with Na_2Te (123 mg, 0.710 mmol) and a stoichiometric amount of 15-crown-5 (0.280 mL, 1.419 mmol) in 5 mL of dry and degassed acetonitrile. The reaction was allowed to proceed overnight under an atmosphere of argon at room temperature. The mixture was then filtered through a glass frit separating NaCl and unreacted Na_2Te from the red reaction solution. The solvent was then removed at reduced pressure into a secondary trap. Following the removal of the solvent, the crude red product was analyzed by ^1H NMR and ^{125}Te NMR spectroscopy. The ^1H NMR spectrum revealed two major products in an approximate 2:1 ratio. Product a: ^1H NMR (500.13

MHz, CD_3CN, 1.94 ppm): δ = 3.52 ppm (s, $CH_{2\ crown\ ether}$), 3.98 (s, 4H, CH_2), 5.15 (d of d, 1H, H_{vinyl}), 5.70 (d of d, 1H, H_{vinyl}), 6.63 (d of d, 1H, H_{vinyl}), 7.13 (d, 2H, H_{aryl}), 7.20 (d, 2H, H_{aryl}), 7.22 (d, 2H, H_{aryl}). Product b: 5.16 (d of d, 1H, H_{vinyl}), 5.74 (d of d, 1H, H_{vinyl}), 6.68 (d of d, 1H, H_{vinyl}) 7.13 (d, 2H, H_{aryl}), 7.32 (d, 2H, H_{aryl}). ^{125}Te NMR: δ = 16.99 ppm (s), 23.12 (s_{broad}).

2.23 Bromination of 1,3,5-tri-tert-butylbenzene.

Following a procedure developed by Pearson,[56] elemental bromine (5.00 g, 0.0314 mol) dissolved in 25 mL of triethylphosphate was mixed in a round bottom flask with 1,3,5-tri-tert-butylbenzene (5.00 g, 0.0203 mol) in 25 mL of triethylphosphate. Due to the continuous flow of nitrogen, the elemental bromine would dissipate over time. After one week, the initial dark orange colour had faded to a pale orange. NMR analysis of the sample revealed 20% of conversion. Another 10 g of bromine was added over the course of a second week resulting in 65% transformation. The solvent was removed at 100 mTorr and 65˚C. The white solid residue was then recrystallized from ethanol yielding 2.47 g, 33% yield of crystalline 2,4,6-tri-tertbutylbromobenzene. ^{1}H NMR (500.13 MHz, CD_2Cl_2, 5.32 ppm): δ = 1.32 ppm (s, 9H, CH_3), 1.59 (s, 18H, CH_3), 7.43 (s, 2H, H_{aryl}).

2.24 Synthesis of (bis)supermesitylditelluride.

Following a preparation by Lange[57], 2,4,6-tri-tertbutylbromobenzene (0.500 g, 1.525 mmol) was dissolved in a solution of 1 mL of dry THF and 5 mL of dry hexanes at -78˚C. To this solution, 2.5M n-BuLi in hexane (0.8 mL, 2 mmol) was added dropwise. The reaction was allowed to proceed for four hours, at which time the

solvent was removed under vacuum into a secondary trap at 0˚C over the course of one hour to ensure the removal of the bromobutane side product. The isolated white organolithium salt was then redissolved in 5 mL of toluene. This solution was transferred by cannula into a sidearm schlenk flask charged with powdered elemental tellurium (200 mg, 1.525 mmol). This reaction was allowed to proceed for 4 hours between -20˚C and 0˚C, during which time the reaction mixture turned a light green. After most of the tellurium was consumed, elemental oxygen was bubbled for 20 minutes turning the reaction a deep red. The contents of the flask were gravity filtered, and the solvent was removed by rotary evaporation. The red solid was isolated and recrystallized from THF yielding a dark red microcrystalline solid. ^{1}H NMR (500.13 MHz, CD_2Cl_2, 5.32 ppm): δ = 1.29 ppm (s, 9H, CH_3), 1.36 (s, 18H, CH_3), 7.24 (s, 2H, H_{aryl}).

2.25 Synthesis of phenyltellurium(IV) trichloride 47.

Using a preparation by Farrar[58], phenyl-mercuric chloride (3.00g, 9.58mmol) was refluxed under an atmosphere of nitrogen for one hour in 20 mL of dry dioxane. After one hour, the reaction was cooled to room temperature. The addition compound of dioxane and mercuric chloride precipitated as white plates from the reaction mixture, and were filtered off. The solvent was removed, and the residue was recrystallized from tetrachloroethane yielding 1.87 g (63%) of a beige crystalline solid. Mp. 207-212 ˚C, IR (cm^{-1}): 453(s), 337(s), 320(s), 310(s), 255(s), 251(s).

2.26 Synthesis of 2,4,6-tri-tert-butylphenyltellurenyl(II) chloride 45.

Using a preparation by Beckmann[59], SO_2Cl_2(0.018 g, 0.134 mmol) was added to a solution of (bis)supermesitylditelluride (100 mg, 0.134 mmol) in 6 mL of dry diethyl ether in an inert amosphere. A dark blue colour was observed almost immediately, and the reaction was allowed to stir for two hours. The ^1H NMR spectrum of the crude product was obtained. The solution was concentrated, and the Schlenk flask was stored in the freezer of a dry box for crystallization. Dark blue plates were observed two days later and prepared for far-IR characterization. IR (cm^{-1}): 393(w, br), 312(s), 247(s), 174(w). ^1H NMR (500.13 MHz, CD_2Cl_2, 5.32 ppm): δ = 1.34 ppm (s, 9H, CH_3), 1.71 (s, 18H, CH_3), 7.62 (s, 2H, H_{aryl})

2.27 Synthesis of 2,4,6-tri-tert-butylphenyltellurium(IV) trichloride 46.

SO_2Cl_2(0.054 g, 0.402 mmol) was added to a solution of (bis)supermesitylditelluride (100 mg, 0.134 mmol) in 6 mL of dry diethyl ether in an inert atmosphere. A bright yellow colour was observed almost immediately, and the reaction was allowed to stir for two hours. The ^1H NMR spectrum of the crude product was obtained. The solution was concentrated, and the Schlenk flask was stored in the freezer of a dry box for crystallization. Bright yellow prisms were observed two days later and prepared for far-IR characterization. IR (cm^{-1}): 357(m), 271 (s, shoulder), 258(s), 181(m) 164(m). ^1H NMR (500.13 MHz, CD_2Cl_2, 5.32 ppm): δ = 1.32 ppm (s, 9H, CH_3), 1.35 (s, 18H, CH_3), 7.25 (s, 2H, H_{aryl}).

2.28 Computational Details.

The structures studied computationally were optimized using the ADF DFT software package.[60,61] Calculations of model geometries were gradient-corrected with the exchange and correlation functionals of the gradient correction proposed in 1991 by Perdew and Wang (PW91).[62,63] Geometry optimizations were conducted using a triple-ζ all-electron basis set with two sets of polarization functions (TZ2P) applying the Zeroth Order Relativistic Approximation (ZORA[64]). Visualization of the computational results was done with the ADF native GUI (SCM), Mercury CSD 2.0[65], or Olex2[48].

3 Chapter 3: Direct Functionalization of Polystyrene with n-BuLi and TMEDA.

3.1 Introduction.

Two synthetic pathways reported in the literature were considered for the telluration of polystyrene. The first involves the synthesis of *para*-brominated polystyrene by the addition of bromine to a solution of TMEDA and polystyrene in methylcyclohexane. The para-brominated polystyrene would then be treated with n-BuLi to produce *para*-aryl lithium groups pendant from the backbone of the polymer. The second considers the direct lithiation of polystyrene with n-BuLi and TMEDA. Various functional groups could then be used to substitute the lithiated polystyrene. This method was developed by Fréchet and was chosen over the first route as it is reportedly more efficient.[45] This technique was tested with the introduction of S-H groups on the aromatic rings, but the extent of functionalization was not conclusively established. Instead, the efficiency of derivatization of the polymer was tested by introducing trimethylsilyl (TMS) groups, which provide a convenient NMR label.

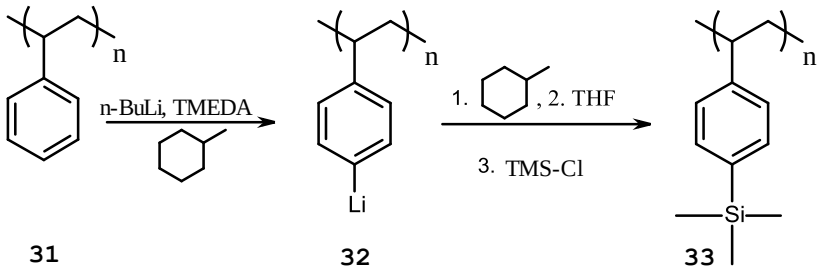

Scheme 3.1: Functionalization of polystyrene with TMS.

3.2 Functionalization of polystyrene with TMS.

This experiment was based on the Xue method depicted in Scheme 3.1. Polystyrene (Mn = 170,000, Mw = 350,000) was treated with n-butyllithium and TMEDA in methylcyclohexane in 1:1 stoichiometry, within four to six hours a dark brown gel separated.[51] The gel-like precipitate is the lithiated polymer and is likely crossslinked by aryl-lithium pairs bridged by molecules of tmeda as it is observed in the dimeric structure of phenyllithium Figure 3.1.[66] The gel was suspended in THF and TMS-Cl was added. After stirring overnight the product, **33**, was precipitated from its THF solution using methanol. The product was purified by cycles of dissolution in THF and precipitation with methanol. The beige solid was characterized by ^{1}H NMR, ^{13}C NMR, and ^{1}H-^{13}C and ^{1}H-^{29}Si HMBC.

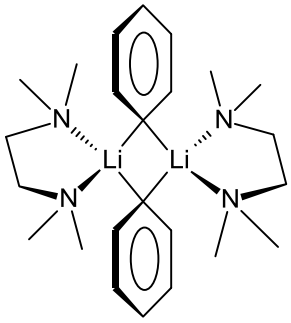

34

Figure 3.1: Structure of TMEDA - phenyllithium dimer as determined by X-Ray diffraction.

The ^{1}H-NMR spectrum shows the presence of the shielded TMS protons centred at 0.20 ppm in addition to the resonances of the aromatic rings and aliphatic polymer backbone. The complete assignments are shown in Figure 3.5. The extent of the functionalization of polystyrene was evaluated by comparing the ratio of the integrations of the resonances

of the TMS group and the aromatic protons. While the quotient would be 9/4 = 2.25 for fully derivatized polystyrene, the experimental value was 0.79/1.71 = 0.46 based on the assigned integrations; this translates into functionalization of 20.7% of the aromatic rings. Thermogravimetric analysis was done in an attempt to verify the extent of the functionalization of the aromatic rings.

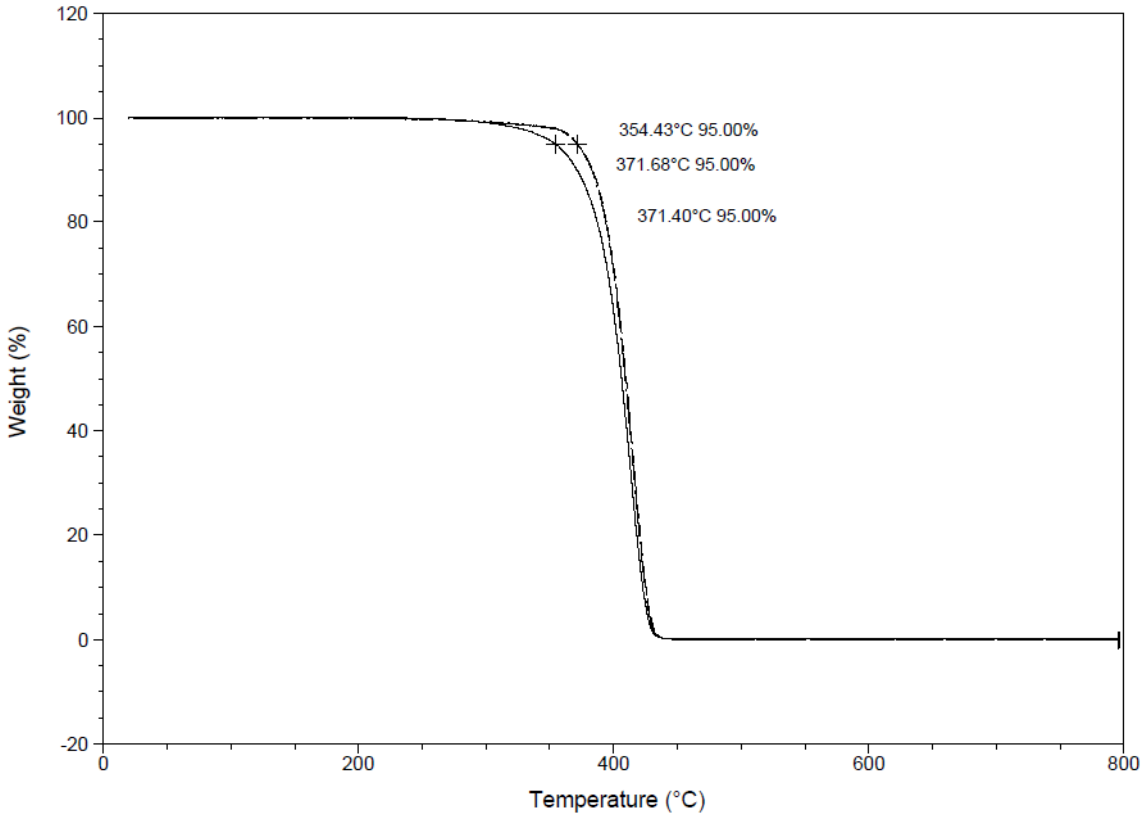

Figure 3.2: Triplicate thermograms of the decomposition of polystyrene.

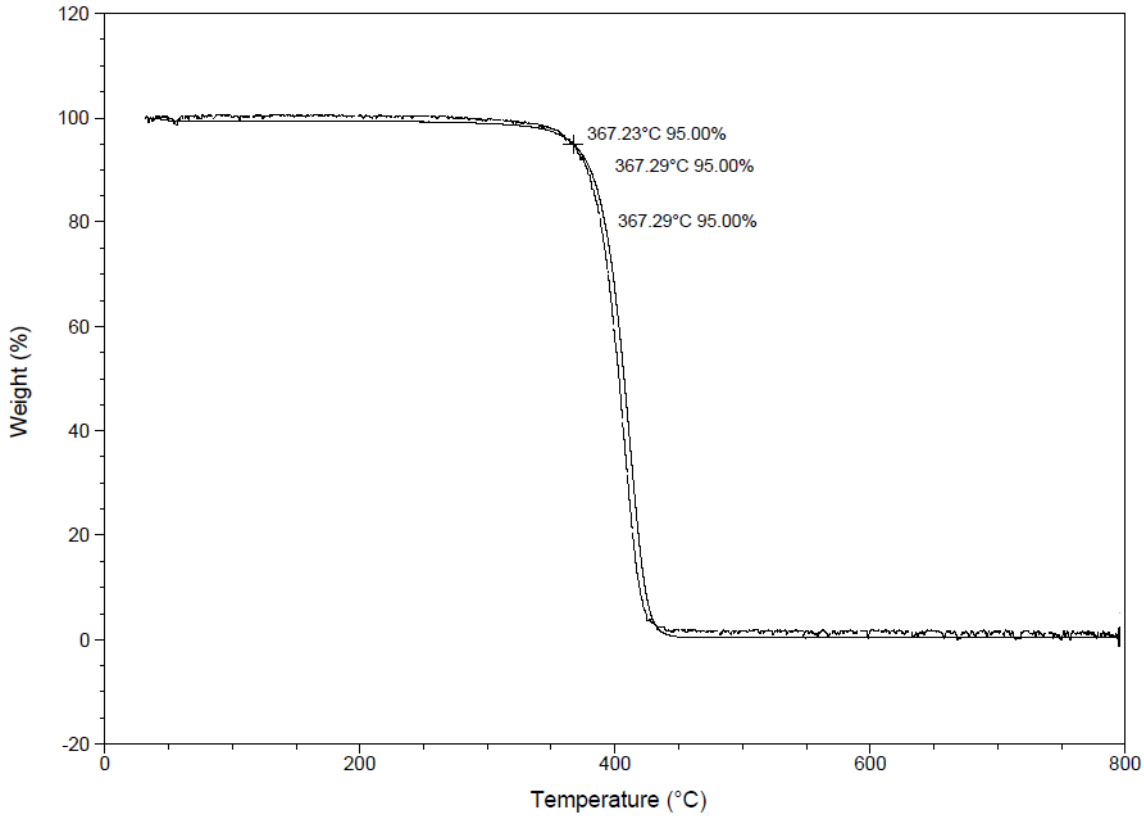

Figure 3.3: Triplicate thermograms of the decomposition of polystyrene functionalized with TMS.

Thermogravimetric analysis was performed for polystyrene and polystyrene functionalized with TMS under a continuous flow of argon gas. Thermograms were obtained in triplicate for both plain polystyrene and polystyrene functionalized with TMS. The images in Figure 3.2 and Figure 3.3 display the decomposition temperature at 5% weight loss, or the "initial decomposition temperature" (IDT). The IDT is an indication of the thermal stability of a material, and can be used as a gauge for the chemical content of a material. In hopes of quantifying the amount of silicon in the TMS functionalized polystyrene, the residual mass was measured. The results of the analysis are summarized in Table 3.1.

Table 3.1: Summarized thermogravimetric data for polystyrene and polystyrene functionalized with TMS.

	Mean IDT and SD (°C)	**Mean residual mass and SD (%)**
Polystyrene	365.84 ± 9.88	-0.03 ± 0.13
TMS-Polystyrene	367.27 ± 0.03	0.49 ± 0.12

In Table 3.1, it is apparent that the values obtained for the IDT of both the plain and TMS functionalized polystyrene are similar. As a result, it is difficult to draw evidence for the inorganic content of the polymers from this analysis.

The ^{13}C NMR spectrum revealed detailed structural information, and the ^{1}H-^{13}C HMBC experiment helped to complete the assignment of the functionalized quaternary carbon. The ^{1}H-^{13}C HMBC spectrum provides clear evidence of coupling between the protons on the TMS group and the carbons on the aromatic ring (Figure 3.7). This 2D NMR experiment provides evidence that the TMS functional groups are chemically bonded to the polymer and not occluded in the polymer matrix.

The presence of silicon was confirmed directly with a ^{29}Si uDEFT experiment at -4.55ppm. This is compared to the chemical shift of -4.71 (C_6D_6) of the analogous trimethyl(phenyl)silane.[67] To further confirm the covalent linking of silicon to the polymer, a ^{1}H-^{29}Si HMBC experiment was conducted. Figure 3.8 shows strong correlation between the ^{29}Si nuclei and the protons responsible for the TMS signal at 0.20ppm and between the ^{29}Si nuclei and the closest protons on the aromatic rings (labeled with 4' on Figure 3.5).

The Infrared spectrum of the TMS functionalized polystyrene was compared to that of a plain polystyrene reference to evaluate changes in the vibrational spectrum of the polymer in the mid-IR range. Typically, samples were made for IR by preparing polymer films. Unfortunately, the TMS functionalized polymer was unsuitable for preparation as a film, and was, instead, prepared as a KBr pellet.

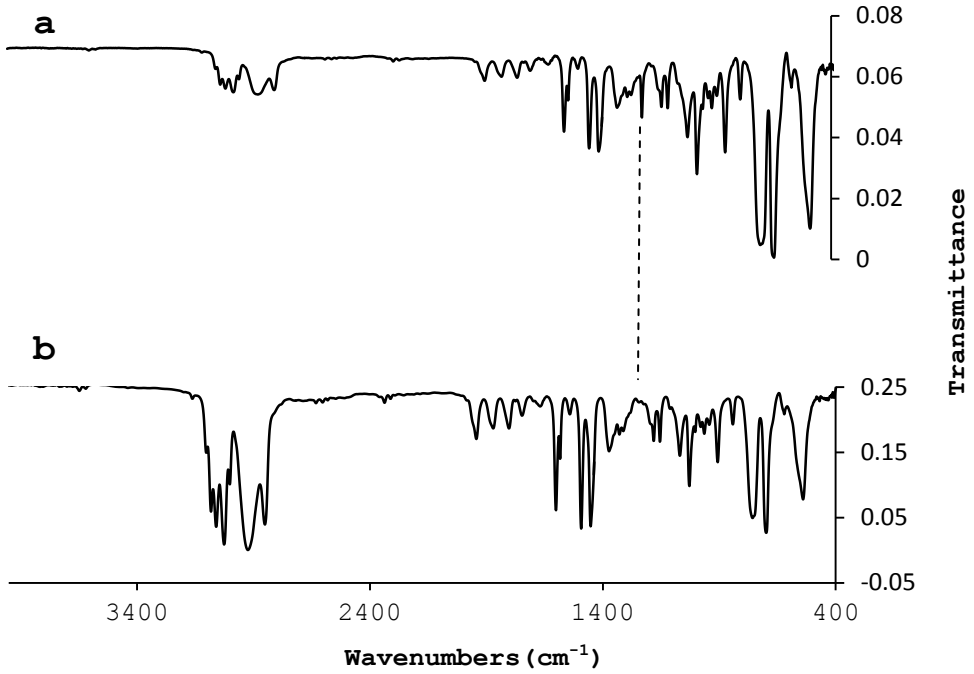

Figure 3.4: Infrared spectra of a) TMS functionalized polystyrene; b) Polystyrene lab reference.

The main difference between the spectra of the plain and functionalized polystyrenes, as indicated in Figure 3.4, is the appearance of a band at 1260cm^{-1} in the functionalized polystyrene. This vibration is most closely related to the symmetrical deformation $\delta_s(CH_3)$ at 1240cm^{-1} in the analogous trimethyl(phenyl)silane.[68]

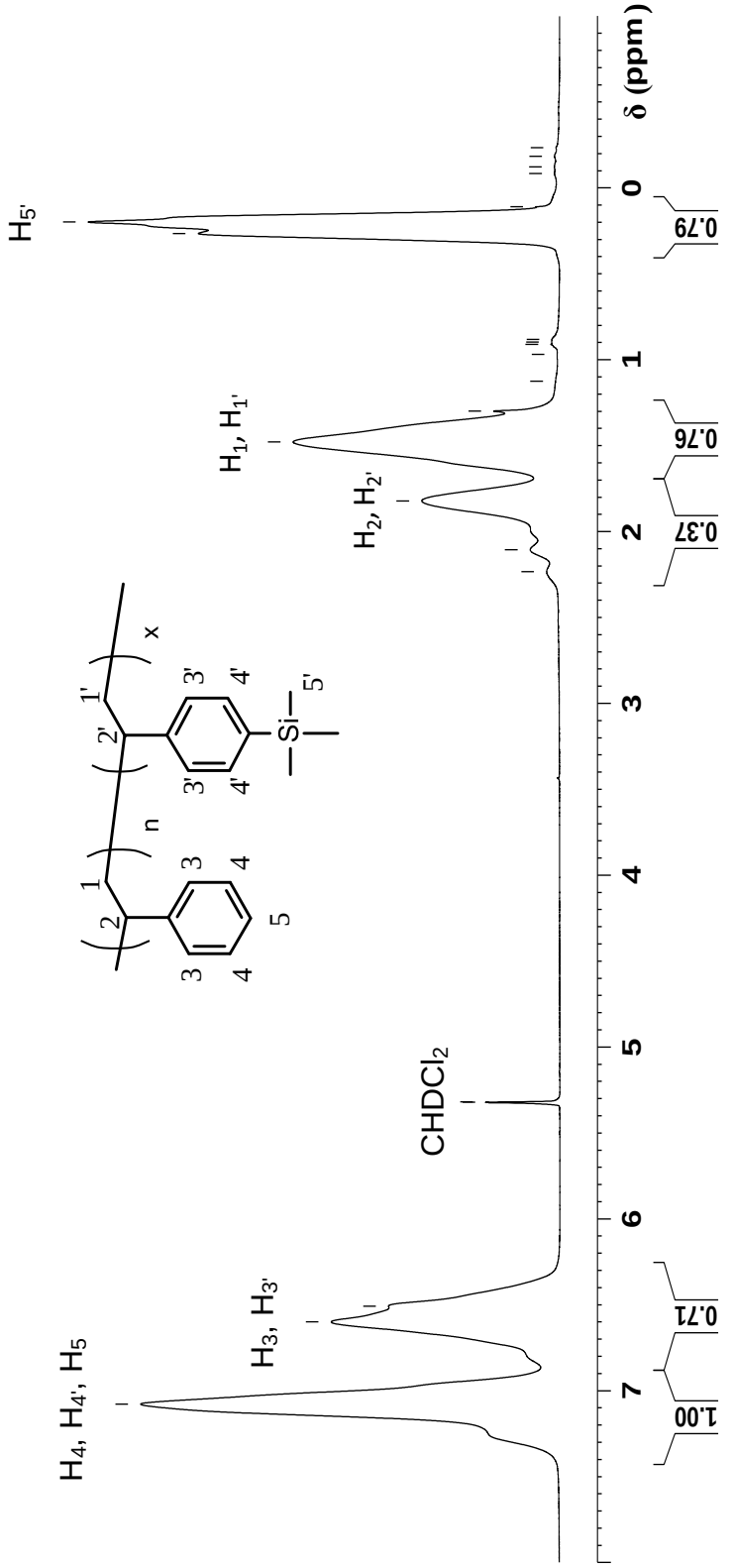

Figure 3.5: ^{1}H-NMR spectrum of a TMS functionalized polystyrene (DCM, 500MHz).

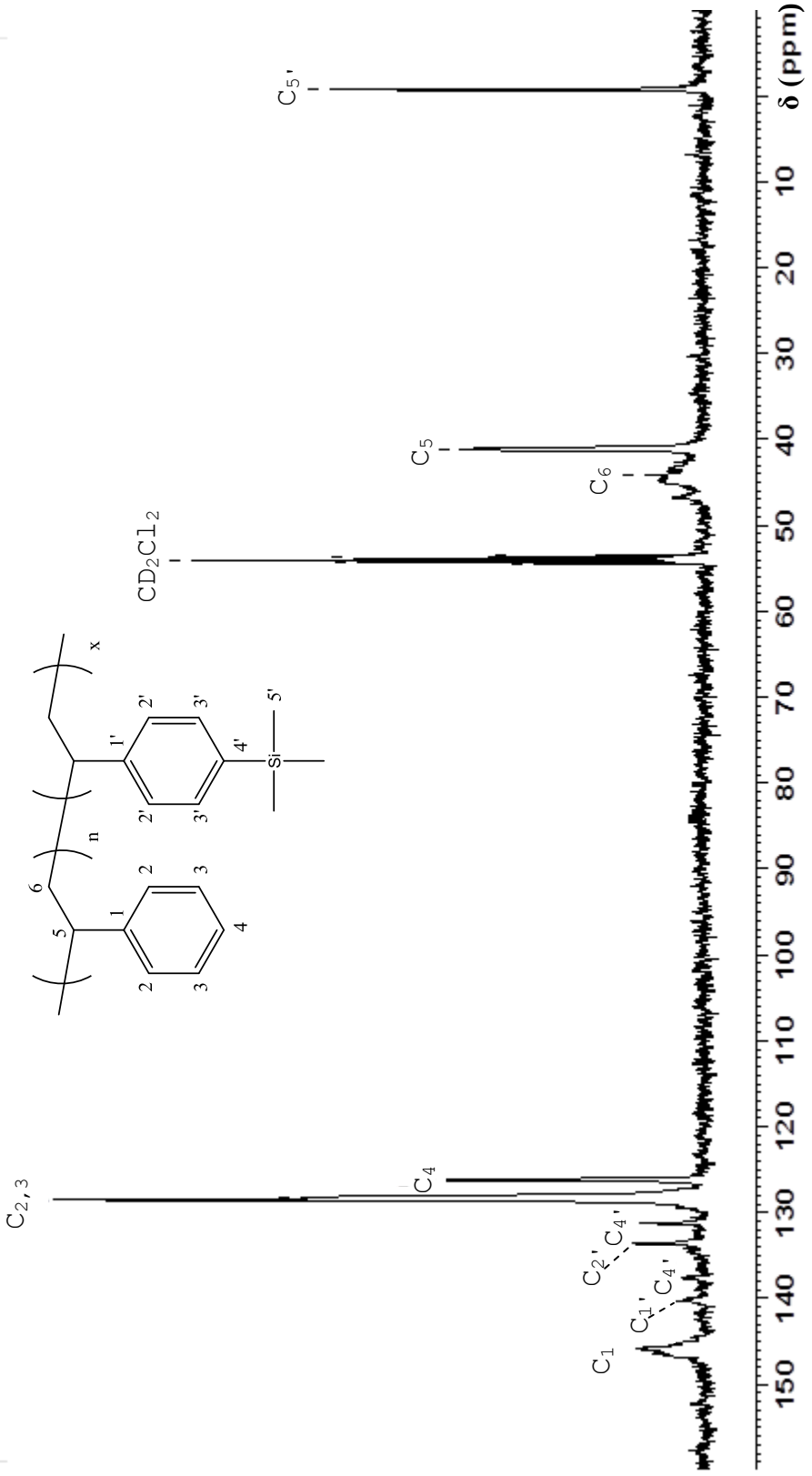

Figure 3.6: ^{13}C-NMR spectrum of a TMS functionalized polystyrene.

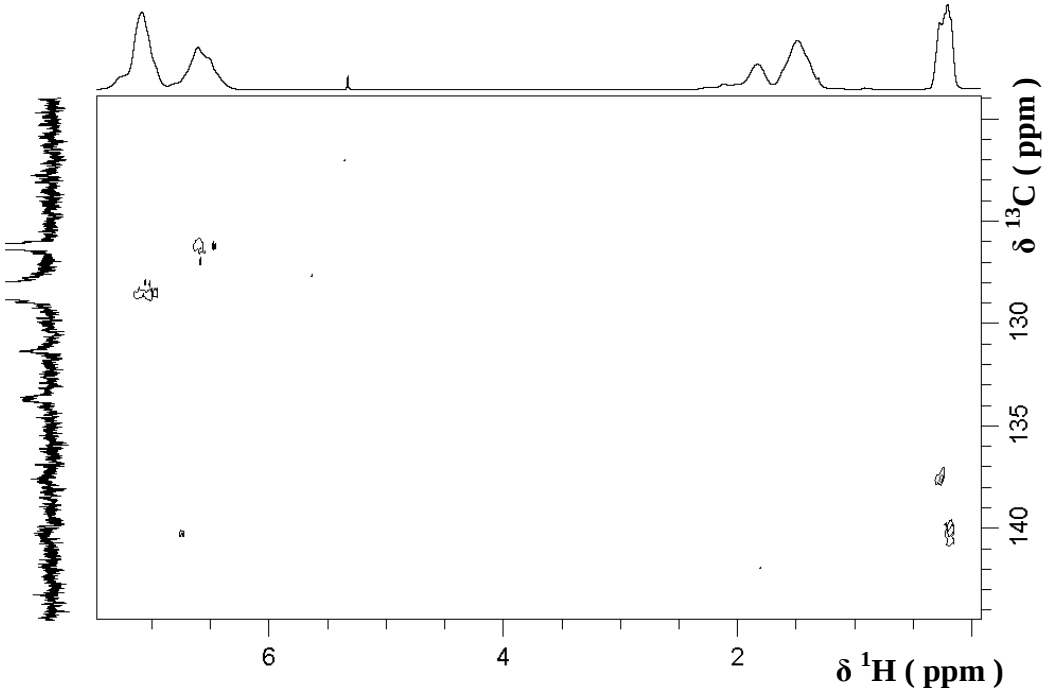

Figure 3.7: ^{1}H-^{13}C HMBC of polystyrene functionalized with TMS by direct lithiation.

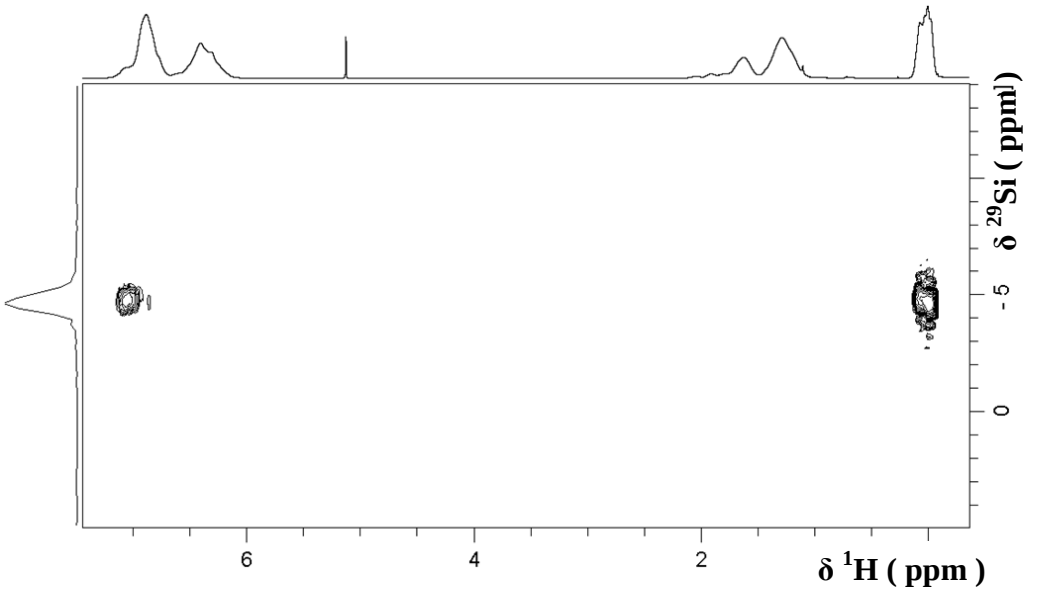

Figure 3.8: ^{1}H-^{29}Si HMBC of polystyrene functionalized with TMS by direct lithiation.

3.3 Reaction of the lithiated polymer with elemental sulfur.

The experiments described in the previous section did demonstrate that it is possible to derivatize polystyrene through the lithiated intermediate. However, the process was rather inefficient. Nevertheless, the lithiated polymer was used in reactions with the chalcogens in elemental form. Such reactions were first attempted before September 2011 but with much smaller amounts of n-butyl lithium (0.1 equivalents).[69] The product of lithiation (**32**) was reacted with elemental sulfur yielding a product which was poorly soluble in common organic solvents and was difficult to characterize.

3.4 Reaction of lithiated polymer with elemental tellurium.

The preparation of a polymer functionalized with Te-H groups was attempted as shown in Eq. 18. Treatment of lithiated polystyrene with elemental tellurium would produce tellurophenolate groups which would be protonated by dilute HCl. However, **36** would be unstable and prone to form ditelluride links and hydrogen as a by-product. The reaction yielded a dark precipitate, the physical appearance would be consistent with a material that is crosslinked by tellurium but its low solubility precluded proper purification and characterization. One complication of this experiment is the insolubility of elemental tellurium, thus the reaction must be performed in a heterogeneous mixture and there is the potential for the presence of long $-Te_n-$ chains within the polymer matrix.

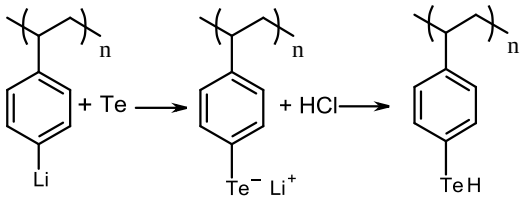

32 **35** **36** (18)

3.5 Reaction of 2 with [Te(bipy)Cl_2].

The recently reported compound [Te(bipy)Cl_2][70] , **39**, was used as an alternative -partly soluble- source of Te(II). The compound was prepared by the sequence of reactions depicted in Eq. 19 and Eq. 20. The product **39** was then used in a reaction with lithiated polystyrene, as shown in Eq. 21. This reaction was also attempted in investigations before the M.Sc. work, but the identity of the product could not be conclusively established at the time. Moreover, the design of the experiment was improved by the knowledge of the extent of polymer lithiation established in the reaction with TMS-Cl.

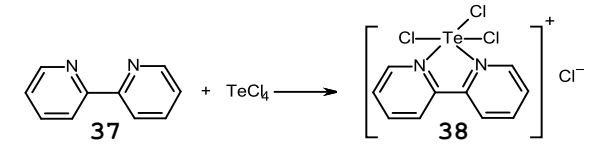

(19)

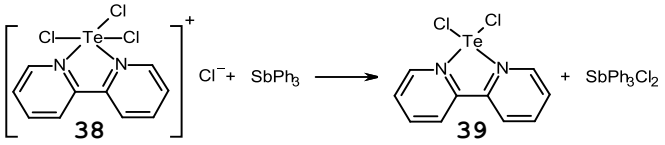

(20)

The reaction between **32** and **39** in THF produced a very dark solution from which a black solid was precipitated with MeOH the following morning (Eq. 21). It was expected that the product of this reaction, **40**, would contain embedded aryl-tellurenyl chloride groups. Similarly to the case of **36**, it is also possible that the tellurenyl

chloride would undergo disproportionation resulting in the formation of ditelluride bonds and other pendant groups such as $TeCl_3$, TeOMe, and $TeOMe_3$. These groups could in principle be identified by spectroscopic techniques. Unfortunately, once isolated the product was difficult to re-solubilize, likely due to cross-linking.

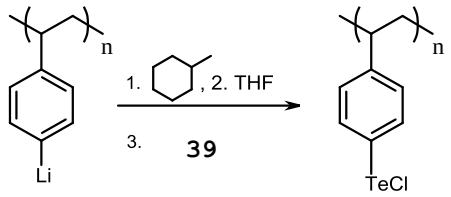

32 **40** (21)

Given the difficulty in characterization of insoluble materials, there is a need to explore suitable methods for the analysis of tellurium containing functional groups. Problems with solubility complicate NMR analysis, and the high molecular weights of the polymers are not ideal for mass spectrometric characterization. As a result, attention was turned to vibrational spectroscopy. Vibrational spectroscopy is advantageous in that there are standard methods for the analysis of solid samples and that both Raman and infrared techniques provide the ability to characterize the environment of tellurium.

4 Chapter 4: Vibrational Analysis of R-$TeCl_n$ Groups.

4.1 Synthesis and vibrational analysis of organo-tellurium chlorides.

Proper identification of tthe tellurium functional groups introduced into polystyrene would require spectroscopic measurements. ^{125}Te NMR measurements would be difficult because of the low receptivity and natural abundance of the isotope. In addition, issues with solubility complicate conventional methods of characterization such as NMR. To circumvent problems associated with insoluble products, and to address the need to assess the functionality of tellurium, vibrational spectroscopy could be employed. Unfortunately, to date, there is no published vibrational study of organotellurium halides which could be used as a point of reference for the identification of R-TeX_n groups. This is in part because the vibration should appear in the low-energy region of the spectrum, and the complications introduced by crystal symmetry and extensive secondary bonding.

Therefore, and in order to support the investigations of the derivatization of polystyrene, a detailed vibrational study of organotellurium halides was performed. This included structurally characterized examples of $RTeCl_n$ (n = 1, 3) compounds. While tellurenyl chlorides (RTeCl) would display only one Te-Cl stretch, three vibrations of this type would be observable for a trichlorotellurane ($RTeCl_3$). Scheme 4.1 displays the composition of the corresponding normal vibrational modes, classified under C_s symmetry.

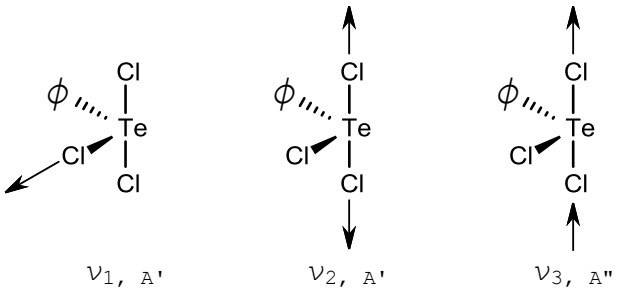

Scheme 4.1: Te-Cl stretch vibrations of a trichlorotellurane and their symmetries under the C_s point group.

Experimental measurements were performed for selected examples. Organotellurium(II) halides are in general unstable, they readily undergo disproportionation to the corresponding ditelluride and trichlorotellurane unless the organic group provides steric protection or enables an intramolecular *secondary bonding interaction* (SBI). These are closed-shell interactions which are longer than typical hypervalent single bonds, yet much shorter than the sum of their corresponding van der Waals radii.[71] The only structurally authenticated example of the former case is that of supermesityl-tellurenyl(II) chloride (**45**), which was prepared by the sequence of reactions in Scheme 4.2[56,57] and Scheme 4.3[59]. An excess of SO_2Cl_2 yielded the corresponding trichlorotellurane. A second trichlorotellurane was synthesized as shown in Scheme 4.4.[58] The far IR experimental spectra of these compounds is displayed in Figure 4.1, Figure 4.3 and Figure 4.5. The spectra were interpreted with the aid of DFT calculations; the corresponding calculated spectra are compared to the experimental in the same figures.

Figure 4.1 compiles the spectra for $PhTeCl_3$. There is, in principle, a good agreement between the experimental spectrum and the position and intensity of the bands calculated for a single molecule

(gas phase). However, in the former case, the most intense band is significantly broadened and appears to consist of the superposition of multiple bands. Splitting of the stretch bands for polar bonds such as Te-Cl is common and could be due to intermolecular interactions and/or crystal symmetry. Perhaps the more notable intermolecular interactions in this case are those between tellurium and chlorine. Dimers of this type, specifically for the $[Te\text{-}Cl]_2$ supramolecular synthon, have been observed in the crystal lattices of the halo-telluranes discussed in this chapter.

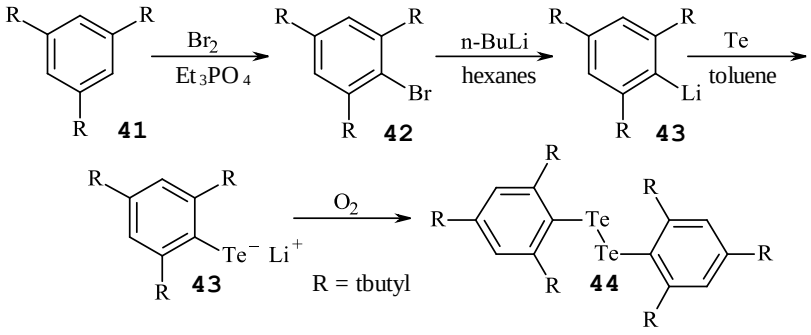

Scheme 4.2: Synthesis of supermesityl ditelluride.

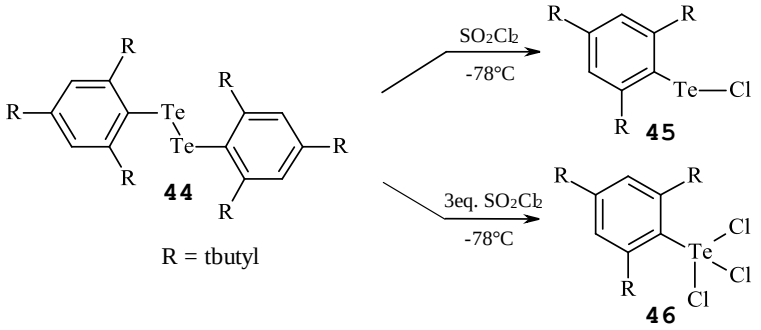

Scheme 4.3: Synthesis of supermesityltellurenyl(II) chloride and supermesityltellurium(IV) trichloride.

Scheme 4.4: Synthesis of phenyltellurium(IV) trichloride.

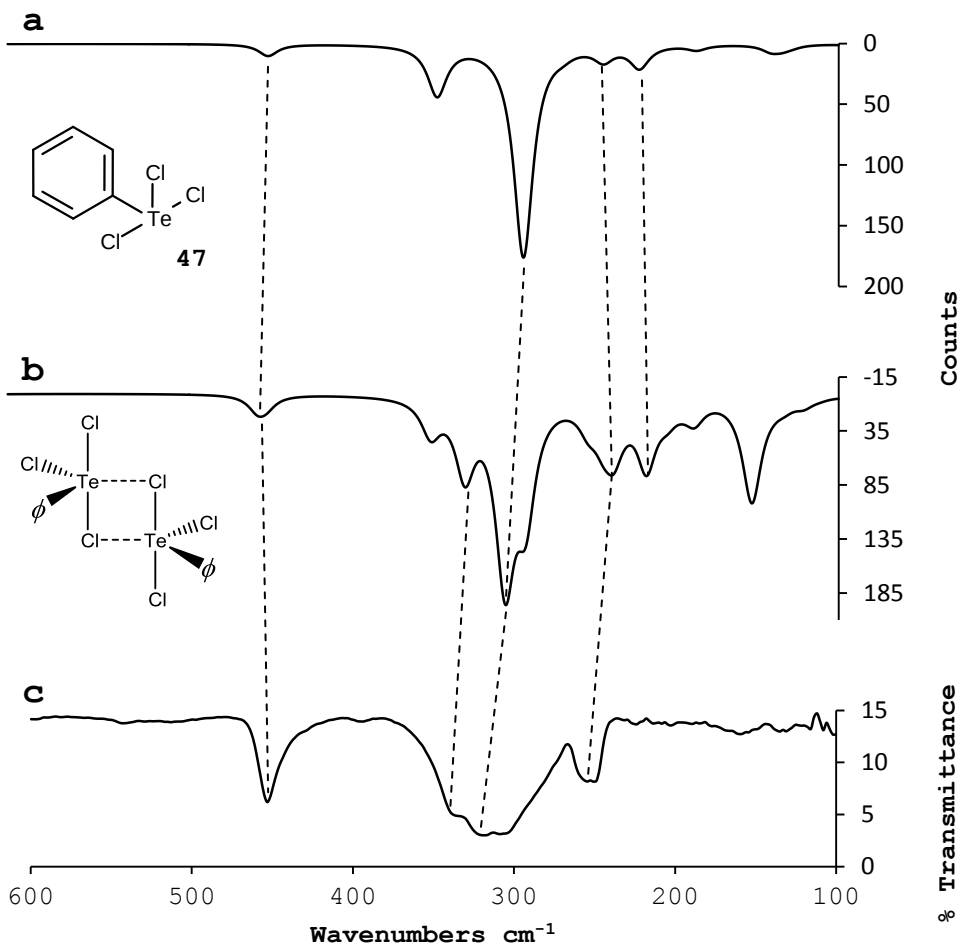

Figure 4.1: Far IR spectra of Ph-$TeCl_3$. a) calculated for a single molecule; b) calculated for an SBI dimer forming the $[Te\text{-}Cl]_2$ supramolecular synthon; c) experimental.

$PhTeCl_3$ crystallizes in the P_{-1} space group and displays the polymeric arrangement of the molecules shown in Figure 4.2.[72,73] There is a significant difference between the terminal (avg. 2.378 Å) and bridging (avg. 2.760 Å) Te-Cl bond distances. Therefore, the single molecule model cannot account for all the features of the experimental spectrum. The effect of crystal symmetry can be predicted by factor group analysis. In the crystalline lattice, there are four molecules per unit cell, the molecules sit in general positions, and the factor group is C_i. Therefore the total of 12 Te-Cl stretch vibrational degrees of freedom would split evenly into 6 A_g (Raman active) and 6 A_u (IR active) vibrations. The experimentally observed broadening and apparent splitting would be consistent with this analysis. All this information makes it possible to propose assignments for some of the bands in the experimental spectrum as shown in Figure 4.1 and Table 4.1.

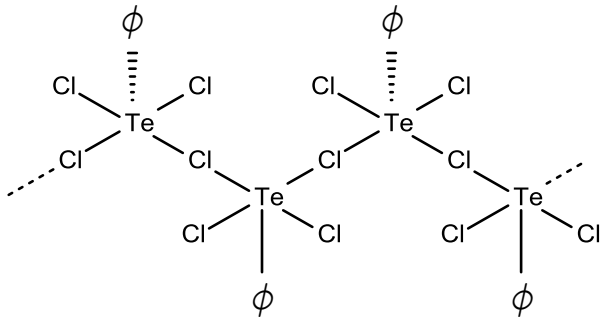

Figure 4.2: Schematic representation of the organization of $PhTeCl_3$ molecules in the crystal.

Table 4.1: Experimental and calculated far-IR vibrations for the dimeric structure of $PhTeCl_3$.

Wavenumber (cm^{-1})		Assignment
Experimental	**Calculated (dimer)**	
453	443	(C-H) out-of-plane umbrella
337, shoulder	341	ν_1(A'), ν(Te-Cl)$_{eq}$
320		
310, shoulder	289	ν_3(A"), ν_{as}(Te-Cl)$_{ax}$
255	241	ν_2(A'), ν_s(Te-Cl)$_{ax}$
251	220	

The supermesityl-trichlorotellurane (**46**) has a simpler crystalline structure, consisting of dimers as shown in Figure 4.4. In this case there are two molecules per unit cell, also sitting in general positions of the P_{-1} space group. Therefore, it is expected that the Te-Cl stretch vibrations would yield 3 A_g and 3 A_u, which are mutually exclusive modes observable in Raman and IR spectroscopy, respectively. The experimental spectrum closely resembles the spectrum of the phenyl analogue, the main differences being the position of the main band, shifted to lower wavenumber, and its splitting into fewer daughter bands.

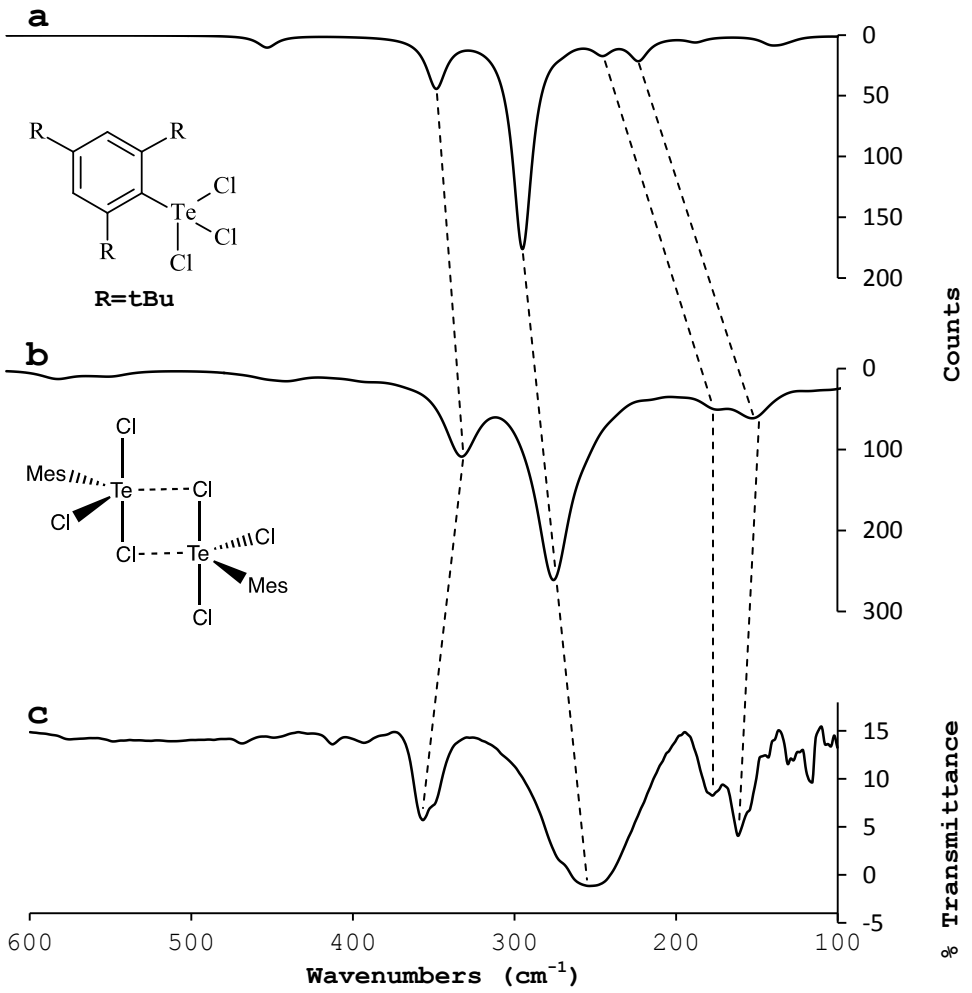

Figure 4.3: Far IR spectra of $SMesTeCl_3$. a) Calculated for a single molecule; b) calculated for a dimer; c) experimental.

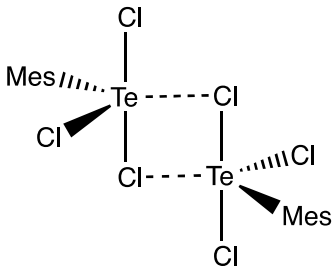

Figure 4.4: Bonding motif of the dimer observed in the crystal of $SMesTeCl_3$.

Table 4.2: Experimental and calculated far-IR vibrations of the dimeric structure of $SMesTeCl_3$.

Wavenumber(cm^{-1})		**Assignment**
Experimental	**Calculated (dimer)**	
357	326	ν_1(A'), ν(Te-Cl)$_{eq}$
258	271	ν_3(A"), ν_{as}(Te-Cl)$_{ax}$
181	172	δ(Te-Cl)$_{ax}$, SBI
164	151	δ(Te-Cl)$_{ax}$, SBI

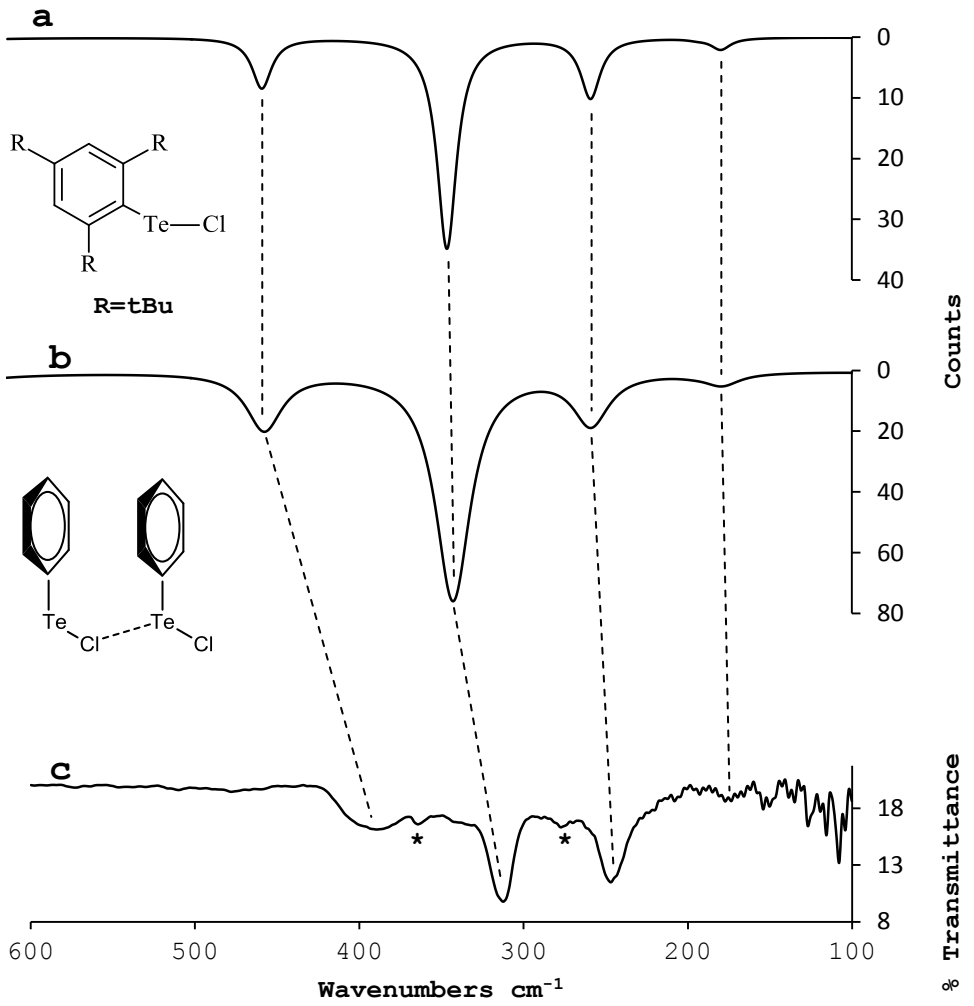

Figure 4.5: Far IR spectra of RTeCl. a) Calculated for PhTeCl; b) calculated for a dimer; c) experimental. The bands marked with a "*" are attribitued to the trichloride present as an impurity.

Alternatively to IV, the chalcogen could be in state II, in which case it would make an aryltellurenyl(II) chloride. Figure 4.5 displays the experimental spectrum of SMesTeCl and compares it to the spectrum calculated for PhTeCl, which is in good agreement. The positions and assignments of the bands are compiled in Table 4.3. The most significant band arises from the Te-Cl stretch and is observed at 312 cm^{-1}.

Table 4.3: Experimental and calculated far-IR vibrations of SMesTeCl.

Wavenumber(cm^{-1})		**Assignment**
Experimental (SMesTeCl)	**Calculated (PhTeCl Dimer)**	
393, sh	450	δ(C-H) out-of-plane bending
368 (impurity)		
312	341	ν(Te-Cl)
270 (impurity)		
247	254	ν(Te-C)
174	173	δ(C-Te-Cl) bending

The factor group analysis of crystalline spectra can be used to explain features that are observed in experimental infrared spectra. This interpretation was done for the Te-Cl bond in supermesityltellurenyl(II) chloride with an idealized C_s symmetry. One stretch vibration of A' symmetry is expected for the Te-Cl bond.

Table 4.4: Factor group splitting analysis of SMesPhTeCl.

$(Z = 4)$ f^Y		C_s		C_1	c	a	f^Y	D_2	c	a	activity
4	1	A'	———	A	1	4	4	A	1	1	R
		A"						B_1	1	1	IR
								B_2	1	1	IR
								B_3	1	1	IR

The factor group analysis predicts three bands in the infrared spectrum for the symmetric Te-Cl stretch. The main band is observed at 312cm^{-1}, however there is no splitting observed in the spectrum.

Given a method to characterize the environment of tellurium by far-infrared spectroscopy, an attempt was made to characterize the polymer **40** by dispersing a sample of the material in polyethylene. Figure 4.6 shows the far-IR spectra of both the polyethylene standard and that of the dispersion.

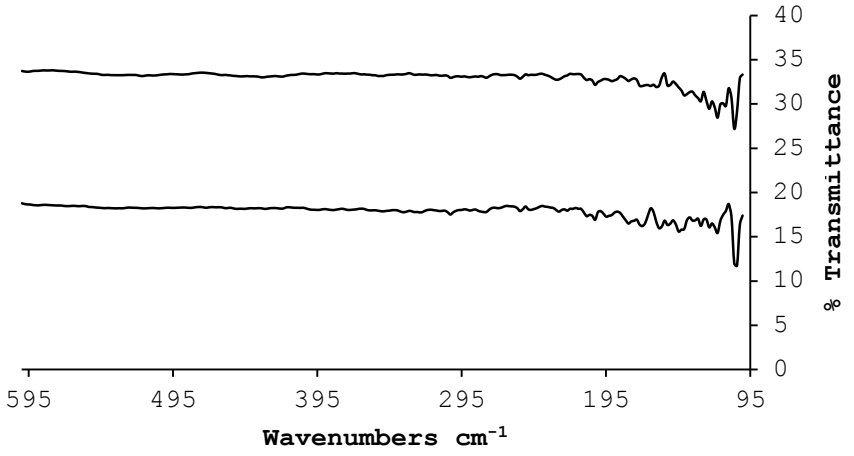

Figure 4.6: Far-IR spectra of a polyethylene standard (top) and polyethylene dispersed with **40** (bottom).

The sample spectra shown in Figure 4.6 do not provide structural information for the product of the reaction in Eq. 21. It is possible that these spectra are not good enough quality to observe the expected bands. The plan to characterize the environment of tellurium in the product **40** has been unsuccessful despite several attempts at both dispersive Raman spectroscopy and far-IR spectroscopy. Given the difficulty in preparing a tellurium containing polymer by direct functionalization, attention was turned to the preparation of polymerizable cross-linking agents.

5 Chapter 5: Polymerizable Cross-Linking Agents

5.1 Introduction.

The first synthesis of a vinyl ditelluride was published in 1962. This unique report describes the preparation of Di-(2-chloro-1,2-diphenylvinyl)ditelluride by the reduction of 2-chloro-1,2-diphenylvinyltellurium trichloride using the hydrate of sodium sulfide. It was claimed that the ditelluride crystallized as orange needles after the addition of water to the crude product followed by recrystallization from petroleum ether. The product was identified on the basis of its melting point and elemental analysis.[74] Few examples exist of (bis)vinyl tellurides and ditellurides, unfortunately, those that have been reported have not been structurally authenticated. The most studied example is that of divinyl ditelluride, which is synthesized by the reaction of the vinyl Grignard reagent with elemental tellurium. Oxidiation of the vinyl tellurolate in air yields the ditelluride as a red oil. Original reports of this ditelluride only provided characterization by ^{1}H NMR, IR spectroscopy and elemental analysis. The purity of the sample was never properly assessed, and the only band identified in the vibrational spectrum is that of the C=C symmetric stretch.[75,76] A report in 2012 described the synthesis of (bis)vinyl ditelluride from tellurium and acetylene. In this case, the ditelluride was characterized by ^{1}H NMR, ^{13}C NMR, and ^{125}Te NMR. The reaction of tellurium with acetylene produced bis(vinyl) telluride as a byproduct and no characterization was provided of the monotelluride.[77]

Given lack of complete characterization for the examples found in literature, our attention was turned to common methods for the synthesis of diorganyl mono- and ditellurides in order to obtain a polymerizable cross-linking agent.

5.2 bis(4-vinylphenyl)ditelluride.

This reagent was conceived as a cross-linking agent for polystyrene, its synthesis is outlined in Scheme 5.1. The method is based in a "one-pot" synthesis that is reportedly highly efficient; the lowest reported yield was 72% for 3-iodopyridine.[52] The alcohol **50** would be used to synthesize the crosslinking agent **51**, using a process developed by J. McNulty for the direct synthesis of functionalized styrenes via aqueous Wittig chemistry (Scheme 5.1).[53] This process uses triethylphosphine hydrobromide to generate a phosphonium salt from benzyl alcohol derivatives. A Wittig reaction with aqueous formalin, of the phosphonium salt, then yields the corresponding styrene. The initial attempt to produce **51** yielded a red solid that was difficult to separate from the DMSO used as the solvent. The ^{1}H NMR spectrum of the sample revealed an impure product. Several attempts were made to purify the compound by sublimation, extraction or recrystallization. The ^{1}H NMR spectrum revealed the two sets of doublets that would be expected for a para-functionalized aromatic ring, a triplet corresponding to the alcohol, and a doublet for the benzyl protons. ^{125}Te NMR spectrum of the residue of CH_2Cl_2 extraction revealed a single transition at 667 ppm, a chemical shift that corresponds to most organo-monotellurides (R-Te-R). Unfortunately, the pure product could not be isolated.

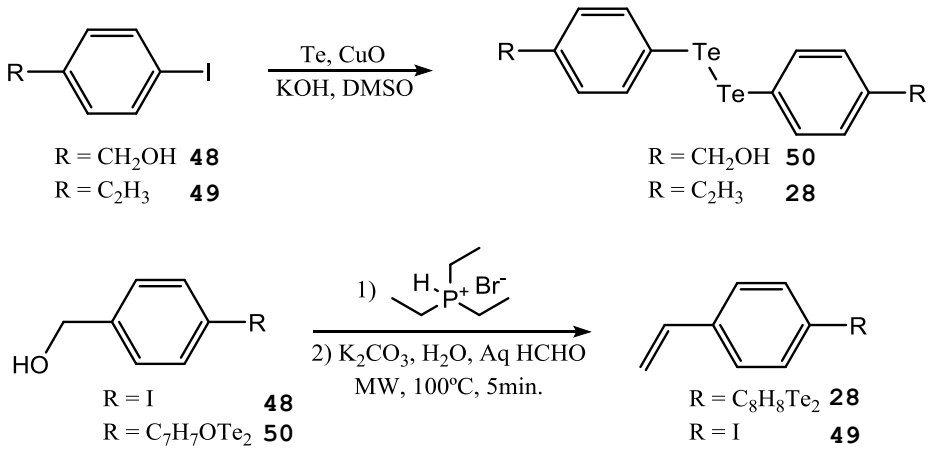

Scheme 5.1: Proposed synthesis of the polymerizable cross-linking agent **28.**

In the presence of alcohols, organo-ditellurides undergo a photochemical reaction that results in tellurium extrusion by a complex kinetic pathway,[78] such processes would explain the difficulties experienced during the synthesis of **51.**

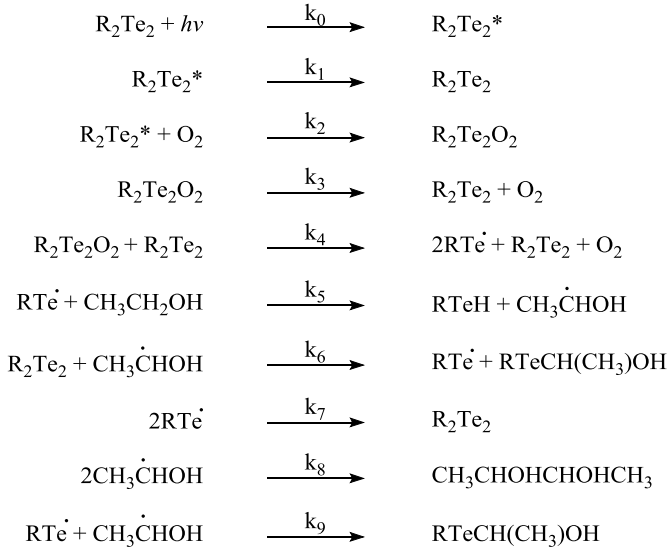

Scheme 5.2: Decomposition pathway of diorganyl ditellurides in the presence of alcohols adapted from.[78]

Scheme 5.2 shows the decomposition stages of a photosensitive ditelluride in alcoholic solution. Ditellurides are prone to photoexcitation and relaxation (k_1 and k_2). The excited state produced from k_1 can react with O_2 and release organotellurium radicals (k_3 and k_4). These tellurium radicals formed through the dissociation of ditelluride bonds can abstract protons from the α carbon in the presence of alcohols, or in alcoholic solution (k_5). This ultimately results in a variety of undesired radical cross-couplings (k_9). Since the preparation of **50** replicates similar conditions, it is likely that the product is decomposing following a similar pathway.

An alternative synthesis of the ditelluride **28** was attempted by first preparing 4-iodostyrene (**49**) by the Wittig of the corresponding phosphonium salt, followed by conversion to the ditelluride as described in Scheme 5.1. 4-iodobenzyl alcohol reacted with triethylphosphine hydrobromide to generate the corresponding phosphonium salt. This product reacted with aqueous formalin in basic medium, yielding 4-iodostyrene after 30 minutes of microwave irradiation. The product, **49**, was isolated by extraction with pentane, followed by filtration through a silica plug. The 4-iodostyrene was then used as above outlined in the ditelluride synthesis. The corresponding product was very sensitive to light and could not be characterized before decomposition.

5.3 Bis(methacryloyl)ditelluride.

The proposed synthesis of compound **30** was based on a method developed by Klapoetke and is shown in Scheme 5.3.[54]

$$4Te + 4NaOH + 2N_2H_4 \cdot H_2O \longrightarrow 2Na_2Te_2 + 2N_2 + 5H_2O$$

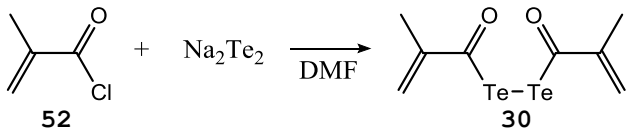

52 **30**

Scheme 5.3: Synthesis of bis(methacryloyl)ditelluride.

Hydrazine hydrate, elemental tellurium and NaOH were mixed in DMF. After stirring for six hours, a thick purple mixture was obtained. Such colour is characteristic of the Te_2^{2-} anion, which has been useful in the synthesis of pyrimidyl dichalcogenides.[54] An excess of methacryloyl chloride was used to consume the water produced in the first step. The product was purified by extraction into toluene and was kept in a dry ice/acetone bath to minimize decomposition. The ^1H NMR spectrum in Figure 5.1 indicated that the reactant methacryloyl chloride (δ = 1.90 ppm (s, 3H, CH_3), 6.06 (s, 1H, CH_2), 6.41 (s, 1H, CH_2)) was consumed in the reaction. A complex mixture of products was obtained.

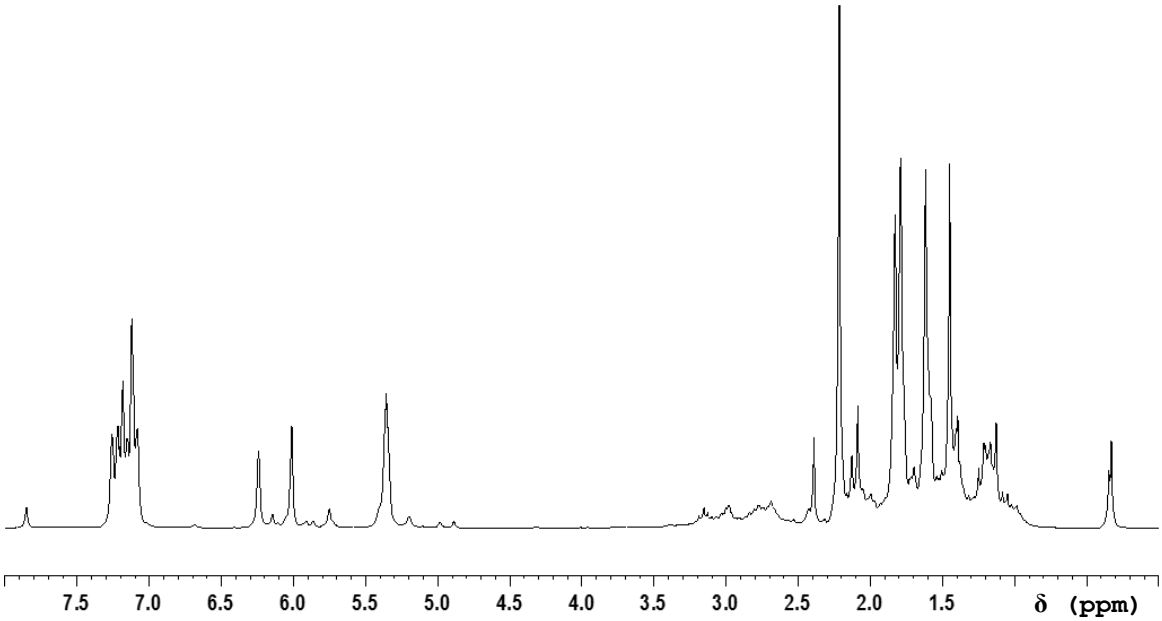

Figure 5.1: ^{1}H NMR spectrum of the crude reaction mixture from the reaction in Scheme 5.3.

An alternative method was proposed, which consists of the initial preparation of the tellurocarboxylate anion by reaction of methacryloyl chloride with Na_2Te (Scheme 5.5). The method is analogous to the synthesis of the alkyl counterparts.[79] The synthesis of sodium telluride was carried out using the free elements in DME and naphthalene as an electron transfer agent[55] (Scheme 5.4). The identity and quality of the product was verified by powder X-ray diffraction. Figure 5.2 displays the experimental diffraction pattern and Table 5.1 compares the experimental with the literature data.

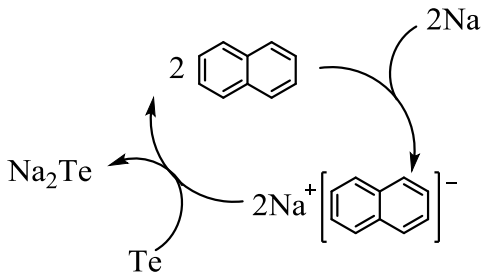

Scheme 5.4: Synthesis of sodium telluride.

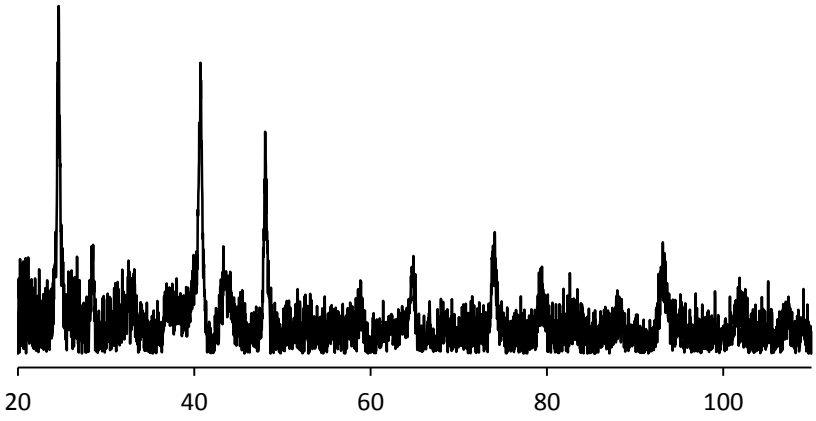

Figure 5.2: Powder diffraction pattern of Na_2Te.

Table 5.1: Experimental and calculated reflections of Na_2Te.

Reflections (2θ, degrees)	
Experimental	**Calculated**
24.62	24.46
28.54	28.30
40.70	40.45
48.04	47.86
50.66*	50.32
58.30	58.48
64.82	64.37
66.68*	66.70
74.16	73.57
78.94	78.84
87.86	87.50
92.64	92.59
95.14*	94.52
101.48	101.07
105.94	106.52
108.86*	108.70

Given the low signal to noise ratio of the diffraction pattern, reflections which were below 6.7% of the reflection at 24.62° were not observed (Table 5.1). With the successful isolation of Na_2Te, a new route was developed for the preparation of vinyl ditelluride cross-linking agents. This was done both for the methacryloyl and vinylbenzyl systems as shown in Scheme 5.5.

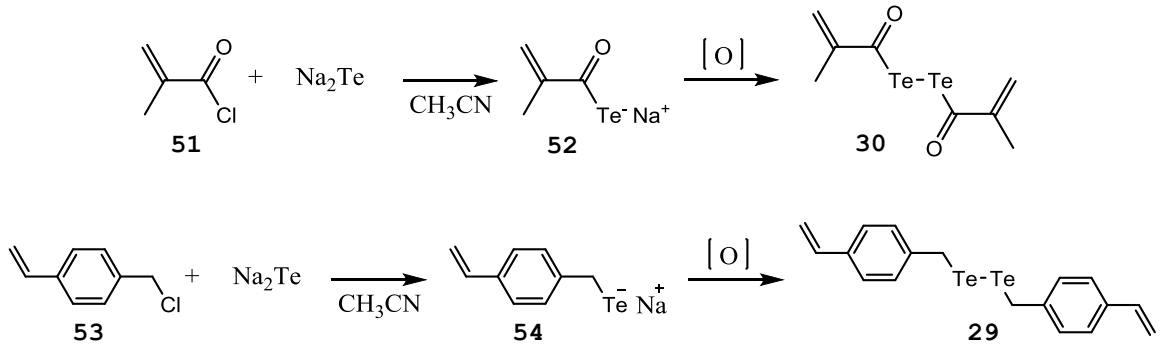

Scheme 5.5: Proposed syntheses of bis(methacryloyl) ditelluride and (bis)vinylbenzyl ditelluride from Na_2Te.

The reaction of Na_2Te with methacryloyl chloride would proceed via an S_N2 mechanism that generates the methacryloyl tellurocarboxylate anion **52**. Given the successful synthesis of the anion, simple oxidation would yield the desired ditelluride.

The reaction of methacryloyl chloride with sodium telluride in acetonitrile produced a red solution from which a dark solid (assumed to be elemental tellurium) precipitated; an orange glassy residue was obtained from the solution upon in-vacuo solvent removal. The ^1H NMR spectrum of gave a spectrum that suggests corresponds to a complex mixture of products, none of which could be identified. Moreover, this yellow solution in CD_3CN decomposed rapidly with extrusion of elemental tellurium.

5.4 bis(4-vinylbenzyl)ditelluride 55.

The synthesis of this compound was attempted from 4-vinylbenzyl chloride as described in Scheme 5.5. The reaction was allowed to proceed overnight and the product was extracted with hexanes the following day. After removal of the solvent and crystallization from

hexanes, a bright yellow crystalline solid was obtained. The ^{1}H-NMR and ^{125}Te spectra of the product in Figure 5.3 and Figure 5.4 are indicative of a single product which was identified as (bis)vinylbenzyl telluride (**55**). The ^{1}H spectrum displays the AA'BB' spin system of the *para*-substituted aromatic ring with two doublets of doublets centred at 7.3 and 7.2 ppm and show the asymmetric distortion that arises from second-order effects. Three sets of doublets of doublets are observed in this spectrum for the vinylic protons. These transitions were assigned based on their chemical shifts and coupling constants. The satellite doublets from the $^{2}J(^{1}H_{6}-^{125}Te)$ = 26.2 Hz and $^{1}J(^{13}C_{6}-^{125}Te)$ = 143.3 Hz couplings were also observed in the ^{1}H NMR spectrum. These are comparable to the coupling constants of $^{2}J(^{1}H-^{125}Te)$ = 21.0 Hz and $^{1}J(^{13}C-^{125}Te)$ = 158 Hz which have been observed for dimethyl telluride.[80] Correspondingly, the ^{125}Te NMR spectrum shows a quintet corresponding to the tellurium nucleus coupling to the four surrounding proton nuclei with $^{2}J(^{125}Te-^{1}H_{6})$ = 26.1 Hz. This demonstrates that two benzylic carbons are attached to one tellurium atom.

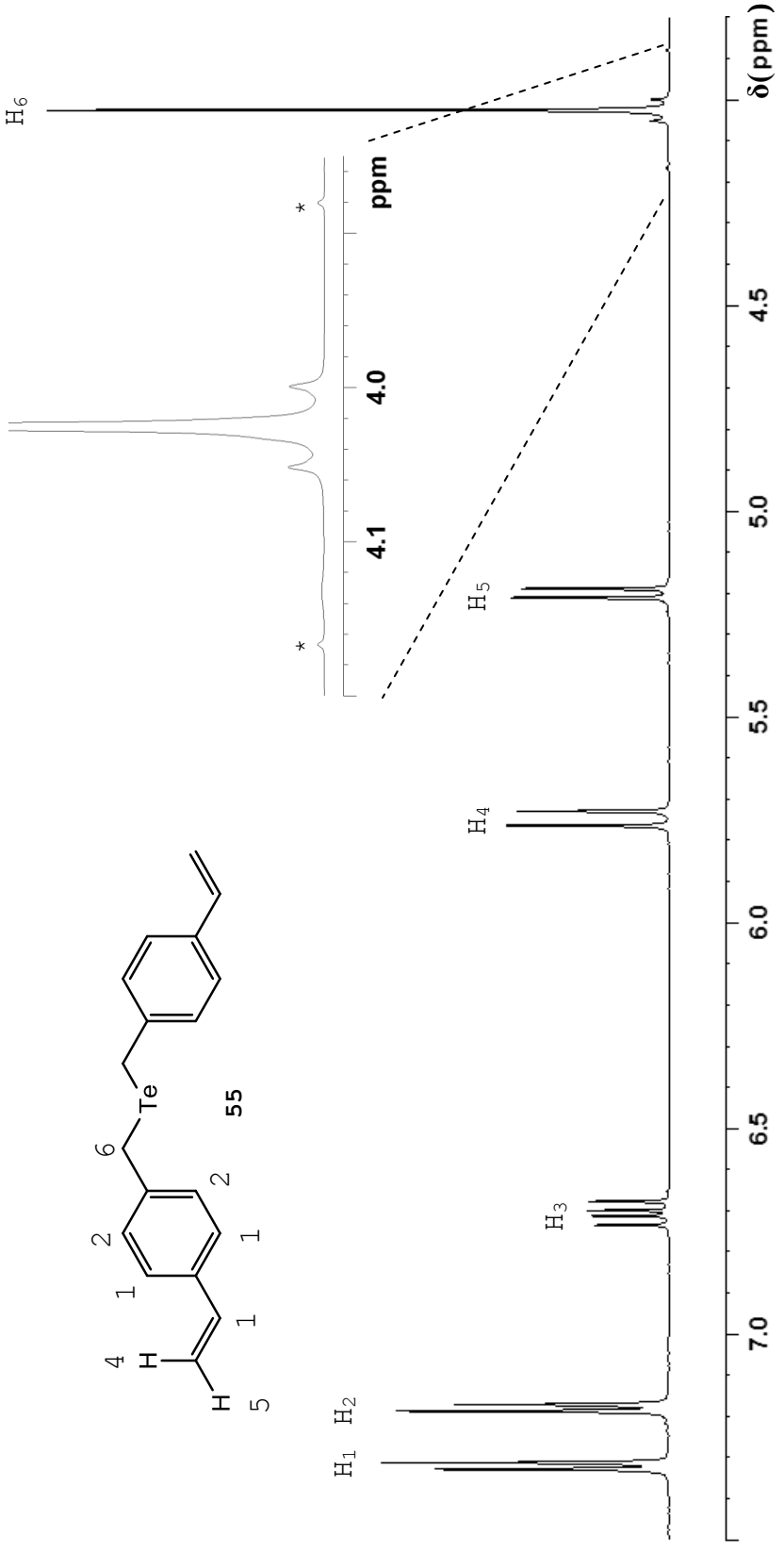

Figure 5.3: ^{1}H NMR spectrum of 4-vinylbenzyl telluride.

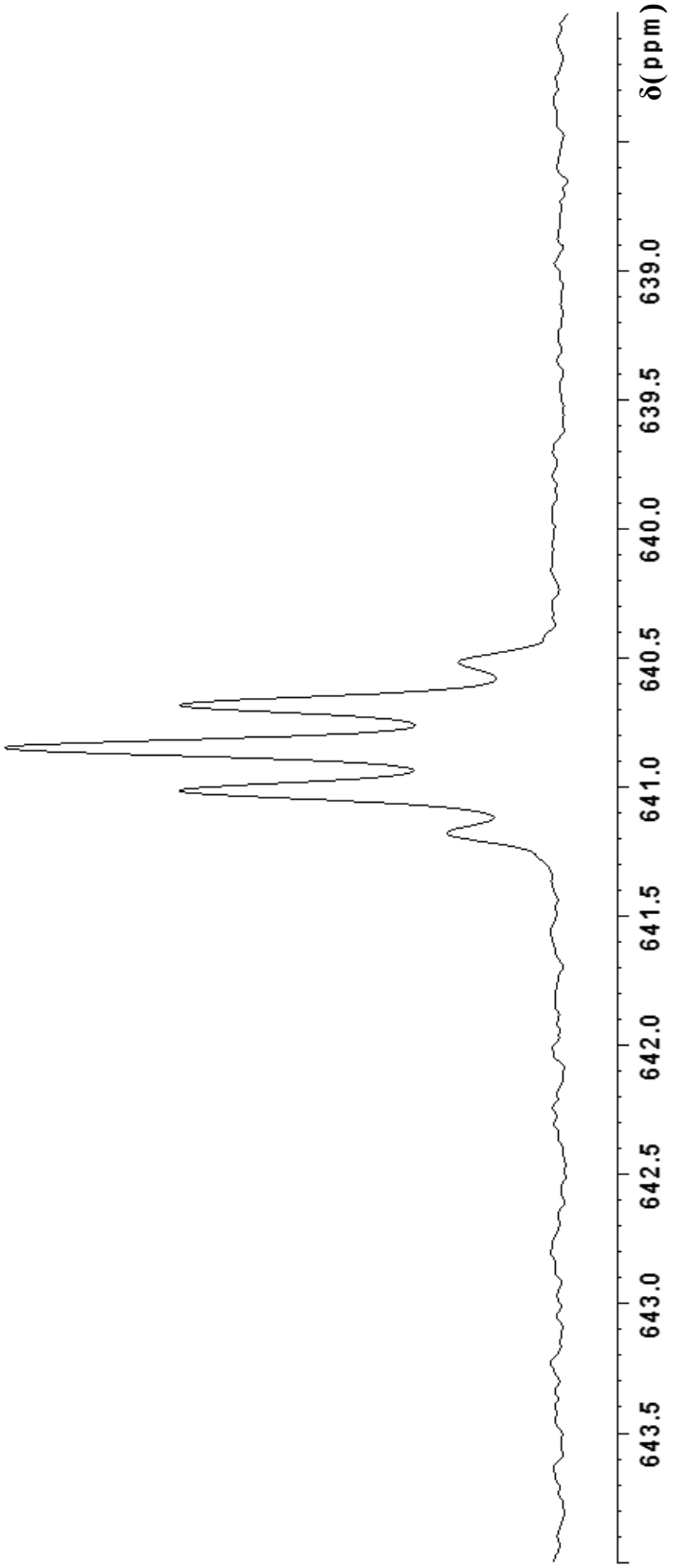

Figure 5.4: ^{125}Te NMR spectrum of 4-vinylbenzyl telluride.

High resolution mass spectrometry was used as a tool to further confirm the identity and purity of (bis)vinylbenzyl telluride **55**. The high resolution mass spectrometric data shown in Figure 5.5 was obtained from a crystalline sample of **55**.

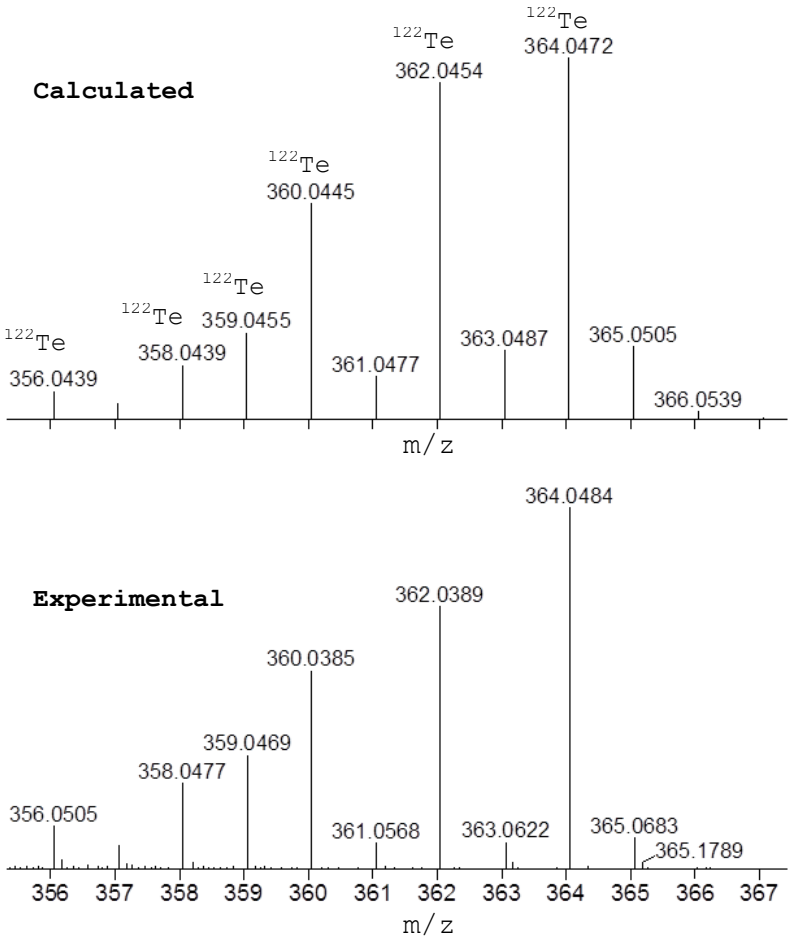

Figure 5.5: Mass spectrometric data of (bis)vinylbenzyl telluride, **55**.

The experimental spectrum shows good agreement with the calculated spectrum for the molecular formula $C_{18}H_{18}Te$. A mass value of 364.0484 m/z was obtained experimentally as compared to the calculated 364.0472 m/z. The calculated isotopic distribution pattern is also shown in the experimental spectrum; the peaks in Figure 5.5 have been labeled with the corresponding tellurium isotope. There is a small

discrepancy in the relative abundances of the calculated isotopomers versus the experimentally observed isotopomers. This can be explained by natural variations in the isotopic composition of elements.[81]

Single crystal X-ray diffraction was used for the structural characterization of **55**. The X-ray crystallographic data for **55** is summarized in Table 5.2. The structure itself displays significant positional disorder in the aromatic rings, and in the pendant vinyl groups. It is clear that there is rotation about the Te-C bond in the crystal lattice. In order to identify the disordered atoms within the structure, the site occupancy factor of the strongest reflections were changed from 11.0000 to 10.5000. This revealed the reflections that corresponded to the disordered atoms by changing general positions to special positions about which a mirror plane exists. The PART instruction was then used to split the two components of the disorder into separate groups. Similarity restraints were applied using the SAME instruction setting the bond lengths and angles of the two components of the disorder equal. For the final refinement, equal atomic displacement parameters were assigned to the atoms of the disorder using the EADP instruction. A perspective view of **55** is shown for both parts of the disorder in Figure 5.6 and a packing diagram is shown in Figure 5.7. The diffraction data confirms the presence of the pendant vinyl groups, and the structure is in agreement with the ^{1}H NMR, ^{125}Te NMR, and high-resolution mass spectrometry data. This is the first structurally authenticated example of a classical cross-linking agent containing tellurium.

Table 5.2: Crystallographic information for (bis)vinylbenzyl telluride.

Crystal Data		
Empirical formula	$C_{18}H_{18}Te$	
Formula weight	361.92g/mol	
Temperature/K	100	
Wavelength	0.71073 Å	
Crystal system	Monoclinic	
Space group	C2/c	
Unit cell dimensions	a = 28.522(5)Å	α = 90º
	b = 6.464(1)Å	β = 107.311(3)º
	c = 9.025(2)Å	γ = 90º
Volume, Z	1588.4(5)Å^3, 4	
Density (calculated)	1.5134	
Crystal colour	Yellow	
Absorption coefficient	1.858	
F(000)	712	
Crystal Size	0.018 x 0.302 x 0.441mm	
Data Collection		
Theta range for data collection	4.72 to 53.54º	
Limiting indices	-36≤h≤35, -3≤k≤8, -11≤l≤11	
Reflections collected	7782	
Independent reflections	1682 [R(int)=0.0394]	
Refinement		
Refinement method	Full-matrix least-squares on F^2	
Data/restraints/parameters	1682/17/128	
Goodness-of-fit on F^2		
Final R indices [I>2σ(I)]	R1 = 0.0377	
R indices (all data)	R1 = 0.0674, wR2 = 0.1035	
Highest diff. peak and hole	1.6 and -0.80	

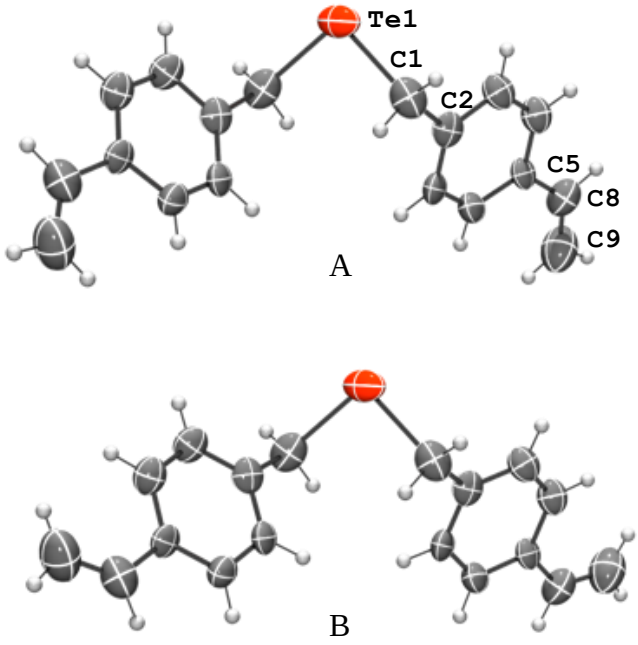

Figure 5.6: Perspective view of the two components of the crystal structure of (bis)vinylbenzyl telluride with populations 46.6%:53.4% A:B (ellipsoids plotted at 50% probability).

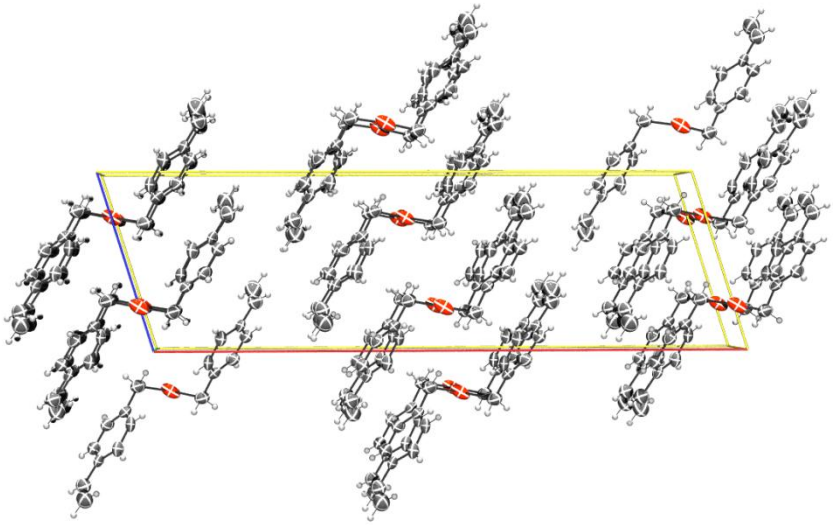

Figure 5.7: Packing view of the "A" component perpendicular to (010) (ellipsoids plotted at 50% probability).

Bis(vinylbenzyl) telluride was also analyzed vibrationally in order to identify bands characteristic of the carbon-carbon double bond and the carbon-tellurium stretch vibrations in the Raman spectrum. Three normal modes, depicted in Figure 5.8, are expected for the C-Te stretches given an idealized C_{2v} geometry. One key band is expected for the carbon-carbon double bond stretch.

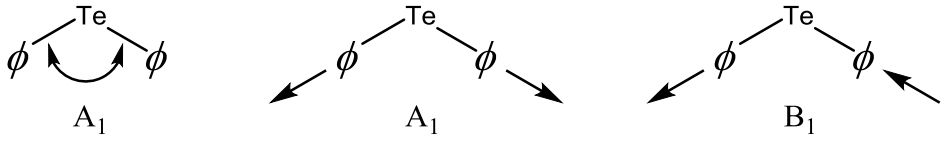

Figure 5.8: Normal coordinate analysis of a C_{2v} idealized (bis)vinylbenzyl telluride.

To support the assignment of the Raman spectrum in Figure 5.10, DFT calculations were employed to obtain the frequencies of the vibrational modes. The geometry of the molecule in gas phase was optimized from the experimental structure. A comparison of selected bond lengths between the experimental and calculated structures are presented in Table 5.3.

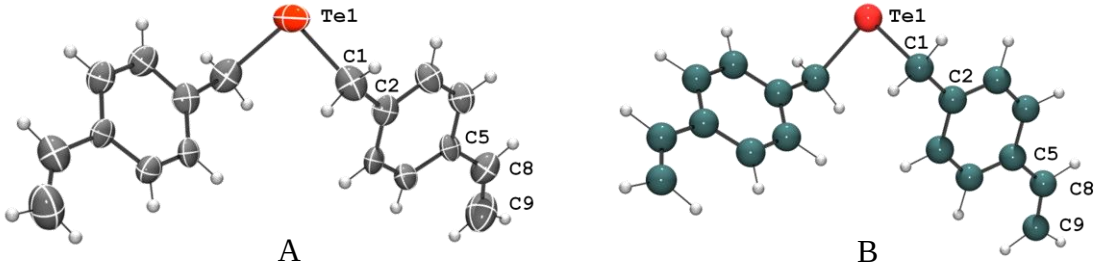

Figure 5.9: Comparison of the experimentally determined (A) and geometry optimized structure (B) of (bis)vinylbenzyl telluride.

Table 5.3: Comparison of experimental and calculated bond lengths (Å).

Atoms	A	B	Calculated
Te1-C1	2.1604(3)	2.1604(3)	2.208
C1-C2	1.5038(2)	1.4709(2)	1.490
C5-C8	1.4804(2)	1.4805(2)	1.465
C8-C9	1.3037(2)	1.3037(2)	1.341

Table 5.4: Bond and torsion angle comparison of experimental and calculated structures.

Atoms	A	B	Calculated
C1-Te1-C1	96.0(2)	96.0(2)	95.2
C5-C8-C9	128.7(6)	128.7(6)	127.7
C2-C1-Te1-C1	81(1)	81(1)	77

Given good agreement between the calculated and experimental structures, the vibrational frequencies were calculated using DFT. The assignments of the representative bands are summarized in Table 5.5.

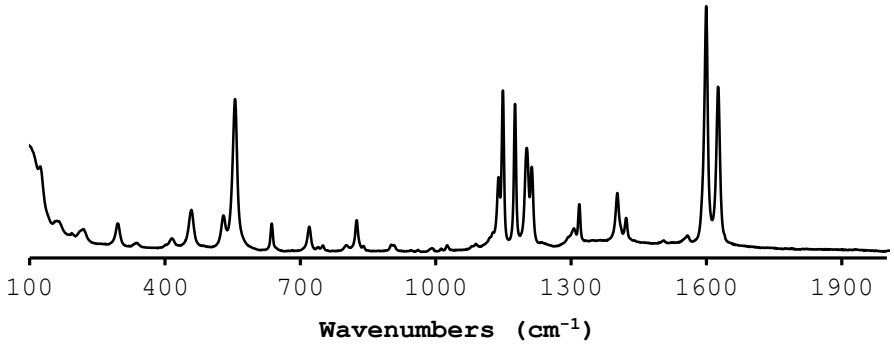

Figure 5.10: Stokes Raman spectrum of (bis)vinylbenzyl telluride (785nm).

Table 5.5: Raman assignments based on the calculated frequencies.

Wavenumber (cm^{-1})		Assignment
Experimental	**Calculated**	
1626, s	1636	ν(C=C) vinyl
556, s	539	$\nu_1(B_1)$, ν_s (C-Te-C)
531	534	$\nu_2(A_1)$, ν_a (C-Te-C)
214	211	$\delta_1(A_1)$, (C-Te-C)

The Raman assignments in Table 5.5 show the key vibrations for the three vibrational modes expected from the normal coordinate analysis shown in Figure 5.8, and the strong C=C vibration characteristic of a vinyl group. As expected, the intensity of the band arising from the symmetric ν_s (C-Te-C) stretch is greater than that of the band from the asymmetric ν_a (C-Te-C). In the calculated infrared spectrum, the asymmetric stretch was found to be more intense. The vibrational

assignments compliment the information from NMR, mass spectrometry, and X-Ray crystallography.

One of the requirements of a suitable tellurium cross-linking agent towards the goal of this project, is that it should be sensitive to green light (λ=532nm). However, the UV-Visible spectrum of (bis)vinylbenzyl telluride in hexanes shows a wavelength of maximum absorption at λ=258nm. A more concentrated sample was acquired, and the tail of the spectrum is examined to assess the absorption at green wavelengths. The expanded spectrum shows weak absorption in the green range.

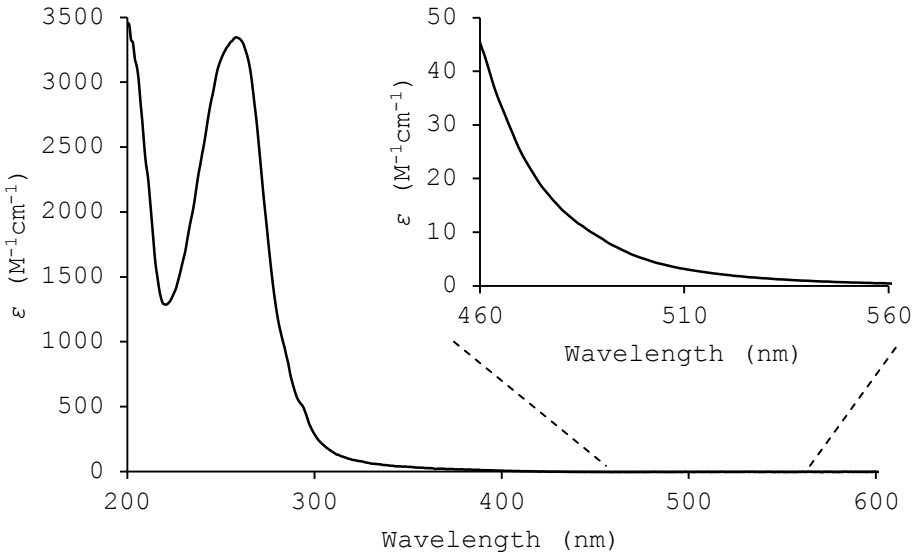

Figure 5.11: UV-Visible spectra of (bis)vinylbenzyl telluride in hexanes.

Following an attempt to acquire the Raman spectrum of a sample of **55** (flame sealed in a capillary tube) with a 514 nm laser, a black spot was observed in the sample. Because of this decomposition, a photolysis

experiment was attempted on a solid sample of **55** (flame-sealed in a capillary tube) using a $NdYVO_4$ laser to assess the light sensitivity of the monotelluride cross-linking agent. The sample was irradiated for 25 minutes using a 532 laser at 5 mW. No visible change was observed in the sample. The ^1H NMR spectrum shows clean **55,** the baseline was expanded in order to view decomposition.

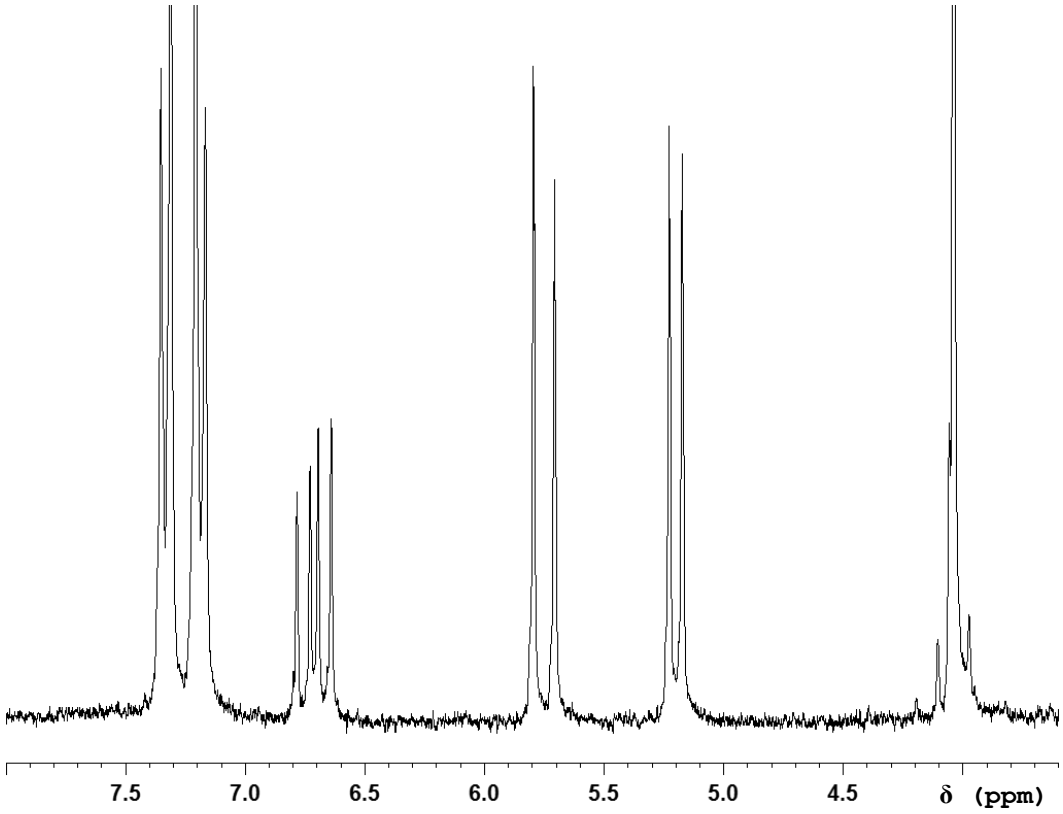

Figure 5.12: NMR spectrum of **55** following attempted photolysis with 532nm light.

With the successful synthesis of (bis)vinylbenzyl telluride, attention was again turned towards the preparation of the ditelluride through the sodium tellurolate intermediate. A possible explanation for the preference for the monotelluride product over the tellurolate anion

is the insolubility of Na_2Te in acetonitrile. A possible process for the monotelluride synthesis is proposed in Scheme 5.6. This is a heterogeneous reaction with Na_2Te in the solid state throughout the course of the reaction. It is likely that the tellurolate anion is generated in solution and reacts faster than Na_2Te with vinylbenzyl chloride due to the insolubility of Na_2Te.

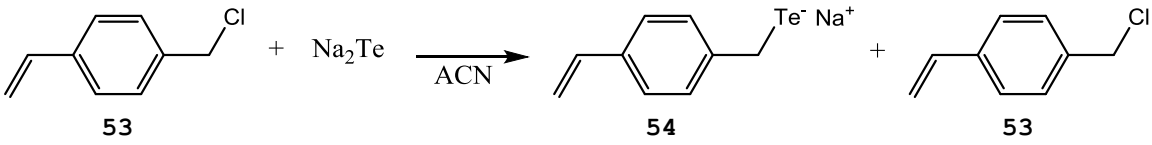

53 **54** **53**

Scheme 5.6: Synthesis of (bis)vinylbenzyl telluride.

To circumvent the issues with the solubility of the monotelluride, a synthesis involving 15-crown-5 was attempted.

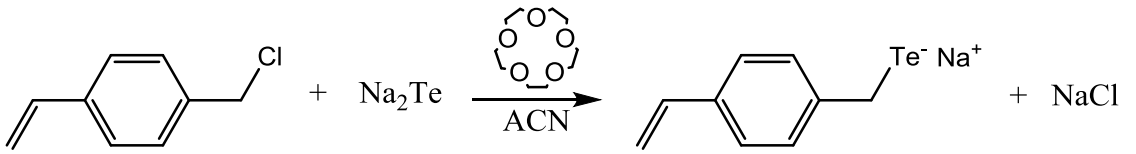

53 **54**

Scheme 5.7: Synthesis of sodium vinylbenzyl tellurolate.

This reaction was conducted with both a catalytic and stoichiometric amount of the crown ether. In the reaction done with a catalytic amount of 15-crown-5, ^1H NMR analysis revealed a 3:1 ratio of **55** and an unidentified product. The spectrum of the minor product shows patterns that would be expected for a compound containing both vinyl and benzyl groups. However, the tellurium resonance for this species could not be observed. In the case of the reaction done with a stoichiometric amount of crown ether, two new products were found in the ^1H NMR spectrum (Figure 5.13), both of which have patterns that would be expected for a

compound containing vinyl and benzyl groups. The ^{125}Te NMR spectrum of this compound however, shows two broad singlet transitions at 16.99 and 23.12 ppm (Figure 5.14). If either the sodium tellurolate anion **54** or the corresponding ditelluride was present, triplets would be expected in the ^{125}Te NMR spectrum from coupling to the two neighbouring protons. However, the breadth of the main transitions at 16.99 and 23.12 ppm span much larger than the expected coupling constant of approximately 25 Hz, rendering the coupling to adjacent protons unobservable. It is possible that the NMR spectra show a mixture of the sodium tellurolate **54** and the corresponding ditelluride **29**. The broad signal at 23.12 ppm is consistent with what would be expected for a species coordinated to 15-crown-5. The chemical shift ranges of dialkyl tellurolates and dialkyl ditellurides overlap in the region in which the ^{125}Te chemical shifts are observed in Figure 5.14. The ^{125}Te chemical shift ranges from -520 to 117 ppm for tellurolate anions, and from -74 to 499 ppm for dialkyl ditellurides.[82,83] This experiment would need to be repeated with a more concentrated sample and larger number of scans to better observe the ^{125}Te signals in the NMR spectrum.

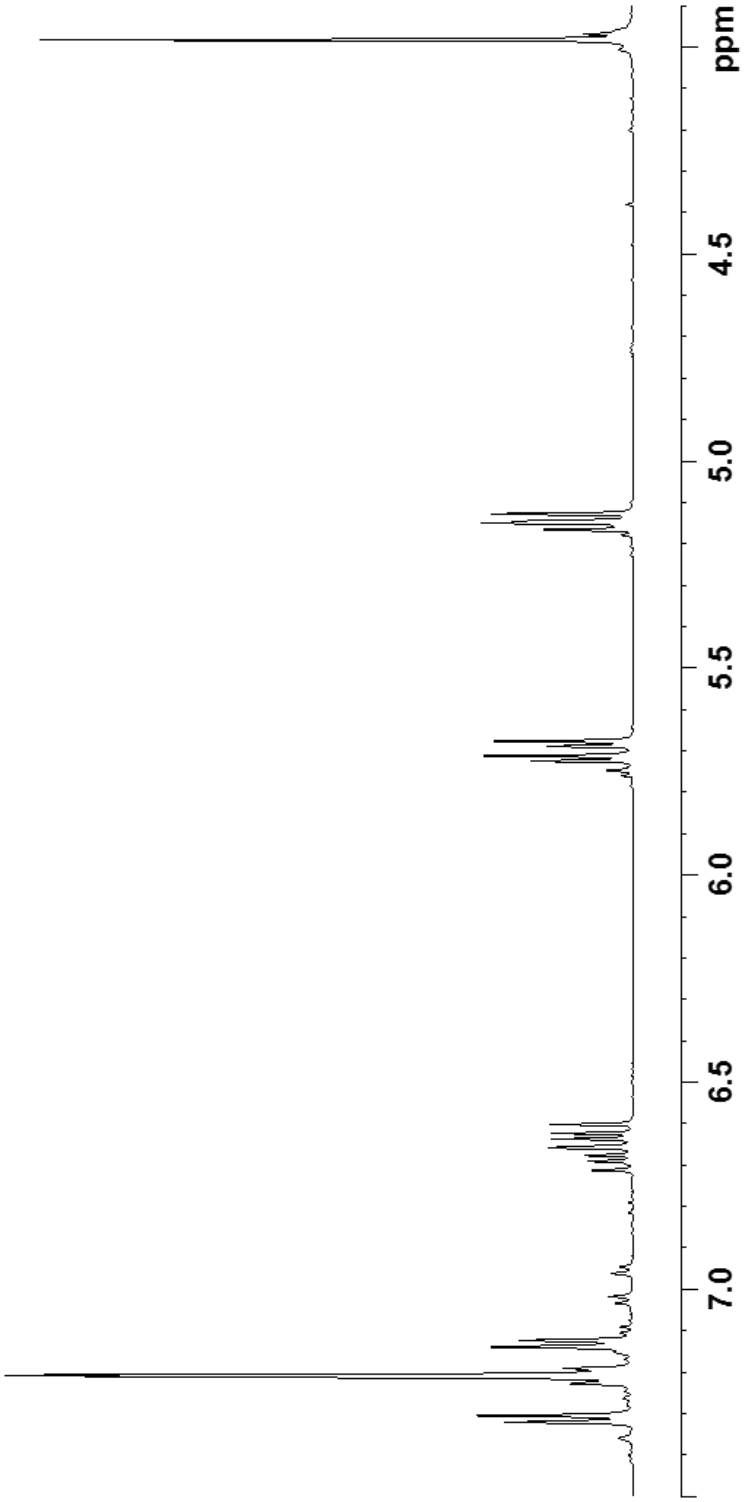

Figure 5.13: ^{1}H NMR spectrum of the product from the reaction of sodium telluride with vinylbenzyl chloride using a stoichiometric amount of 15-crown-5.

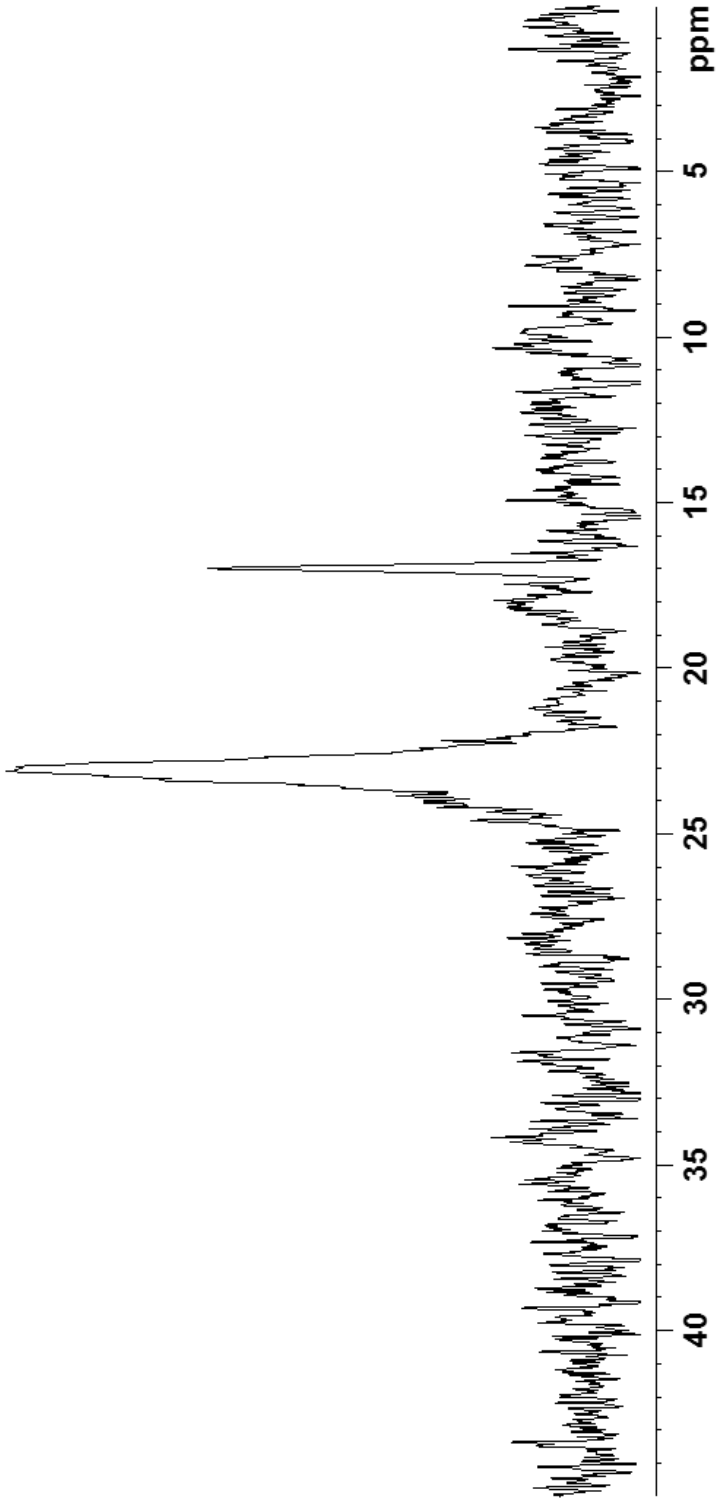

Figure 5.14: ^{125}Te NMR spectrum of the product from the reaction of sodium telluride with vinylbenzyl chloride using a stoichiometric amount of 15-crown-5.

6 Chapter 6: Conclusions and Suggestions for Future Work

6.1 Conclusions.

Two approaches for the synthesis of a polymer cross-linked by photosensitive ditelluride groups were explored: direct functionalization of polystyrene, and the preparation of a ditelluride-based cross-linking agent. The two-step functionalization of polystyrene was complicated by the inefficiency of the initial lithiation and the insolubility of the products when chalcogenation was attempted. However, functionalization with TMS groups was successful with this method, and the expected product was confirmed using 1D and 2D NMR methods.

Working with molecules that simultaneously contain two reactive functionalities such as a polymerizable alkene and a ditelluride group was also challenging. The products, if formed, were too unstable to be purified and conclusively characterized. The most promising result discussed in this thesis is the formation of bis(4-vinylbenzyl)telluride. This is the first structurally authenticated example of a tellurium containing cross-linking agent. The product is cleanly formed and is stable, unfortunately it is not sensitive enough to green light to permit using it as the cross-linking agent in a photo-responsive polymer gel. This finding is also significant because several vinyl tellurides have been previously reported, but the claims

have lacked proper spectroscopic evidence and structural characterization.

Because it seems that (bis)vinylbenzyl telluride is not sensitive enough to be used as a potential cross-linking agent in a photo-responsive polymer, efforts should be made towards the synthesis of a polymerizable ditelluride containing cross-linking agent.

6.2 Suggestions for future work.

6.2.1 Synthesis of a ditelluride cross-linking agent.

Reported in this thesis are both conventional and new approaches to the synthesis of diorganyl ditelluride containing cross-linking agents. A less classic method to the synthesis of a ditelluride cross-linking agent which involves the synthesis of a (bis)trialkylsilyl telluride intermediate can also be explored.

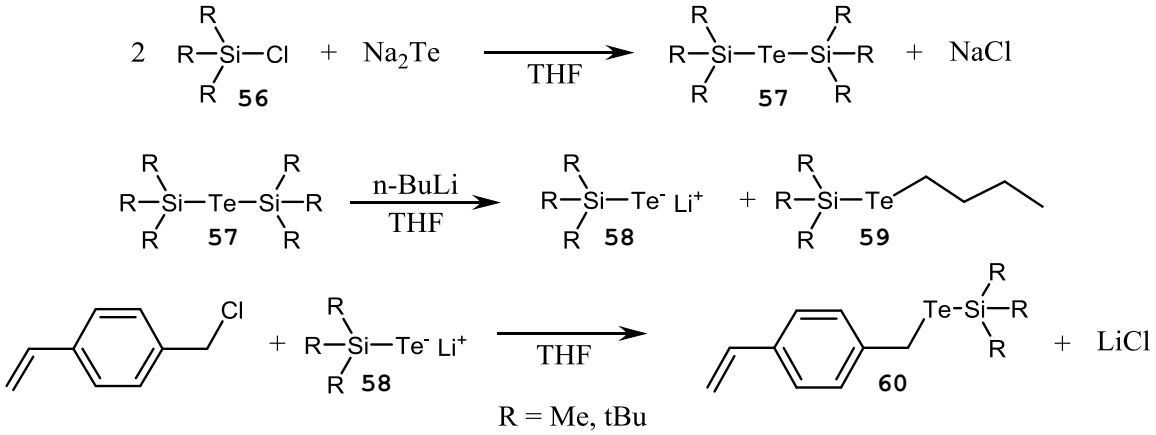

Scheme 6.1: Synthesis of a trialkylsilyl protected organotellurium species through a (bis)trialkylsilyl telluride intermediate.

To accomplish this, two equivalents of sodium telluride would be reacted with a trialkylsilyl chloride reagent to prepare the (bis)trialkylsilyl telluride intermediate **58**.[84] The isolation of (bis)trialkylsilyl tellurides can be made difficult by their volatility, and instability in air. They could be reacted further with alkyllithium reagents to form the corresponding tellurolate salt **58**. **58** would then be reacted with vinylbenzyl chloride to give **60**. From the final product, the ditelluride could be formed by protonation and removal of the silyl protecting group. Tellurols are known to be unstable and decompose to the corresponding ditelluride and hydrogen gas.

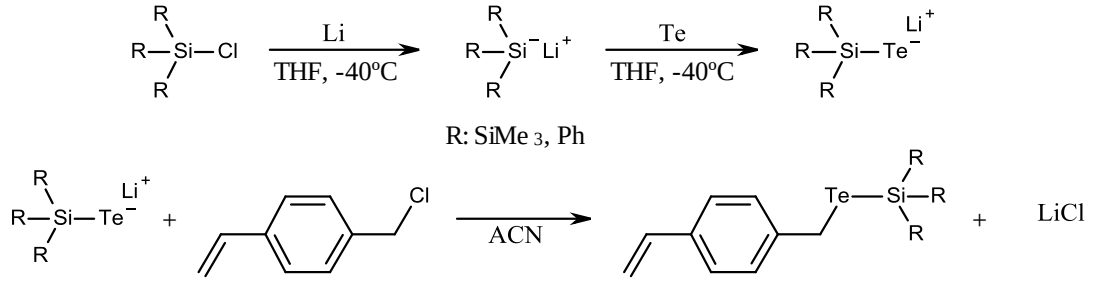

Scheme 6.2: Synthesis of a trialkylsilyl protected organotellurium species through a sterically hindered trialkylsilyl tellurolate.

To circumvent the synthesis of the volatile and sensitive (bis)trialkylsilyl telluride intermediate, the more stable sterically hindered trialkylsilyl tellurolate anions could be directly synthesized. The syntheses of the supersilyltellurolate and triphenylsilyltellurolate anions are both known stable species. Following the procedure described in Scheme 6.2 and acid workup, this reaction scheme should yield (bis)vinylbenzyl ditelluride.

6.2.2 Tellurium cross-linking agents from acetylides and elemental tellurium.

A synthesis of a compound simultaneously containing vinyl groups and tellurium was reported in 1979 by Petrov.[85] Initially, the reported method included the preparation of the red-orange 1,3-ditellurole using the following process in Scheme 6.3.

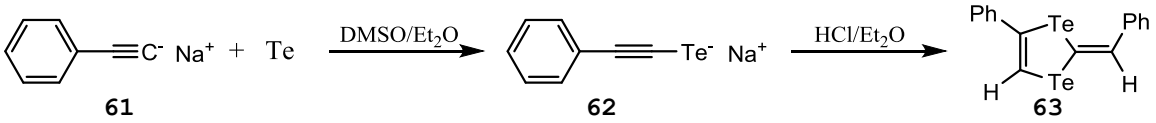

61 **62** **63**

Scheme 6.3: Preparation of a 1,3-ditellurole.

This chemistry was later repeated in 1981, and the final product was structurally characterized by X-ray diffraction. The synthesis was actually shown to yield the dimer **64**.[86]

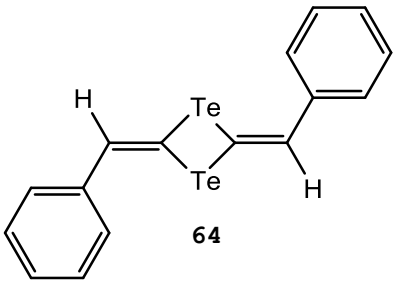

64

Figure 6.1: *trans*-2,4-dibenzylidine-1,3-ditelluretan.

Interest in this compound stems from its red colour, and the presence of both the carbon-carbon double bond and tellurium. This chemistry could also be attempted using tert-butylacetylene as a starting material.

REFERENCES

(1) Trenor, Scott R.; Shultz, Allan R.; Love, Brian J.; Long, Timothy E. *Chem. Rev.* **2004**, *104*, 3059.

(2) Brown, Glenn H. *Techniques of Chemistry Volume III (Photochromism)*. John Wiley & Sons, Inc., Kent, Ohio. **1971**.

(3) Lewis, G. N.; Lipkin, D. J. Amer. Chem. Soc. **1942**, *64*, 2801.

(4) Holt, P.F.; Hughes, B.P. *J. Chem. Soc.* **1955**, 98.

(5) Weiss, J. *Trans. Faraday Soc*. **1940**, *36*, 856.

(6) Lyons, W.E.; *Nature*. **1948**, *162*, 1004.

(7) Alessandri, L. *Atti Accad. Nazl. Lincei, Rend. Cl.-Sci. Fis. Mat. Nat.* **1910**, *19*, 122.

(8) Jeger, O.; Schaffner, K.; Wehrli, H. *Pure Appl. Chem.* **1964**, *86*, 5050.

(9) Zimmerman, H.E. *A New Approach to Mechanistic Organic Photochemistry, Vol. 1.* **1963**. Interscience, New York.

(10) Henry, A. J. *J. Chem. Soc.* **1946**, 1156.

(11) Schulte-Frohlinde, D.; Blume, H.; Güsten, H. J. Phys. Chem. **1962**, *66*, 2486.

(12) Brode, W. R.; Pearson, E.G.; Wyman, G.M. *J. Amer. Chem. Soc*. **1954**, *76*, 1034.

(13) Irie, M.; Hirano, Y.; Hashimoto, S.; Hayashi, K. *Macromolecules*. **1981**, *14*, 262.

(14) Bullock, D. J. W.; Cumper C. W. N.; Vogelm, A. I. *J. Chem. Soc.* **1965**, 5316.

(15) Eisenback, C. D. *Polymer*. **1979**, *20*, 196.

(16) Menju, A.; Hayashi, K.; Irie, M. *Macromolecules*. **1981**, *14*, 755.

(17) Irie, M. Hayashi, K. Menju, A. *Polym. Photochem*. **1981**, *1*, 233.

(18) Takemoto, Kilichi; Ottenbrite, Raphael M.; Kamachi, Mikiharu. *Functional Monomers and Polymers (2nd Edition)*. Marcel Dekker, Inc., New York, New York. **1997**.

(19) Irie, M. Hosoda, M. *Makromol. Chem. Rapid Commun*. **1985**, *6*, 533.

(20) Irie, M.; Hosoda, M. *Makromol. Chem. Rapid Commun*. **1984**, *5*, 829.

(21) Irie, M.; Kungwatchakun, D. *Macromolecules*. **1986**, *19*, 2476.

(22) Imori, Toru; Tilley, T.D. *J. Chem. Sov., Chem. Commun*. **1993**, 1607.

(23) Trummer, Markus; Nauser, Thomas; Lechner, Marie-Luise; Uhlig, Frank; Caseri, Walter. *Polym. Degrad. Stab*. **2011**, *96*, 1841.

(24) Shultz, G.V.; Tyler, D.R. *Inorg. Organomet. Polym. Mater*. **2009**, *19*, 423.

(25) Tenhaeff, S. C.; Tyler D. R. *Organometallics*. **1991**, *10*, 473.

(26) Meyer, T. J.; Caspar, J.V. *Chem Rev*. **1985**, *85*, 187.

(27) Geoffroy, G. L.; Wrighton, M. S. *Organometallic Photochemistry*. Academic Press, New York. **1979**.

(28) Shultz, G. V.; Zemke, J. M.; Tyler, D. R. *Macromolecules*. **2009**, *42*, 7644.

(29) Wong, Wai-Yeung; Abd-El-Aziz, Alaa S. *Molecular Design and Applications of Photofunctional Polymer and Materials*. RSC Publishing. **2012**.

(30) Ramakrishna, S. *Anantha. Rep. Prog. Phys.* **2005**, 68, 449.

(31) Kaminow, I.P.' Turner, E.H. *Appl. Opt.* **1966**, *5*, 1612.

(32) Chen, Zhigang; Segev, Mordechai. *J. Opt. Soc. Am. B.* **1997**, *14* 1407.

(33) Besancon, Robert M. *The Encyclopedia of Physics Second Edition.* Litton Educational Publishing Inc. **1974**.

(34) *CRC Handbook of Chemistry and Physics*. 55th ed. CRC Press: Cranwood Parkway Cleveland, Ohio, **1974**; E222.

(35) Atkins, P.W. *Physical Chemistry, 4th ed.*; W.H. Freeman and Company: New York, **1990**, 652.

(36) Zhang, Jihua; Saravanamuttu, Kalaichelvi. *J. Am. Chem. Soc.* **2006**, *128*, 14913.

(37) Villafranca, Ana B.; Saravanamuttu, Kalaichelvi. *J. Phys. Chem. C.* **2008**. *112*, 17388.

(38) Villafranca, Ana B.; Saravanamuttu, Kalaichelvi. *J. Opt. A: Pure Appl. Opt.* **2009**, *11*, 125202/1.

(39) Villafranca, Ana B.; Saravanamuttu, Kalaichelvi. *Opt. Express.* **2011**, *19*, 15560.

(40) Burgess, Ian B.; Shimmell, Whitney E.; Saravanamuttu, Kalaichelvi *J. Am. Chem. Soc.* **2007**, *129*, 4738.

(41) Kasala, K.; Saravanamuttu, Kalaichelvi. *J. Am. Chem. Soc.* **2012**, *134*, 14195.

(42) Ogawa, Akiya; Yokoyama, Kazuyuki; Ryoichi, Obayashi; Han, Li-Biao; Kambe, Nobuaki; Sonoda, Noboru. *Tetrahedron*. **1993**, *49*, 1177.

(43) Pauling, Linus. *J. Phys. Chem*. **1954**, *58*, 662.

(44) Vogel, Arthur I. *J. Chem. Soc.* **1948**, 1820.

(45) Farrall, M. Jean; Frechet, M.J. *J. Org. Chem*. **1976**, *41*, 3877.

(46) Bruker (**2007**). APEX2. Bruker AXS Inc., Madison, Wisconsin, USA.

(47) Farrugia, L.J. *J. Appl. Cryst.* **1999**, *32*, 837.

(48) Dolomanov, O. V.; Bourhis, L. J.; Gildea, R. J.; Howard, J. A. K.; Puschmann, H. *J. Appl. Cryst.* **2009**, *42*, 339.

(49) Farrugia, L.J. *J. Appl. Cryst.* **1997**, *30*, 565.

(50) Persistence of Vision Pty. Ltd. **(2004)**. Persistence of Vision Raytracer (Version 3.6). Persistence of Vision Pty. Ltd., Williamstown, Victoria, Australia. http://www.povray.org/.

(51) Xue, Thomas J.; Jones, Mark S.; Ebdon, John R.; Wilkie, Charles A. *J. Polym. Sci., Part A: Polym. Chem.* **1997**, *35*, 509.

(52) Singh, Devender; Deobald, Anna M.; Camargo, Leandro R.S.; Tabarelli, Greice; Rodrigues, Oscar E.D.; Barga, Antonia L. *Org. Lett.* **2010**, *12*, 3288.

(53) Das, Priyabrata; Mcleod, David; Mcnulty, James. *Tetrahedron Lett.* **2011**, *52*, 199.

(54) Bhasin, K.K.; Arora, Ekta; Kaur, Kushwinder; Kang, Sung-Kyu; Gobel, Michael; Klapoetke, T.M.; Mehta, S.K. *Tetrahedron.* **2009**, *65*, 247.

(55) Thiele, K.H.; Steinicke, A.; Dümichen, U.; Neümuller, B. *Z. anorg. allg. Chem.* **1996**, *622*, 231.

(56) Pearson, D.E.; Frazer, M.G.; Frazer, V.S.; Washburn, L.C. *Synthesis*. **1976**, 621.

(57) Lange, Lutz; Du Mont, Wolf-Walther. *J. Organomet. Chem*. **1985**, *286*, C1.

(58) Farrar, W.V. *Research (London)*. **1951**, *4*, 177.

(59) Beckmann, Jens; Heits, Stephan; Hesse, Malte. *Inorg. Chem.* **2007**, *46*, 3275.

(60) te Velde, G.; Bickelhapt, F. M.; Baerends, E. J.; Fonseca Guerra, C.; van Gisbergen, S. J. A.; Snijdfers, J. G.; Ziegler, T. *J. Comput. Chem*. **2001**, *22*, 931.

(61) Fonseca Guerra, C.; Visser, O.; Snijders, J. G.; te Velde, G.; Baerends, E.J. *Methods and Techniques for Computational Chemistry.* **1995**, 303.

(62) Perdew, J. P. *Phys. Rev. B*. **1986**, *33*, 8822.

(63) Perdew, J. P.; Wang, Y. *Phys. Rev. B*. **1992**, *45*, 13244.

(64) van Lenthe, E.; Ehlers, A.; Baerends, E. J. *J. Chem. Phys.* **1999**, *110*, 8943.

(65) Macrae, C.F.; Bruno, I.J.; Chisholm, J. A.; Edgington, P. R.; McCabe, P.; Pidcock, E.; Rodriguez-Monge, L.; Taylor, R.; van de Streek, J.; Wood, P. A. *J. Appl. Cryst*. **2008**, *41*, 466.

(66) Elschenbroich, Christoph; Salzer, Albrecht. *Organometallics a concise introduction, Second Revised Edition.* VCH Verlagsgesellschaft mbH, Weinheim (Federal Republic of Germany) & VCH Publishers Inc. **1992.**

(67) Fortier, Skye; Zhang, Yongqiang; Sharma, Hemant K.; Pannell, Keith H. *Organometallics*. **2010**, *29*, 1041.

(68) Moerlein, S. M. *J. Organomet. Chem.* **1987**, *319*, 29.

(69) Gendy, C. Senior Undergraduate Thesis, McMaster University. **2011**.

(70) Dutton, J.L.; Farrar, G. J.; Sgro, M. J.; Battista, T. L.; Ragogna, P. J. *Chem. Eur. J.* **2009**, *15*, 10263.

(71) Alcock, N.W.; *Adv. Inorg. Chem. Radiochem*. **1972**, *15*, 1.

(72) Alcock, N.W.; Harrison, W.D. *J. Chem. Soc., Dalton Trans.* **1982**, 251.

(73) Einstein, F.W.B.; Jones, T. *Acta Crystallogr., Sect. B: Struct. Sci*. **1982**, *38*, 617.

(74) de Moura Compos, M.; Petragnani, N. *Tetrahedron*. **1962**, *18*, 527.

(75) Dabdoub, M.J.; Dabdoub, V.B.; Comasseto, J.V. *J. Organomet. Chem.* **1986**, *308*, 211.

(76) Dabdoub, M.J.; Comasseto, J.V. *J. Organomet. Chem.* **1988**, *344*, 167.

(77) Musalova, M.V.; Potapov, V.A.; Panov, V.A.; Amosova, S.V. *Russ. J. Org. Chem*. **2012**, *48*, 743.

(78) Mehdi, Rahim T.; Miller, J. David; Tahri, Tahir A. *Inorg. Chim. Acta*. **1948**, *90*, 85.

(79) Kato, Shiuzi; Niyomura, Osamu; Nakaiida, Shohou; Kawahara, Yasuyuki; Kanda, Takahiro; Yamada, Ryo; Hori, Shinya. *Inorg Chem.* **1999**, *38*, 519.

(80) Gedridge, Robert W.; Higa, Kelvin T. Jr.; Nissan, Robin A. *Magn. Reson. Chem.* **1995**, *33,* 441.

(81) Ignacio García Alonso, J.; Rodríguez-González, P.; González-Gago A.; González-Antuña, A. *Anal. Chim. Acta.* **2010**, *664,* 68.

(82) Arnold, John. *Prog. Inorg. Chem*. **1995**, *43*, 353.

(83) Jones, C.H.W.; Sharma, R.D. *J. Organomet. Chem*. **1983**, *255*, 61.

(84) Detty, Michael R.; Seidler, Mark D. *J. Org. Chem*. **1982**, *47*, 1354.

(85) Petrov, M.L.; Laishev, V.Z.; Petrov, A. A. *Zh. Org. Khim*. **1979**, *15*, 2596.

(86) Bender, Steven L.; Haley, Neil F.; Luss, Henry R. *Tetrahedron Letters*. **1981**, *22*, 1495.